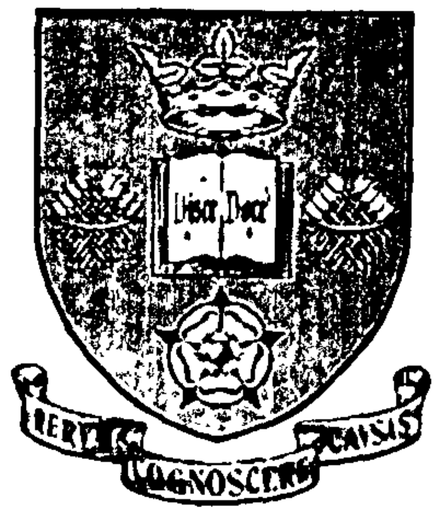

DEPARTMENT OF CIVIL AND STRUCTURAL ENGINEERING

UNIVERSITY OF SHEFFIELD

LIQUEFACTION OF SAND-TYRE CHIP MIXTURES

VOLUME 1

by

PANU PROMPUTTHANGKOON

A THESIS SUBMITTED TO THE UNIVERSITY OF SHEFFIELD

FOR THE DEGREE OF DOCTOR OF PHILOSOPHY

JULY 2009

ABSTRACT

This research attempts to address the two problems of soil liquefaction in reclaimed land and a growing number of discarded tyres by mixing liquefiable sand with tyre chips and using them as fill materials with the aim reducing the liquefaction potential. The cyclic strength of sand-tyre chip mixtures was investigated using a cyclic triaxial system which was modified to house bender elements for measuring the shear wave velocity and small strain shear modulus. In addition, the behaviour of the mixtures under monotonic loading conditions was studied using a standard triaxial apparatus with pore water pressure measurements.

The triaxial test results showed that the addition of rubber alters the stress-strain, pore water pressure, and stress path behaviours, depending on the amount of rubber added. It was found that the cyclic strength of mixtures with 5% to 30% rubber content were lower than that of pure sand. However, when the rubber was increased to 40% and above, the cyclic strength was increasingly improved. The bender element tests showed that the higher the percentage of rubber, the lower was the shear wave velocity and shear modulus.

The seismic response of the layered soils comprising sand, clay, and sand-tyre chips has been analysed using equivalent linear elastic analysis. This showed that the sand-rubber mixtures actually amplify the ground accelerations and generate higher shear strains, compared to pure sand; however, the generated shear stress did not vary with the addition of rubber. Nevertheless, it was found that the mixtures improve the overall factor of safety against liquefaction, suggesting that they may be used to mitigate the hazard.

ACKNOWLEDGEMENTS

The author wishes to thank the Office of the Higher Education Commission, Thai Government, for their financial aid through the Office of Educational Affairs, Royal Thai Embassy in London. They provided the support for all aspects of living and studying in the UK from the first day right to the completion for which the author is gratefully indebted.

This research was guided throughout by Prof Adrian FL Hyde who offered advice and opinions, provided suggestions, and answered questions; in particular, read and corrected the drafts of this thesis. His experiences and knowledge about soil liquefaction have broadened the author to a new perspective of geotechnical engineering research. Most importantly, his door was always wide open for the author when encountering the difficulties and problems during the research. The author would like to express his heartiest gratitude to the supervisor for all of these.

A special thanks is due to Dr Charles C Hird for the permission of using the equipment and materials used for the bender element test as well as providing useful suggestions. A computer program used to conduct the cyclic triaxial test was provided by ELE International free of charge which is kindly acknowledged.

In addition, the author would like to extend his gratitude to the following people for their help in the laboratories: (1) Mr Paul Osborne, for his expertise in the laboratory, including discussion, designing and assembling of special instruments, and purchasing of test materials, (2) Mr Mark Foster, for assisting and providing support relating to all technicalities of the test machines, and (3) Mr David Callaghan, for introducing the basic triaxial test as well as offering miscellaneous assistance.

Lastly, the author is very grateful and appreciative of all of the assistance and support offered from colleagues, researchers, and lecturers of the Geotechnical Engineering Group.

TABLE OF CONTENTS

VOLUME 1

VOLUME 2

NOTATION

a parameter for curve fitting (for *CRR* determination); factor (for *CSR* determination); factor (for e_s determination)

a_{max} maximum acceleration

A tyre chips CT0515

A pore water pressure coefficient; parameter (for V_s calculation)

A_c area of specimen after consolidation

A_f pore water pressure coefficient at failure

b parameter for curve fitting (for *CRR* determination); factor (for *CSR* determination); factor (for e_s determination)

c factor (for $\Delta u_p/\sigma'_{3c}$ determination)

B tyre chips CT1030

B pore water pressure coefficient

BE bender element

C tyre chips CT2060

$CC_{xy(t)}$ cross correlation function

$CC_{xy,max}$ maximum value of cross correlation of two signals

C_c coefficient of curvature

C_B correction for borehole diameter

CC cross correlation

C_E correction for hammer energy ratio

C_{Fines} corrected value due to find contents for $(N_1)_{60}$

C_N correction for effective overburden pressure

C_R correction for rod length

C_S correction for samples (with or without liners)

CT undrained cyclic triaxial test

C_u coefficient of uniformity

C_v factor to correct measured shear wave velocity for overburden pressure

CRR cyclic resistance ratio

CSR cyclic stress ratio

CSR_{20} cyclic strength

d average grain size; factor(for $\Delta u_p/\sigma'_{3c}$ determination)

D tyre chips CT4010

D diameter of specimen; damping ratio

D_{10} maximum size of the smallest 10 per cent

D_{30}	maximum size of the smallest 30 per cent
D_{50}	mean particle size
D_{60}	maximum size of the smallest 60 per cent
D_r	mean particle size of tyre chips
D_s	mean particle size of Leighton Buzzard 16/30 sand
e	consolidated void ratio
e_o	initial void ratio
e_r	inter-rubber void ratio
e_s	inter-sand void ratio; inter-granular void ratio
f	frequency
f_{in}	frequency of input voltage
FA	first arrival
FC	fine content
F_e	factor (for e determination)
FFT	Fast Fourier Transform
F_G	factor (for G_{max} determination)
F_L	factor of safety against liquefaction
FS_L	factor of safety against liquefaction
F_V	factor (for V_s determination)
g	acceleration of gravity
G	shear modulus
G_{max}	small strain shear modulus
$Gxy(f)$	cross power spectrum
IFFT	Inverse Fast Fourier Transform
K_o	coefficient of earth pressure at rest
l	distance
l_{rb}	length of individual rubber
$l_{t\text{-}t}$	tip to tip distance between transmitter and receiver
L	earthquake-induced cyclic shear stress ratio; length of specimen
$Lx(f)$	linear spectrum of input signal
$Ly(f)$	linear spectrum of output signal
$Ly^*(f)$	complex conjugate of linear spectrum of output signal
m	stress exponent (for V_s calculation)
M	slope of critical state line
MSF	magnitude scaling factor
M_w	moment magnitude of earthquake

n	exponent (for *MSF* determination)
N	number of load cycles; SPT-N value
N_f	number of load cycles at liquefaction
$(N_1)_{60}$	corrected SPT-N value
$(N_1)_{60,CS}$	adjusted $(N_1)_{60}$ due to fine contents
p'	mean normal effective stress
P_a	reference stress of 100kPa or about atmospheric pressure
P_c	magnitude of cyclic load
P'_f	mean effective normal stress at failure
PP	first major peak to peak
PT	phase transformation
q	deviator stress
q_{cyc}	cyclic deviator stress (single amplitude)
q_f	deviator stress at failure
r_d	stress reduction coefficient
R	cyclic strength ratio of soil
RC	rubber content in per cent
S	Leighton Buzzard 16/30 sand
SA	Leighton Buzzard 16/30 sand + tyre chips CT0515
SB	Leighton Buzzard 16/30 sand + tyre chips CT1030
SC	Leighton Buzzard 16/30 sand + tyre chips CT2060
SD	Leighton Buzzard 16/30 sand + tyre chips CT4010
t	travel time; time shift between two signals
t_o	arrival time of shear waves
$t_{pk\text{-}pk}$	peak to peak travel time
TC	undrained triaxial compression test
TE	undrained triaxial extension test
T_r	time record
u_f	pore water pressure at failure
u_o	initial pore water pressure
V_S	volume of solid
V_V	volume of voids
V_s	shear wave velocity
V_{s1}	overburden stress-corrected shear wave velocity
V^*_{s1}	upper limit value of V_{s1}
w_{rb}	width of individual rubber

z	depth below ground surface
$\varepsilon_{a,DA}$	double-amplitude axial strain
$\varepsilon_{a,P}$	axial plastic strain
Γ	specific volume of soil at critical state with $p' = 1.0$kPa
η	aspect ratio
ρ	density
μ	Poisson's ratio
ν	specific volume
λ	slope of normal consolidation line; wave length
γ	shear strain
γ_{max}	maximum shear strain
ϕ'	angle of friction in terms of effective stress
σ'_1	major principal effective stress
σ'_2	intermediate principal effective stress
σ'_3	minor principal effective stress, effective confining pressure
σ'_{3c}	consolidation pressure
σ_1	major principal stress
σ_3	minor principal stress
σ'_h	horizontal effective stress
σ'_v	vertical effective stress
σ'_{vo}	vertical effective overburden stress
σ_{vo}	vertical total overburden stress
σ_{cyc}	cyclic deviator stress
τ_{av}	average horizontal shear stress
τ_{cyc}	cyclic shear stress
τ_{max}	maximum shear stress
ΔP_c	peak cyclic load in compression
ΔP_e	peak cyclic load in extension
Δu	excess pore water pressure, change of pore water pressure
Δu_p	peak pore water pressure
$\Delta \sigma_3$	change of cell pressure

LIST OF TABLES

LIST OF FIGURES

CHAPTER 1

INTRODUCTION

1.1 Research Context

Saturated sand when subjected to seismic loading under undrained conditions will undergo a progressive build up of the pore water pressure. Under certain conditions this can become equal to the initial effective stress resulting in the complete loss of shear strength and stiffness. This phenomenon has been coined as "liquefaction". During the liquefaction, soil grains lose contact with each other and float around and as a result the soil assemblage is transformed from a solid to liquid state. If this happens on sloping ground, flow failure is foreseen. On the other hand, for level ground, after the liquefaction large settlements are likely to occur owing to the re-arrangement of the soil grains after the dissipation of pore water pressure, as illustrated by Figure 1.1.

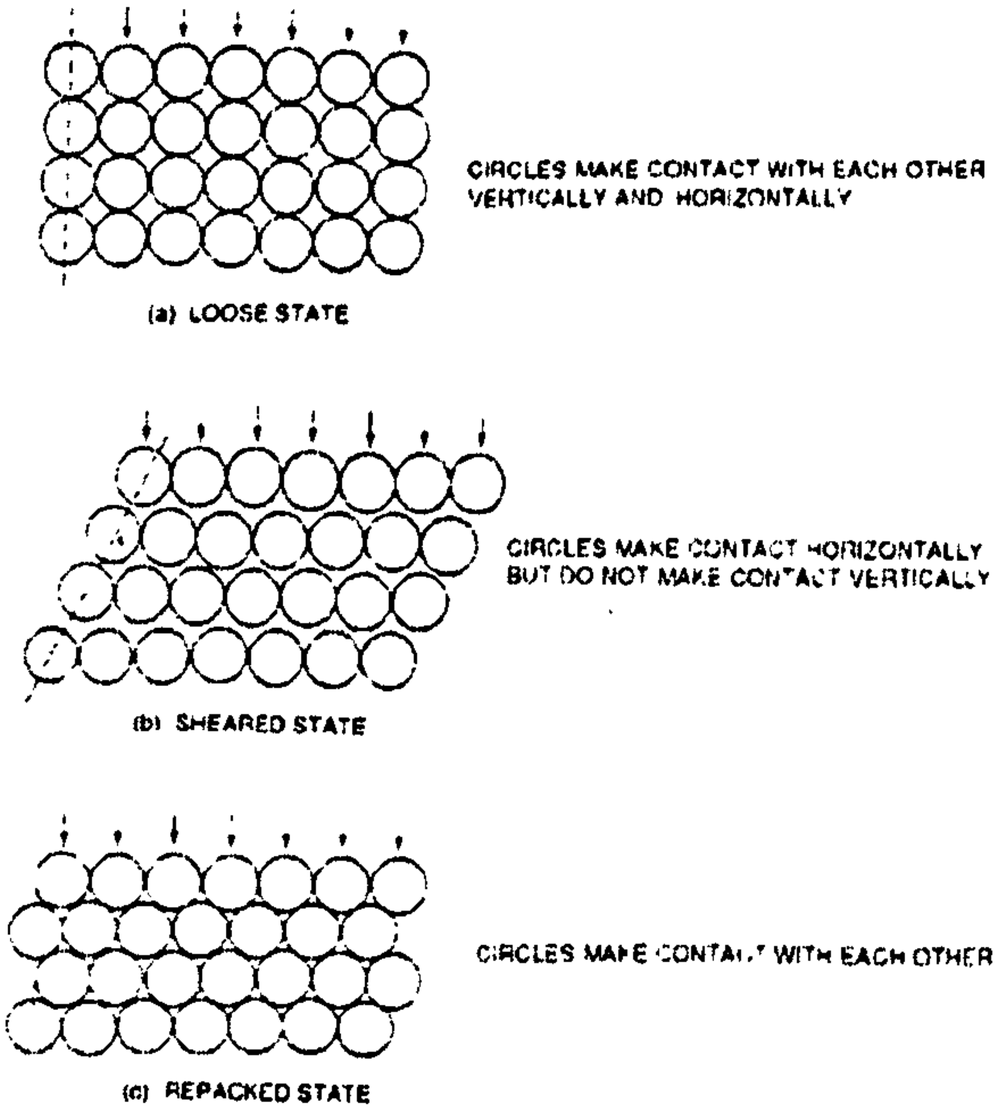

Figure 1. 1 Schematic diagram for sand grain arrangement (after PHRI, 1997)

Geotechnical engineers have studied the behaviour of earthquake-induced liquefaction since the earthquakes in 1964 at Niigata, Japan, and Alaska, USA; nonetheless, many aspects of liquefied soil including the mitigation of potential damage still need to be investigated. It should be noted that the understanding of dynamic behaviour of soils and foundations has lagged behind the study of dynamic behaviour of structures because it was believed that superstructures need to be strengthened more in poor soils than in good soils (Prakash, 1981).

Amongst the geotechnical engineering community, the 1964 earthquakes have been regarded as a milestone of liquefaction study because they led to public recognition of the phenomenon, and of the importance of measures to mitigate the damage caused by earthquakes in general (Ishihara, 1993). The reason is that the phenomenon can be cited symbolically as the first event in the world in which all kinds of modern structures were destroyed due to the liquefaction of soil deposits.

If buildings, dams, bridges, and buried structures are to be constructed in seismic zones containing liquefiable soil, the geotechnical engineer must be aware of the possibility of liquefaction as well as its consequences. As such, the following questions must be satisfied: (1) is the in situ soil susceptible to liquefaction? (2) if the soil is susceptible, will then liquefaction be triggered? and (3) if liquefaction is triggered, will damage occur? The answer to the first question may preclude the other two. If it is negative, then the evaluation of liquefaction hazard may not be necessary. If the answer on the other hand is yes, the following questions must be addressed (Kramer, 1996). The extent of the study of liquefaction potential depends on the value of a project and the level of hazard if the soil liquefies.

If a construction site is found to have a high possibility of liquefaction, mitigation is essential in order to maintain the functions of a structure (PHRI, 1997). Normally, mitigation techniques for soil liquefaction can be classified into two groups: (1) soil improvement, and (2) structural design. The former is intended to prevent the occurrence of liquefaction, whereas the latter aims to minimise the damage to structures if the soil liquefies. Any soil improvement technique that could increase the shear strength and stiffness of soil can be employed. Examples of soil improvement are compaction, pore water pressure dissipation, cementation and solidification, replacement, shear strain restraint and preloading.

An artificial island reclaimed from the open water areas such as oceans, lakes, and harbours is generally constructed by simply dumping the fill materials without any compaction effort. This conventional construction practice results in the island having loose to medium dense sediments. If these loose saturated sediments encounter a strong earthquake, the probability of liquefaction is therefore high. Examples of reclaimed land are waterfront developments, offshore artificial islands, and offshore airport construction (PHRI, 1997).

In recent years, discarded tyres have become an increasing problem around the world because disposing of them in open areas is a danger to the environment. They are vulnerable to fire and subsequently may contaminate ground water. Ground water contaminated by burnt tyres may need hundreds of years to be clean again. As a result, disposing whole used tyres has been prohibited by a new EU Landfill Directive since July 2003 (Khalid and Artamendi, 2004). Thus, making use of them needs to be considered imaginatively and the solution must be sustainable.

Several investigators have studied the shear strength and deformation characteristics of sand mixed with recycled tyre chips. Numerous results indicate that the shear strength of the mixture is increased, depending on tyre chip content as well as the aspect ratios of the tyre chips. Thus, as the shear strength of the mixtures increases, then logically, the cyclic strength may also increase. This implies that it is possible that waste tyres could mitigate the liquefaction susceptibility of land fills.

1.2 Research Objectives

The main objective of this research was to investigate sustainable solutions for landfill materials in seismic zones. It was therefore proposed to investigate the liquefaction potential of recycled waste tyres mixed with liquefiable soil by means of cyclic triaxial tests. Thus soil has been mixed with various sizes of tyre chips and various ratios of sand to rubber in order to determine an optimum mix.

To be able to analyse the liquefaction potential, however, other two parameters were needed, namely small strain shear modulus and damping ratio. The damping ratio can be computed from undrained cyclic triaxial test data. The small strain shear modulus was obtained by measuring the shear wave velocity employing bender elements requiring modification of the cyclic triaxial testing system so that the bender

elements could be housed within a triaxial cell. This allowed the liquefaction strength and the small strain shear modulus to be obtained from the same specimen.

In addition, the undrained shear strength of the mixtures was investigated to provide the stress-strain behaviour as well as the generation of pore water pressure under monotonic loading conditions.

Lastly, the test results obtained from the undrained cyclic triaxial tests and the bender element tests were used to evaluate and compare the liquefaction potential of the mixtures.

1.3 Research Methods

To achieve the aims of the research a sandy soil was obtained that was liquefiable when subjected to simulated earthquake shaking. After that, various sizes of recycled tyre chips were obtained. To minimise the probable boundary problems, the maximum size of tyre chips was limited to 1/10 the diameter of a cylindrical triaxial specimen.

It was recognised that mixing two or more materials having different sizes and specific gravity may cause the segregation. Thus, next task was to trial mixing methods that could cause as little segregation as possible. Both dry deposition and underwater deposition methods were investigated.

A standard triaxial testing system was employed to investigate the undrained shear strength of the mixtures. The liquefaction characteristics were investigated by employing a closed-loop computer-controlled cyclic triaxial testing system. Tests were performed under undrained conditions based on the assumption that the pore water pressure has no time to dissipate during an earthquake because the strong ground motion occurs over a short period. Specimens were subjected to a repeated sinusoidal cyclic deviator stress at a frequency of 0.1Hz until a double amplitude axial strain of 5% was achieved which was defined as liquefaction. The shear wave velocity was measured by means of bender elements. Two bender elements were employed; one attached at a triaxial base and protruded into a specimen about 7mm acted as a transmitter. Meanwhile, the other bender element at the top received the shear waves generated.

Finally an evaluation of liquefaction potential and response of ground containing tyre chip mixtures was accomplished by using an equivalent linear computer analysis called EERA.

CHAPTER 2

LITERATURE REVIEW

2.1 Introduction

Soil liquefaction can be triggered by both static and dynamic loading under undrained conditions. Examples of dynamic loading are earthquakes, blasting, and vibration. Once this has occurred, soil completely loses its shear strength and stiffness, and behaves like a viscous fluid having the unit weight equal to a saturated soil. In such conditions, if superstructures have the unit weight greater than that of the liquefied soil, will sink. On the other hand, underground and buried structures of which the unit weight is smaller will float. The probability of damage is therefore high. The level of hazard, excluding the shaking of structures due to dynamic loading, depends chiefly on degree of soil saturation, drainage conditions, and period of liquefaction.

Since the 1964 earthquake at Niigata and Alaska, civil and geotechnical engineers have paid attention to earthquake-induced liquefaction because even modern structures and bridges were destroyed (Ishihara, 1993). Unfortunately, with current technology and knowledge, engineers and scientists are still unable to accurately predict the occurrence of an earthquake as well as its magnitude.

Structural engineers are able to choose materials and a specific design code for structural design if they know that a structure is to be constructed in seismic zones. In fact, they could design the structure to resist any magnitude of earthquakes, irrespective of types of foundation soil. Geotechnical engineers, on the other hand, cannot choose materials for their design, but have to deal with in situ soils which are deposited naturally. The obvious differences between structural materials (e.g., steel and concrete) and geomaterials are that most soils are not homogenous and contain voids. If it is found that a construction site contains soil that is prone to the liquefaction, then the

countermeasures are essential for maintaining the serviceability of the structure, and, most importantly, for saving human lives.

Even though 1964 is regarded as the beginning of liquefaction study; in fact, it can be traced back to the work by Casagrande (1936, 1940) and Terzaghi and Peck (1948). Since then, liquefaction has been studied extensively (e.g., Seed and Idriss, 1971; Ishihara *et al.*, 1975; Ladd and Chan, 1976; Seed, 1979; Kramer and Seed, 1988; Ishihara, 1993; Vaid and Sivathayalan, 2000; Vaid *et al.*, 2001; Hyde and Higuchi, 2005). Nevertheless, many aspects of liquefied soil are still not well understood because of the complexity of earthquake patterns as well as the behaviour of soil particles during liquefaction.

This chapter reviews the literature related to all aspects of soil liquefaction, undrained behaviour of saturated sand, critical and steady state concepts, assessment of soil liquefaction, mitigation of soil liquefaction, and sand-tyre chip mixtures.

2.2 Liquefaction of Soil

2.2.1 Definitions and Terms

In broader senses, liquefaction is a phenomenon in which soils progressively lose shear strength and stiffness due to earthquakes, vibration, blasting, or rapid loading. It occurs in saturated soils, normally sand, in which the pore space is completely filled with water. During dynamic loading, if drainage is prevented, the pore water pressure builds up gradually, and eventually causes the effective stress of the soil to become zero. The soil then behaves like a fluid, i.e., soil particles float in the pore water. Both undrained monotonic and cyclic loading can trigger the soil to liquefy. However, the earthquake-induced liquefaction is of most interest because it is the most catastrophic to built environments and humans.

It is noteworthy herein to introduce the definition of cyclic loading because it has the most significant influence on soil liquefaction. According to O'Reilly and Brown (1991), the term cyclic loading suggests a system of loading which exhibits a degree of regularity both in its magnitude and in its frequency. Note that the cyclic loading is not only produced by earthquake shaking, it is also encountered in practice, e.g., machine operations and offshore structures.

Terzaghi and Peck (1948) are the researchers who early discussed the liquefaction of soils by using the term spontaneous liquefaction to explain the behaviour. Spontaneous liquefaction occurs when a quicksand suddenly loses shear strength and drainage is prevented. As a consequence, the structure of the sand collapses, associated with an increase of pore water pressure. They explained that the phenomenon transforms the sand into a very concentrated suspension.

Mitchell (1993) stated that saturated sand will liquefy if its void ratio is above the critical state or steady state line, and sheared rapidly. If the water cannot escape from the pores instantaneously, the structure will transform the normal stress to pore water pressure. The loss of the effective stress will then reduce the shear strength of the soil to a very low value, and the soil eventually liquefies.

Soil subjected to stress reversals, e.g., wind, wave, and machine loading, or the transient type of loading imposed by earthquakes, can progressively lose shear strength because the pore water pressure builds up, and this was termed liquefaction by Lee *et al.* (1983). Poulos *et al.* (1985) described the term liquefaction as a phenomenon wherein the shear resistance of a mass of soil decreases when subjected to monotonic, cyclic, or dynamic loading at a constant volume. Youd and Idriss (2001) explained the liquefaction as a phenomenon of seismic generation of large pore water pressure and consequent softening of granular soils. Consequently, the soil is transformed from a solid to liquefied state as a result of increased pore water pressure and reduced effective stress due to earthquakes, vibration, or rapid loading.

The liquefaction of soil by means of cyclic triaxial test in laboratories was described by Ishihara (1993). In cyclic triaxial tests, a sequence of constant amplitude cyclic axial stresses under undrained conditions is applied to saturated sand specimens until they deform to a certain level of peak-to-peak axial strain (or double amplitude). The applied load creates stress conditions on a plane of 45 degree through the specimen similar to those produced on the horizontal plane in the ground during earthquake shaking. During cyclic loading, it is observed that the pore water pressure builds up progressively, and eventually approaches a value equal to the initial confining stresses, thereby producing an axial strain of about 5% in double amplitude. Notice that, such a state has been referred to as initial liquefaction or simply liquefaction.

The liquefaction phenomenon attracts the researchers because its consequences are catastrophic. However, ongoing research around the world being conducted is using different equipment and assumptions. As a result, research papers, technical notes, and theses have been published for decades. Yet, definitions and terms used in these publications are somewhat different despite the fact that they are the same meaning. Therefore, it is vital to clarify herein the important terms related to the liquefaction phenomenon which are to be used and referred to throughout this research.

(a) Static Liquefaction

According to Kramer and Seed (1988), static liquefaction can only occur if the shear stress acting on a soil is increased by a sufficient amount under undrained conditions. If the induced shear stress is greater than the undrained shear strength of the soil, then the soil will liquefy. The magnitude of an increase in shear stress (under undrained conditions) required to initiate the liquefaction has been referred to as the static liquefaction resistance of the soil. The soil, on the other hand, will not liquefy if it is subjected to an increase in shear stress under undrained conditions of magnitude which is less than the static liquefaction resistance.

The conditions in a triaxial test at which $\sigma'_3 = 0$ and $(\sigma_1 - \sigma_3) = 0$, where σ'_3 and $(\sigma_1 - \sigma_3)$ are the effective confining pressure and the principal stress difference, respectively, were also described as static liquefaction by Yamamuro and Lade (1997). They reported that when this had happened large wrinkles in the membranes surrounding the specimens were also observed.

(b) Flow Liquefaction

Flow liquefaction can be triggered by either monotonic or cyclic loading (transient disturbance), but requires a strain softening response in undrained loading. Flow liquefaction will be initiated if the in situ shear stress (gravitational static stress or driving stress) is greater than the undrained residual (or steady state) strength of the soil (Grozic *et al.*, 2000). Note that the steady state strength is the strength a soil has when undergoing a steady state of deformation, i.e., continuous flow under constant shear stress and constant effective confining stress at constant volume and constant velocity (Poulos, 1981).

(c) Cyclic Liquefaction

Cyclic liquefaction, or simply called liquefaction, requires undrained cyclic loading (e.g., earthquakes and vibration) where shear stress develops. If the cyclic loading is sufficient to cause shear stress reversal, and to cause the effective confining stress to essentially reach zero, cyclic liquefaction occurs (Grozic *et al.*, 2000). Note that in cyclic triaxial test the first time when the effective confining pressure σ'_3 reaches zero has been termed initial liquefaction (Seed, 1979). Large deformations of the soil can develop during cyclic liquefaction; however, they normally stabilise when the cyclic loading stops. Figure 2.1(a) illustrates the cyclic liquefaction of soil.

(d) Cyclic Mobility

Cyclic mobility (Figure 2.1(b)) occurs in a soil that first softens under cyclic loading, but then stiffens when monotonically loaded without drainage as the tendency to dilate reduces the pore water pressure (Rauch, 1997). As a result, the effective stress will not really reach zero and the deformation during cyclic mobility will also stabilise when the loading ceases. It can occur even when the static shear stress is lower than the steady state shear strength of the soil. During cyclic mobility, the residual shear strength of the soil remains greater than the static shear stress and the deformation accumulates only during cyclic loading. For conventional usage, it is sometimes referred to as liquefaction.

(e) Cyclic Strength

In engineering practice which deals with the property of materials, a numerical value is always allocated for a particular behaviour of the material in order to facilitate the design and construction. This is also true for liquefaction. In general, the cyclic strength, also called liquefaction strength, of a soil in cyclic loading tests is the relationship between the magnitude of applied cyclic deviator stress or shear stress and the number of load cycles required to initiate the liquefaction. Liquefaction of the soil in laboratories, e.g., cyclic triaxial tests, cyclic simple shear tests, and cyclic torsional tests occurs in three ways: (1) the induced pore water pressure is approximately equal to the initial effective confining stress, (2) the amplitude of cyclic strain exceeds a certain limit, and (3) the residual strain (steady state strain) exceeds a certain limit (JGS, 1998).

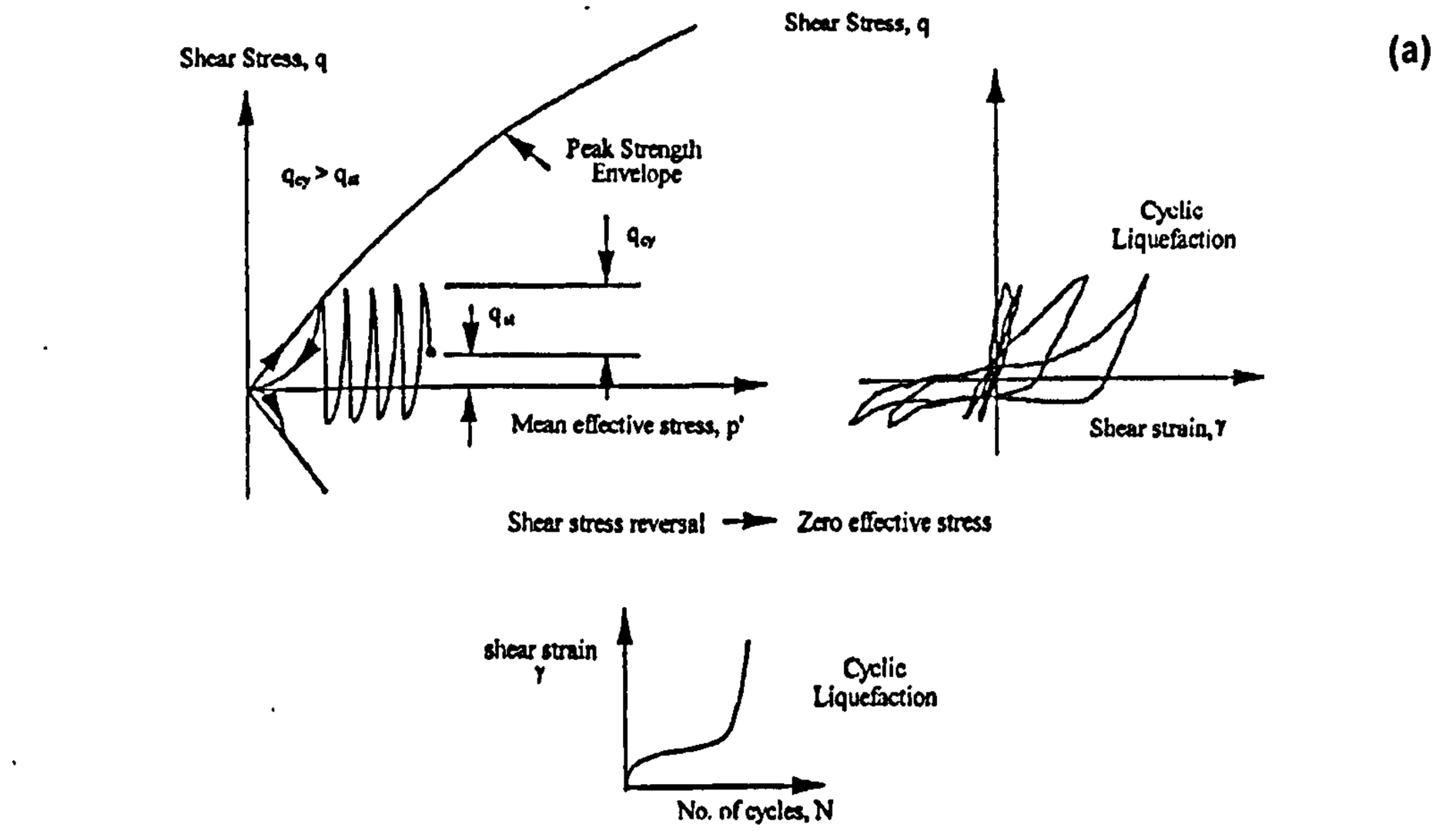

Figure 2. 1 Schematic illustrations of cyclic liquefaction (a) and cyclic mobility (b) (after Grozic *et al.*, 2000)

Ishihara (1993) described the cyclic strength of a soil as the stress level required to cause a specified level of strain after a specific number of load cycles. More precisely, the cyclic strength is the magnitude of cyclic stress ratio required to produce 5% of either double amplitude axial strain $\varepsilon_{a,DA}$ or axial plastic strain $\varepsilon_{a,P}$ in 20 cycles of uniform load application. The particular number of 20 is used because it is similar to

actual time histories of accelerations recorded during past earthquakes. It should be noted that the cyclic stress ratio has been defined as $q_{cyc}/2\sigma'_{3c}$ for the cyclic triaxial loading condition by which q_{cyc} denotes the single amplitude of cyclic axial stress and σ'_{3c} is the initial effective confining stress (Ishihara 1993; Hyodo *et al.*, 1998). In cyclic simple shear tests, however, the cyclic stress ratio is defined as τ_{cyc}/σ'_v, where τ_{cyc} and σ'_v denote the cyclic shear stress and vertical effective stress, respectively.

For cyclic triaxial tests, the criterion number (2), the amplitude of cyclic strain exceeds a certain limit, is always used to determine the cyclic strength by plotting a number of load cycles N required to cause double amplitude axial strain $\varepsilon_{a,DA}$ or axial plastic strain $\varepsilon_{a,P}$ of 5% (Hyodo *et al.*, 1996; Higuchi, 2001; Amini and Chakravrty, 2004; Hyde and Higuchi, 2005). The curve is called a liquefaction strength curve. The typical liquefaction strength curve obtained from cyclic triaxial tests is illustrated by Figure 2.2. It can be concluded that the cyclic strength, liquefaction strength, and cyclic stress ratio required to cause 5% double amplitude axial strain or axial plastic strain in 20 cycles are in fact the same.

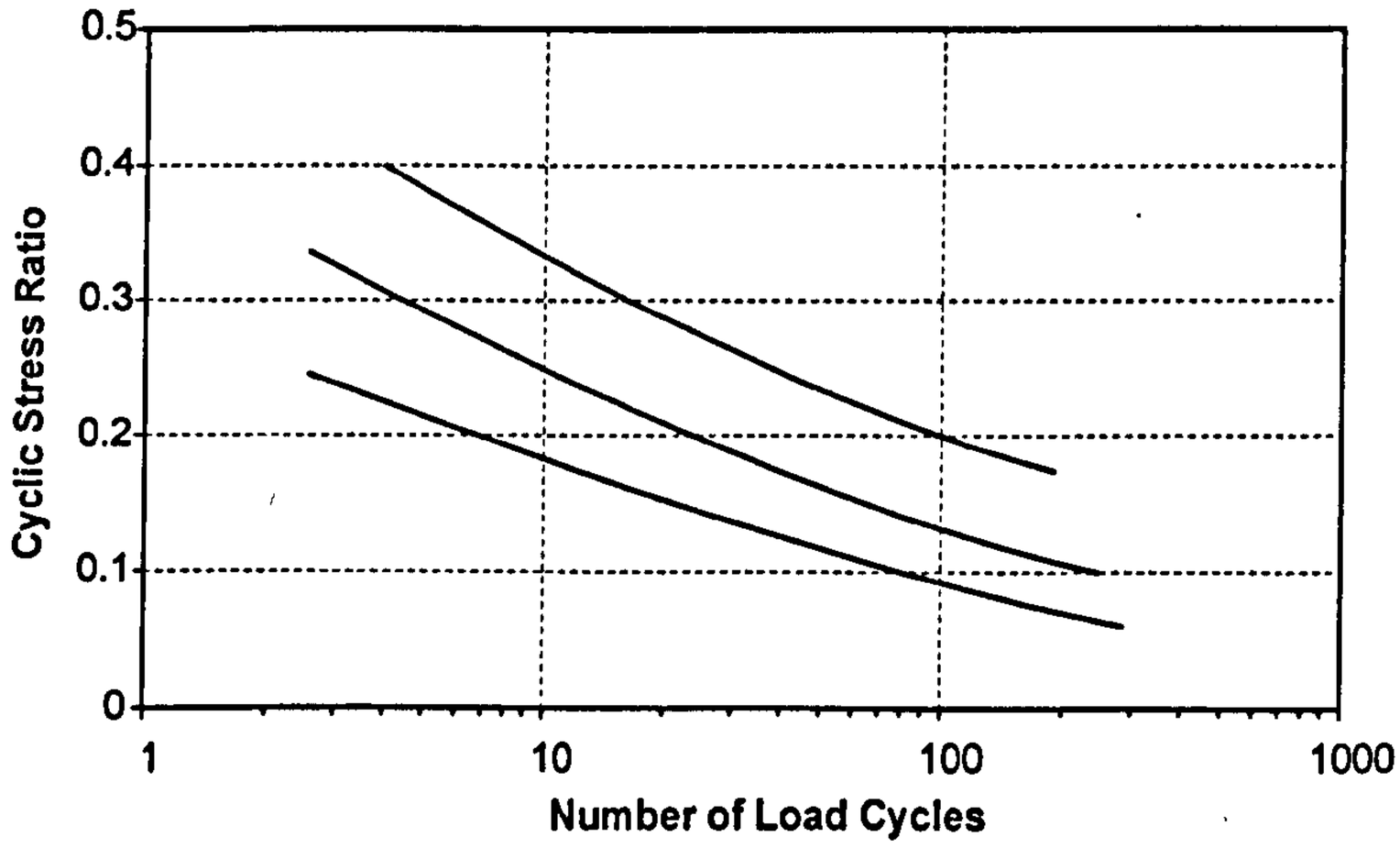

Figure 2. 2 Typical cyclic strength curves

2.2.2 Damage from Soil Liquefaction

When considering ground problems caused by soil liquefaction, they can be classified into two groups: (1) level ground, and (2) sloping ground (Wiegel, 1970). The level ground refers to ground which lies horizontally or slopes gently. The sloping ground includes levees and embankments. The problems encountered in level ground, besides

loss of shear strength and stiffness, are always settlements after the dissipation of pore water pressure.

For sloping ground, there are more problems to concern. If liquefaction is likely to occur in such ground, an analysis of stability, flow deformation, and settlement must be included. Flow slides of clay soil in the sloping ground may occur during ground shaking if an underlying layer is liquefiable soil and the static shear stress induced is greater than the residual stress of the underlying soil.

When soil is liquefied, the shear strength decreases because of the generated pore water pressure resulting in a decrease in effective shear strength; additionally, uplift forces can arise, and buried structures float if their unit weight is less than that of the liquefied soil. In the case of spread foundations, settlement, tilting, or overturning may occur after the liquefaction. Of most concern in geotechnical designs is the settlement and deformation of foundation soils. After the liquefaction, the generated excess pore water pressure will eventually dissipate to equalise the ground water table. As a result, soil particles are rearranged and repacked because of the decreased soil volume. Subsequently, if the settlement exceeds the design value, structures may undergo either structural or functional damage. The structural damage can be simply visualised; on the other hand, the functional damage needs to be investigated and tested.

Large permanent deformations of embankments and earth structures are an example of the functional damage. Although they do not collapse; but, they are not functional any more. Port and harbour structures and retaining walls may be severely damaged because of additional horizontal earth pressure due to liquefied soil (PHRI, 1997). Even though a retaining wall may not be damaged from the additional pressure from back fills, it may no longer be serviceable because of the dislocation due to lateral soil movement. In the case of water pipes even if they do not break, if their elevation has been changed, water may not flow as designed. Other examples of disturbing the function are subsidence and tilting of buildings, lateral movement of bridge abutments and piers, floating of sewage treatment tanks, instability of earth-fill dams causing overflow of its reservoir water, and excessive distortion of harbour revetments (JGS, 1998).

2.2.3 Soils Susceptible to Liquefaction

At the beginning, it was believed that soils most susceptible to liquefaction are loose saturated sand deposits. Figure 2.3 presents the gradations of soil particles that have a possibility to liquefy when encountering dynamic loading. One can use this diagram for the preliminary assessment of liquefaction potential. Soils at which the gradation falls in zones other than the possible ranges shown are considered non-liquefiable. Figure 2.3 has been employed to determine the liquefaction potential of sands with high coefficient uniformity as well as low coefficient of uniformity. These criteria have been confirmed by many researchers. For example, Sitharam *et al.*, (2004) concluded that soil type most susceptible to liquefaction for a given site condition is sand which has uniform gradation and rounded particles, and must be in a very loose state. The other conditions are that it has recently been deposited with no cementation between soil grains, and there is no either prior preloading or seismic shaking.

Subsequently, it was found that sands with some low plasticity silts were also liquefiable. It was also believed that sand containing silt exhibits a greater resistance to liquefaction. However, if the fines comprise minerals with a dry surface texture which is free from adhesion, the particles will separate. As a result, the sand containing such fines will have as great a potential to liquefy as clean sand has (Ishihara, 1993).

Erten and Maher (1995) investigated the effect of fine contents on the pore water pressure generation in sand by performing automated cyclic triaxial tests on pure sand specimens, silt specimens, and sand mixed with silt specimens. Two types of silts were used: a non-plastic silt and a low plasticity silt with the plasticity index of about 10. For sand mixed with both two silts, they found that there is a significant increase in the generated pore water pressure at strain levels of 0.01% and higher. However, for non-plastic silt, addition of silt while maintaining the same void ratio results in an increasing pore water pressure up to a limiting value which corresponds to 30% silt content.

Higuchi (2001) studied the liquefaction and cyclic failure of low plasticity silts using undrained cyclic loading tests on samples reconstituted from slurry. The reconstituted sample was consolidated both isotropically and anisotropically, and then was sheared cyclically and monotonically. The study showed that silt is also liquefiable.

A study by Song *et al.*, (2004) also suggested that silt is susceptible to liquefaction in the same way as clean sand.

The Chi Chi earthquake on 21 September 1999 in Central Western Taiwan triggered extensive soil liquefaction. The majority of sand deposits in the liquefied area had significant amounts of low to medium plastic fines (Huang *et al.*, 2004). In addition, Yamamuro and Lade (1997, 1998) pointed out that at very low pressures, complete static liquefaction in laboratory testing is easily achieved in silty sands.

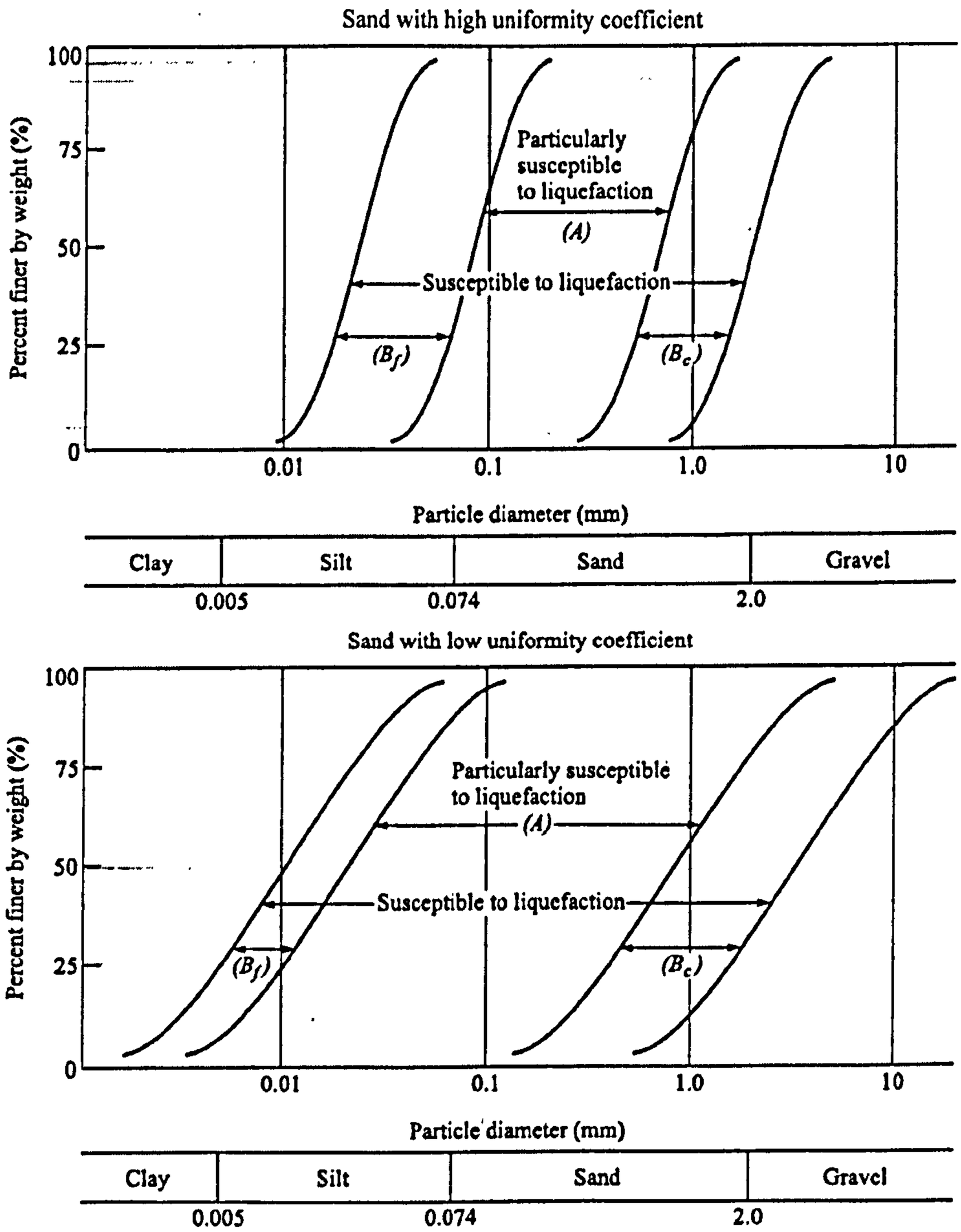

Figure 2. 3 Grain size distribution of soils which are susceptible to liquefaction (after JGS, 1998)

Due to high hydraulic conductivity, gravels and gravelly soils were once thought to be non-liquefiable. As a result, gravels and gravel drains have frequently been used as a remedial measure to improve the liquefaction resistance by means of rapidly dissipating pore water pressure generated during ground shaking.

However, a study by Evans and Zhou (1995) showed that a composite of sand and gravel is also liquefiable depending on the gravel content. They performed undrained cyclic triaxial tests using sand samples mixed with varying gravel contents of 0, 20, 40, 60, and 100%. The results showed that the specimens with an addition of 0% and 20% gravel contents have similar pore water pressure and axial strain responses; and, exhibit the cyclic liquefaction behaviour similar to loose sand. When the mixtures contained gravel of 40% and 60%, on the other hand, the specimens exhibit cyclic mobility behaviour similar to dense sand. From the results, it can be concluded that the higher gravel content in sand-gravel mixtures results in a greater value of resistance to liquefaction. The behaviour of gravelly soils was also studied by Evans (1992) and Evans *et al.*, (1992).

The liquefaction characteristics of uniform and layered sand-gravel composites were studied by Amini and Chakravrty (2004). They found that as the confining pressure increases, the liquefaction strength of the composites decreases. Moreover, they concluded that the ranges of confining pressure of 50 to 250kPa do not significantly influence the liquefaction strength of the composites.

Seabed soils may contain large amounts of gas dissolved in the pore fluid. Gasses found in seabed sand normally comprise carbon dioxide, hydrogen sulphide, ethane and methane. However, only methane is found in considerable quantities (Grozic *et al.*, 2000). Normally, soils containing large quantities of gas are called gassy soils. When these submarine sediments encounter low-tide conditions, with a combination of the presence of gases and sufficiently low density, flow liquefaction may be triggered (Chillarige *et al.*, 1997); and, subsequently, flow slides occur. However, increasing amounts of gas in the specimen will reduce the cyclic liquefaction potential of the soil.

Grozic *et al.*, (2000) studied the behaviour of gassy sand using undrained cyclic loading in the laboratory. They measured gas content in the specimen before and after each test using time domain reflectometry. The results showed that the gassy sand

exhibits little pore-pressure generation before failure. For example, if the loading initiates the specimen to collapse, then the pore water pressure increases noticeably; subsequently, the failure occurs. On the other hand, if the collapse is not triggered within four cycles of loading, then failure does not occur and pore water pressure does not build up. They suggested that the applied cyclic load must be very close to the load required for monotonic failure. They also concluded that gassy sands exhibit a monotonic type failure under high cyclic loads.

Recently, there has been increasing interest in whether or not finer soils, especially silts and silty clays are liquefiable. Wang (1979) and Seed and Idriss (1982) proposed the Modified Chinese Criteria (Figure 2.4) and pointed out that fine soils are considered to be of potentially liquefiable type if: (1) there is less than 15% of clay fines (< 0.005mm, based on the Chinese definition), (2) there is a liquid limit of ≤ 35%, and (3) there is an in situ water content ≥ 90% of the liquid limit (Seed *et al.*, 2003).

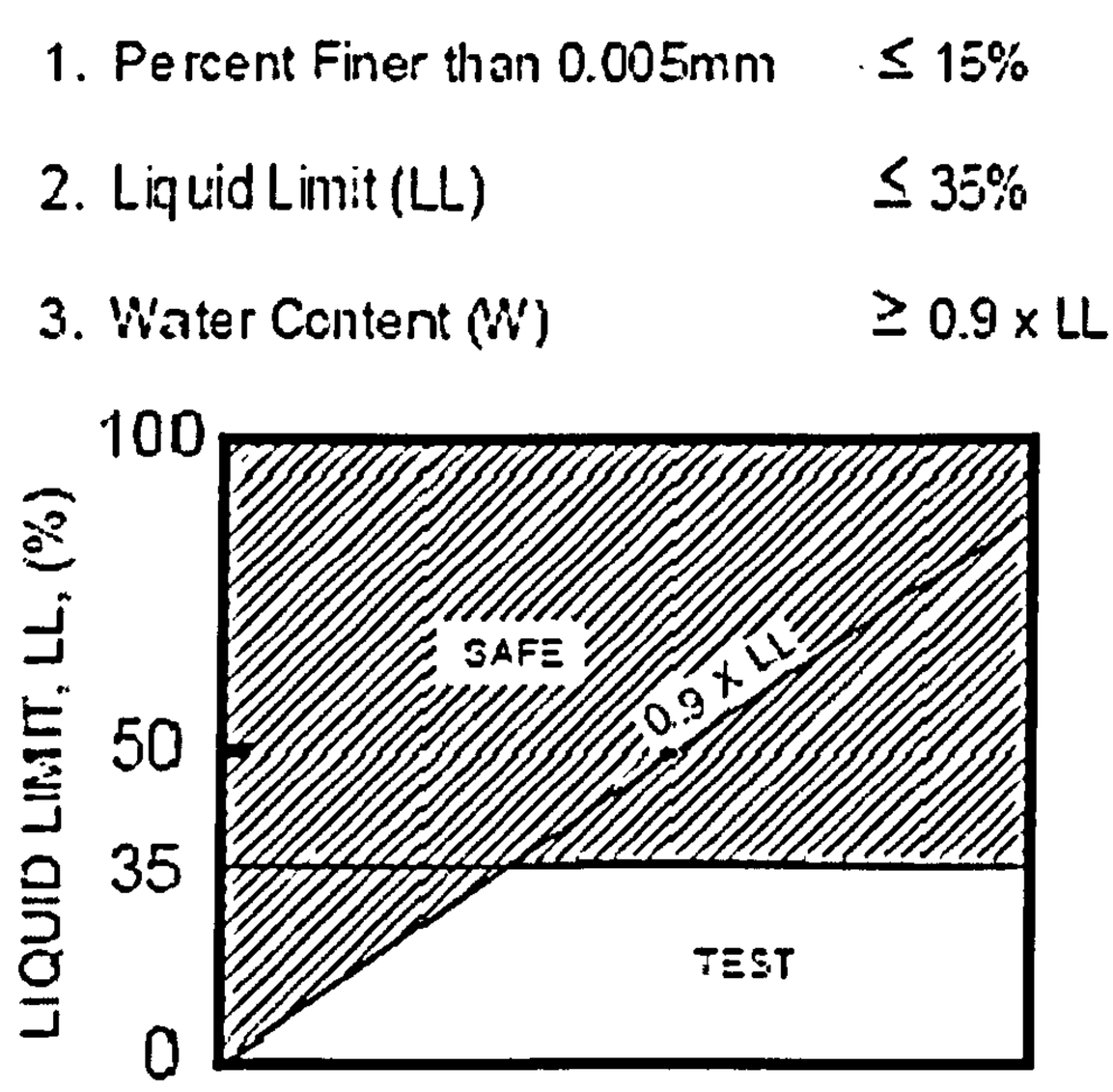

Figure 2. 4 Modified Chinese criteria (after Wang, 1979; Seed and Idriss, 1982)

Andrews and Martin (2000) re-evaluated the Modified Chinese Criteria and proposed that: (1) soils with less than about 10% clay fines, and a Liquid Limit in the minus 40 sieve fraction < 32%, are considered potentially liquefiable, (2) soils with more than about 10% clay fines and liquid limit ≥ 32% are unlikely to liquefy, and (3)

soils intermediate between these criteria should be sampled and tested to assess the liquefaction potential. These criteria are summarised in Table 2.1.

Table 2. 1 Liquefaction susceptibility of silty and clayey sands (after Andrews and Martin, 2000)

	Liquid Limit[1] < 32	Liquid Limit[1] ≥ 32
Clay Content[2] < 10%	Susceptible	Further Studies Required (Considering plastic non-clay sized grains – such as Mica)
Clay Content[2] ≥ 10%	Further Studies Required (Considering non-plastic clay sized grains – such as mine and quarry tailings)	Not Susceptible

Notes:

[1] Liquid Limit determined by Casagrande-type percussion apparatus.
[2] Clay defined as grains finer than 0.002 mm.

2.2.4 Factors Affecting Liquefaction

Even though the liquefaction characteristics of soil have been studied for many years since the 1964 Niigata earthquake; its behaviour is still not clearly understood because there are so many factors that affect liquefaction. Moreover, up to the present, no apparatuses can at once simulate all factors to study the behaviour of liquefied soil because of the complexity of earthquake loading patterns and the controlling of stress and strain levels throughout the test. Therefore, geotechnical engineers must be aware of the limitations and applications of an apparatus employed for evaluating the liquefaction potential of a soil.

Laboratory studies have identified numerous factors influencing the liquefaction strength of a soil, e.g., relative density (or void ratio), effective confining stress, and level of static shear stress. It has also been recognised that sample preparation techniques are an important factor affecting the results from laboratory testing. It is

therefore necessary to study all sample preparation methods and compare the results obtained because the aim of the laboratory testing of soils is to simulate the state of soil specimens as close to the in situ condition as possible. As an example, samples prepared by water sedimentation are suitable for reclaimed lands in which they are constructed by filling materials in open water areas.

Yamamuro and Wood (2003) studied the undrained behaviour of sand containing some non-plastic silt by performing undrained triaxial tests using a variety of depositional methods. They included slurry deposition, water sedimentation, air pluviation, mixed dry deposition and dry funnel deposition. The results showed that dry methods exhibit a more contractile behaviour than wet methods; on the other hand, wet deposition methods exhibit a more dilatant response.

Vaid *et al.*, (2001) investigated the liquefaction strength of sand obtained from Fraser River, Canada, under monotonic and cyclic loading by considering the effect of levels of confining stress and static shear stress. The samples were reconstituted by water pluviation because the technique provides uniform repeatable specimens. The undrained monotonic loading results showed that increasing the static shear stress at constant confining stress increases the level of contractiveness, as does increasing the confining stress at a constant level of static shear stress. Under cyclic loading, they concluded that the resistance to liquefaction decreases when the confining stress increases. However, they suggested that the increase in confining stress has little effect at the loosest state.

The studies by Vaid and Sivathayalan (2000) indicated that the susceptibility to liquefaction of soil under both monotonic and cyclic loading, besides the initial state, is also affected by the effective stress path during undrained shear. They summarised factors affecting the liquefaction into four groups: (1) the capability of the testing apparatus, (2) the effect of initial state variables, (3) the influence of the effective stress path during loading, and (4) the effect of any departure from the undrained deformation assumption. They found that for the capability of the testing device, especially the loading system, the cyclic shear stresses from stress controlled and strain controlled systems yield a different stress-strain response. The study also showed that the stress controlled loading system may modify the true strain-softening of the sand, depending

on the specimen-device interaction and the frequency response of the data acquisition system; while the strain controlled loading system does not alter the response.

Factors such as strain rate, particle shape, compressibility, sample preparation technique, and stress history were studied by Hird and Hassona (1990) to investigate the liquefaction and flow of saturated sands by using load-controlled undrained triaxial tests. They concluded that, at a given effective confining pressure and void ratio, rounded sands are somewhat more susceptible to liquefaction than angular ones of similar grading. The results showed that the sand has less possibility of liquefaction if the compressibility increases. They also suggested that the stress-strain responses from strain- and stress- controlled tests do not coincide. In addition, under monotonic loading, the specimen preparation technique and stress history had a small effect on the liquefaction.

Xenaki and Athanasopoulos (2003) studied the liquefaction resistance of medium sand mixed with non-plastic silt by varying silt contents from 0, 10, 30, 42, 55, and 100% using stress controlled undrained cyclic triaxial tests. They concluded that the mixtures containing fines from 0 to 44% result in an increase of the resistance to liquefaction. On the contrary, if fine contents are greater than 44%, the resistance to liquefaction decreases. It was therefore concluded that the liquefaction characteristic of the mixtures depends on whether the value of fines content is lower or higher than the threshold value which is 44%.

Ishihara *et al.*, (1978) performed two series of undrained cyclic triaxial tests on soils containing fines from 0 to 100%, by weight, to investigate the cyclic strength. The first series was performed on reconstituted samples in the laboratory having overconsolidation ratios ranging from 1.0 to 2.0. The results showed that the higher the overconsolidation ratio of the specimen, the greater the cyclic strength of the soil. Moreover, the cyclic strength at an overconsolidation ratio of 2.0 increases up to 70% compared with normally consolidated specimens. For the second series, it was obvious that the undisturbed samples produce up to 15% more cyclic strength than the reconstituted samples.

Mulilis *et al.*, (1978) investigated the effects of specimen preparation methods as well as testing techniques on sand liquefaction using remoulded specimens of Monterey

No. 0 sand under undrained cyclic triaxial testing. Three specimen preparation methods were studied: dry rodding, moist rodding, and moist tamping. The other effects studied were loading wave form, degree of saturation, and density variations. It was clearly seen that the cyclic strength of the specimens prepared by moist rodding is approximately 38 to 58% higher than those of the specimens prepared by dry rodding. For moist tamping method, at high stress ratios, the tamping foot size had no effects on the strength of the soil. Employing the variable compaction procedure (Silver *et al.*, 1976) and lower *B* values of only 0.91, 0.92, and 0.93 (Skempton, 1954) resulted in somewhat higher strength. The highest cyclic strength was obtained from a sinusoidal wave form; on the other hand, the lowest strength was obtained from a square wave form. An increase of specimen density of 12% resulted in a 22 to 30% increase in the cyclic strength.

The effects of loading frequency on the liquefaction strength have been studied by several researchers. As an example, Tatsuoka *et al.*, (1986) studied the effect of loading frequency on the liquefaction of Toyoura sand and found that a frequency varying between 0.05 and 1.0Hz yields a minimal difference in liquefaction strength (Grozic *et al.*, 2000). Hyodo *et al.* (1998) suggested that the liquefaction does not depend on the frequency of cyclic loading, but depends rather on a number of cycles of loading. Note that ASTM (1996b) recommends a loading frequency range of 0.1 to 2.0Hz; however, the frequency of 1.0Hz is preferred.

According to PHRI (1997), the factors affecting the liquefaction strength of a specimen can be classified into four groups, which are shown in Table 2.2.

Table 2. 2 Factors affecting the occurrence of liquefaction (after PIIRI, 1997)

1. Load conditions	Cyclic shear stress amplitude Waveform Vibrational frequency Irregularity in the waveform Multidirectional shear Reversal of shear stress
2. Soil conditions	Density (relative density) Grain size distribution Degree of saturation Structure of soil skeleton Cyclic shear history Cementation effect
3. Stress conditions	Average effective principal stress Overconsolidation ratio Initial shear stress
4. Test conditions	Specimen dimension Specimen preparation method Consolidation time Membrane penetration *B*-value Type/structure of test equipment

2.2.5 Failure Criteria

In theory, a saturated soil specimen is considered to have liquefied when the pore water pressure generated by cyclic loading is approximately equal to the initial effective stress (Seed *et al*, 2003). During the liquefaction, the soil has almost zero shear strength, and behaves like a viscous fluid having the unit weight equal to a saturated soil. In the case of reconstituted loose to medium dense sands, these conditions can easily be reproduced by any cyclic loading test. For soils deposited naturally, however, it is rare to find only one soil type. In the case of artificial fills, the type of soil to be used also depends mainly on the availability of resources nearby. In addition, the ground is not normally fully saturated all the time. Thus, the criteria for soil liquefaction failure should be able to cover all soil types.

For soils that consist of clay or medium- to high-plasticity silt, the pore water pressure generated by cyclic loading may never reach the initial effective stresses and the classical liquefaction conditions are therefore not met. However, in geotechnical design not only is the shear strength considered, but also the settlement and deformation must be included. Thus, even if the pore water pressure is still below the initial effective

stress, the deformation due to softened soil may be sufficient to cause damage (Promputthangkoon and Hyde, 2008a). As a result, it is customary to deploy a limiting strain in the liquefaction analysis.

For ground that is approximately horizontal in which there is no static shear stress, the generated shear stress will reverse many times during ground shaking. This is known as stress reversal. In this case, the soil is considered to have liquefied when the accumulation of axial strain from both compression and extension - double amplitude axial strain $\varepsilon_{a,DA}$ - reaches 5% (Ishihara, 1993; Hyodo *et al.*, 1996, 1998). The failure criterion for level ground conditions is depicted by Figure 2.5. At low to moderate cyclic stress levels, initially the excess pore water pressure is small resulting in a small strain. This implies that at this stage the soil particles still do not lose contact. However, because it is an undrained test; the excess pore water pressure will gradually build up, causing the soil particles lose contact to each other resulting in a larger strain. Liquefaction is assumed to have occurred when the double amplitude axial strain reaches 5% level.

In the case of sloping ground, there will be a static shear stress in the soil mass due to gravitational force. If the static shear stress is greater than the cyclic shear stress generated by seismic loading, there will no be stress reversal; thus, the strain will be accumulated in compression only. The strain in this case is called plastic axial strain $\varepsilon_{a,P}$, and the soil is considered to reach failure when it also reaches 5% (Higuchi, 2001). Note that in this research only isotropically consolidated specimens representing level ground conditions were tested. The failure conditions for sloping ground are depicted by Figure 2.6. Also note that if the static shear stress is lower than the generated cyclic shear stress, there will also be the stress reversal. As a result, the failure criterion illustrated by Figure 2.5 is employed.

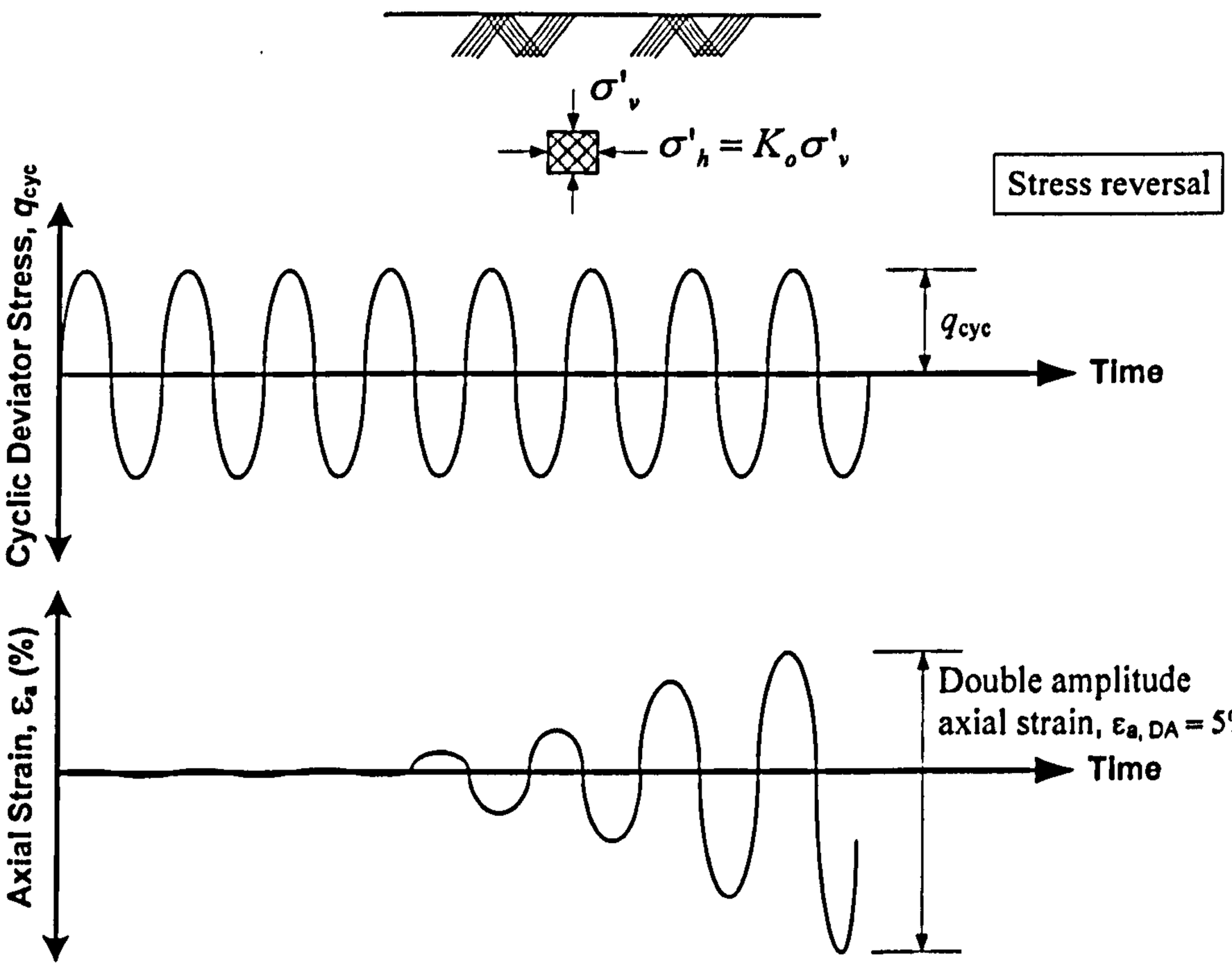

Figure 2. 5 Liquefaction failure conditions for isotropically consolidated samples

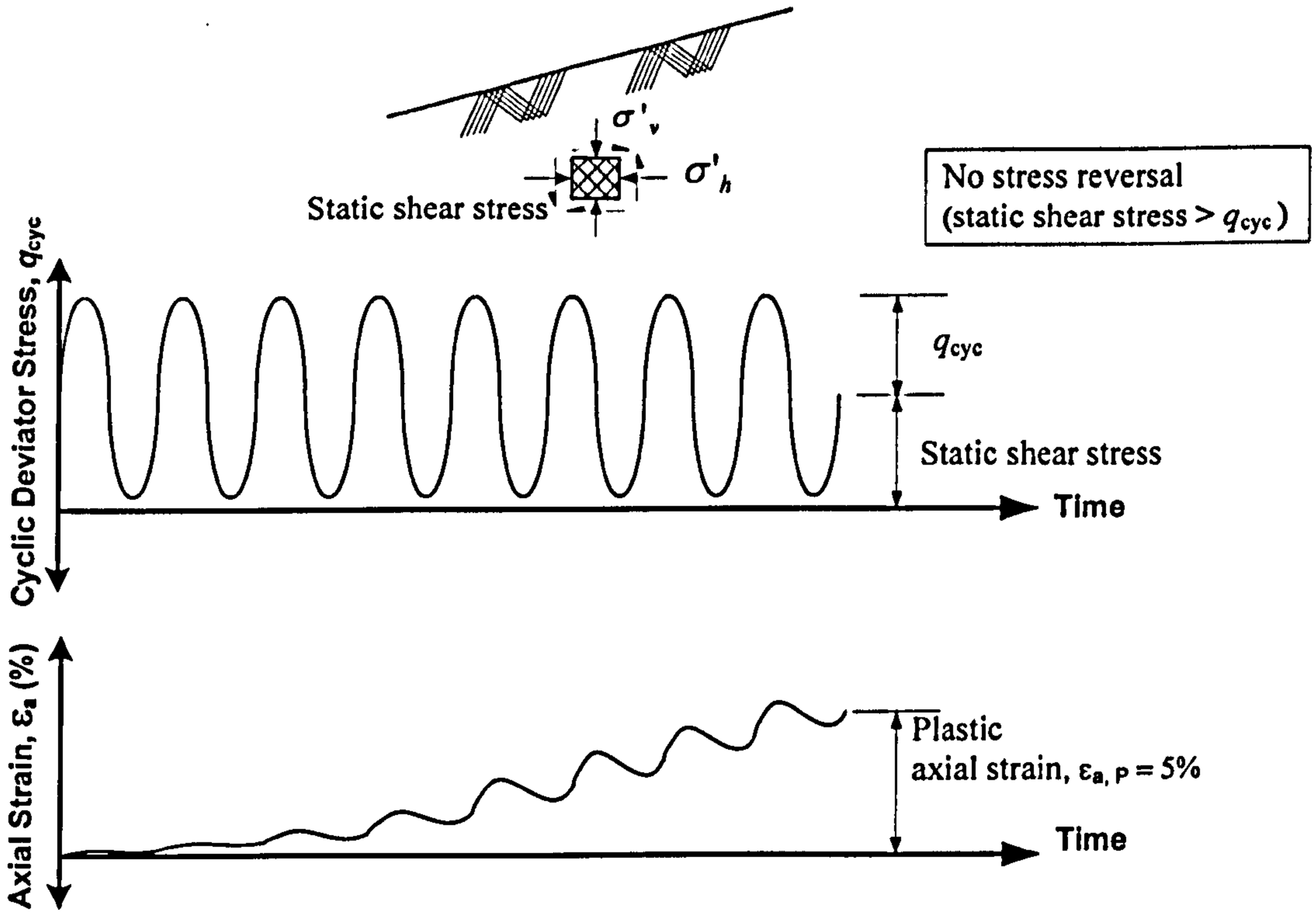

Figure 2. 6 Liquefaction failure conditions for anisotropically consolidated samples

2.3 Undrained Behaviour of Saturated Sand

2.3.1 Monotonic Loading

The undrained shear strength of a sand specimen is normally determined in laboratories using a standard triaxial compression test under monotonic loading conditions. In liquefaction potential determination, the method is also very useful for evaluating the flow deformation of sandy soil. It should be noted that the undrained shear strength of the soil can also be obtained by other methods such as the standard penetration test and the cone penetration test.

Castro (1969) reported that when loose sands are sheared under undrained conditions in triaxial compression, a unique stress condition is achieved at large deformations, irrespective of the initial conditions, but dependent on the density of the sand. A similar concept was also reported by Poulos (1981) and Poorooshasb (1989), but Poulos (1981) called the final condition a steady state whereas Poorooshasb (1989) called an ultimate steady state. It should be noted that the steady state may also occur in drained tests if the strains are large enough (Poulos, 1981).

The shear strength of the sand at the steady state has been considered as the undrained shear strength for a flow failure analysis. The reason is that once the undrained shear deformation is initiated and the static driving force is greater than the undrained shear strength at the steady state; then, the deformation of the sand may continue indefinitely (Yoshimine *et al.*, 1999). As a result, flow failure occurs.

The state at which soils deform continuously without any increment of stress components has simply been called a steady state. The steady state of the sand under undrained monotonic loading conditions is illustrated by Figure 2.7. When loose sand is sheared undrained monotonically under relatively low effective confining stresses, the steady state may occur at two states: (1) the quasi steady state, and (2) the ultimate steady state. The quasi steady state (Zhang and Garga, 1997) appears at the state of phase transformation (the state at which the pore water pressure begins to decrease (Ishihara *et al.*, 1975; Hyodo *et al.*, 1998)), which is the state of minimum effective stress during undrained shear. It should be noted that at the quasi steady state the shear stress components are at a minimum. If initial effective confining stresses are large enough, strain hardening will not occur, and the minimum stress state becomes ultimate

steady state (also called critical steady state (Yoshimine and Ishihara, 1998; Yoshimine *et al.*, 1999)).

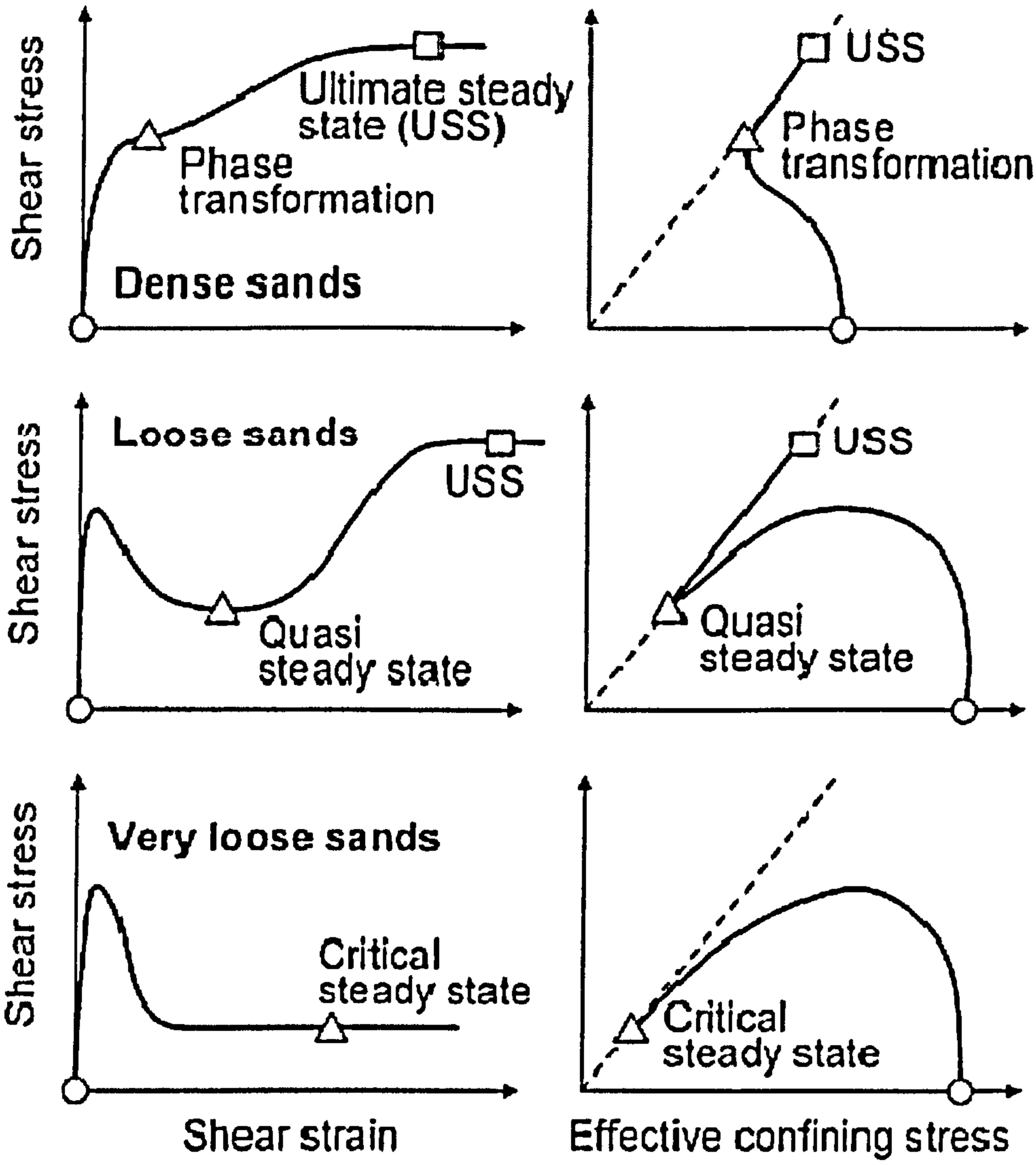

Figure 2. 7 Definitions of ultimate steady state, quasi steady state, and critical steady state (after Yoshimine *et al.*, 1999)

2.3.2 Cyclic Loading

The behaviour of saturated sand subjected to cyclic loading is illustrated by Figure 2.8 and Figure 2.9. In a cyclic triaxial test the stress condition can be divided into two types: (1) stress reversal, where the cyclic deviator stress changes from compression to extension during each cycle; and (2) stress non-reversal, where the cyclic deviator stress remains in one direction, usually in compression (Higuchi, 2001). As a result, the failure of the sand under cyclic loading conditions should also be described separately. In the

case of stress reversal, significant plastic strain does not accumulate and failure occurs rapidly with little resistance to the deformation. If the sand is sheared under non-reversal conditions, the failure will occur when irrecoverable strain is developed in compression (Selig and Chang, 1981).

If the sand specimen is subjected to a cyclic shear stress amplitude smaller than the undrained steady state strength (Figure 2.8), the stress path eventually passes from contractive to dilative as a result of pore water pressure built up, but it cannot reach the critical stress ratio *CSR* line (the locus of points at which strain softening is initiated (Vaid and Chern, 1985)) for that particular void ratio. Thus, the effective stress path traverses below the point corresponding to the steady state strength (point S) and then approaches the failure envelope. When the effective stress path reaches a critical value, dilation will prevail. As a result, it will turn around and move back along the failure line (Alarcon-Guzman *et al.*, 1988).

If cyclic shear stress amplitudes are greater than the steady state strength at the corresponding consolidation void ratio, it may exhibit either complete or limited flow deformation behaviour. In the first case (Figure 2.9(a)), unlimited shear strains will develop. In the second case (Figure 2.9(b)), the effective stress path may cross the phase transformation line after the limited steady state condition is reached (point S′). Subsequently, the soil structure collapses, and results in the occurrence of initial liquefaction. Then, the effective stress path may continue with alternating cycles of zero effective stress state and associated large deformations. It is then followed by hardening with shearing in the opposite direction (Alarcon-Guzman *et al.*, 1988).

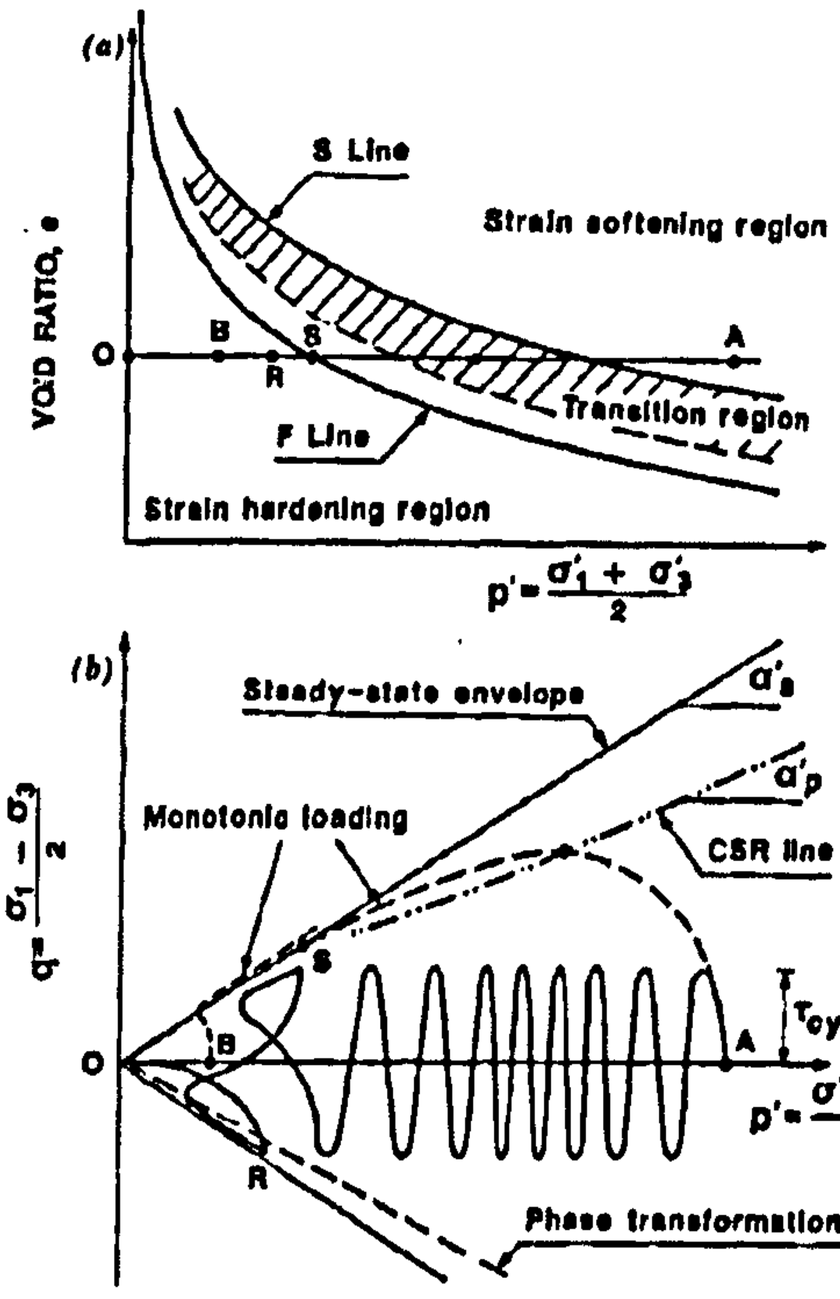

Figure 2. 8 Undrained behaviour under cyclic shear stresses smaller than steady state strength (schematic): (a) state diagram; (b) stress path plot (after Alarcon-Guzman *et al.*, 1988)

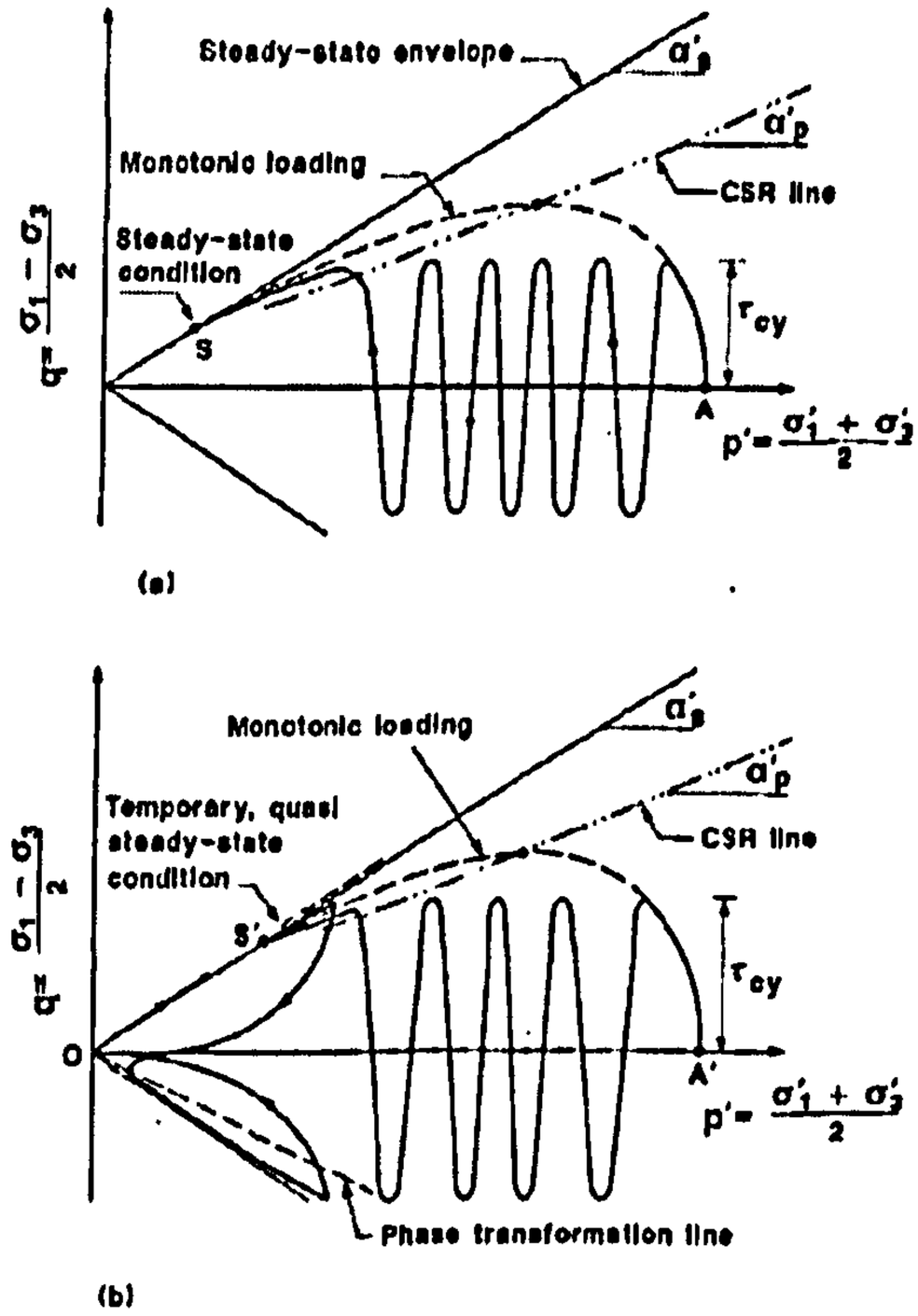

Figure 2. 9 Undrained behaviour under cyclic shear stresses larger than steady state strength (schematic): (a) flow deformation (b) limited flow deformation (after Alarcon-Guzman *et al.*, 1988)

2.4 Critical State and Steady State Concepts

The critical void ratio (Casagrande, 1936) is the state at which soil can undergo any amount of deformation without volume change under drained conditions (Zhang and Garga, 1997). The concept has been regarded as the basis of the steady state of deformation. Later on, it was extended by Roscoe *et al.*, (1958) at Cambridge University; and became the critical state concept of soil and other granular materials. After that, the steady state of deformation for any mass of particles was proposed by Poulos (1981). He stated that it is the state in which the mass is continuously deforming at constant volume, constant normal effective stress, constant shear stress, and constant rate of shear strain. It should be noted that the concept of critical void ratio is not a unique property of a soil, but depends upon the confining stress (Prakash, 1981).

Critical state soil mechanics (Roscoe *et al.*, 1958; Schofield and Wroth, 1968) is a framework used to describe the behaviour of soil and granular materials. The core of the concept is that if the soil is continuously distorted until it flows like a frictional fluid, the critical state will be achieved, and can be determined by the following equations:

$$q = Mp' \qquad \textbf{(Eq. 2. 1)}$$

$$\Gamma = \nu + \lambda \ln p' \qquad \textbf{(Eq. 2. 2)}$$

$$M = \frac{6\sin \emptyset'}{3-\sin \emptyset'} \qquad \textbf{(Eq. 2. 3)}$$

where,

q	=	deviator stress,
M	=	slope of critical state line,
p'	=	mean normal effective stress,
Γ	=	specific volume of soil at critical state with $p' = 1.0$ kPa,
ν	=	specific volume,
λ	=	slope of normal consolidation line, and
ϕ'	=	angle of friction in terms of effective stress.

The position of critical states from Eq. 2.1 and Eq. 2.2 can be represented by Figure 2.10 and Figure 2.11. These equations represent the position of the critical state of a soil sample in q, p', and ν space; therefore, it is very helpful to think of the critical

state in a three-dimensional $q : p' : \nu$ space, as shown in Figure 2.12. Eq. 2.1 determines the magnitude of deviator stress q required to keep the soil flowing continuously as the product of a constant M with the mean normal effective stress ($p' = (\sigma'_1+\sigma'_2+\sigma'_3) / 3$) (Figure 2.10(a)). In Eq. 2.2, the specific volume ν occupied by unit volume of flowing particles will decrease as the mean normal effective stress increases (Figure 2.10(b)). If the soil is looser than the critical state (Figure 2.10(b)), the term *wet* is used to describe such a state. This is because if the wet soil deforms by applied loads, it will transfer some pressure into the pore water causing water to bleed out of the soil. On the other hand, the term *dry* is used if the soil is denser than the critical states. In this state, during deformation the soil structure will expand and tend to suck up water into itself.

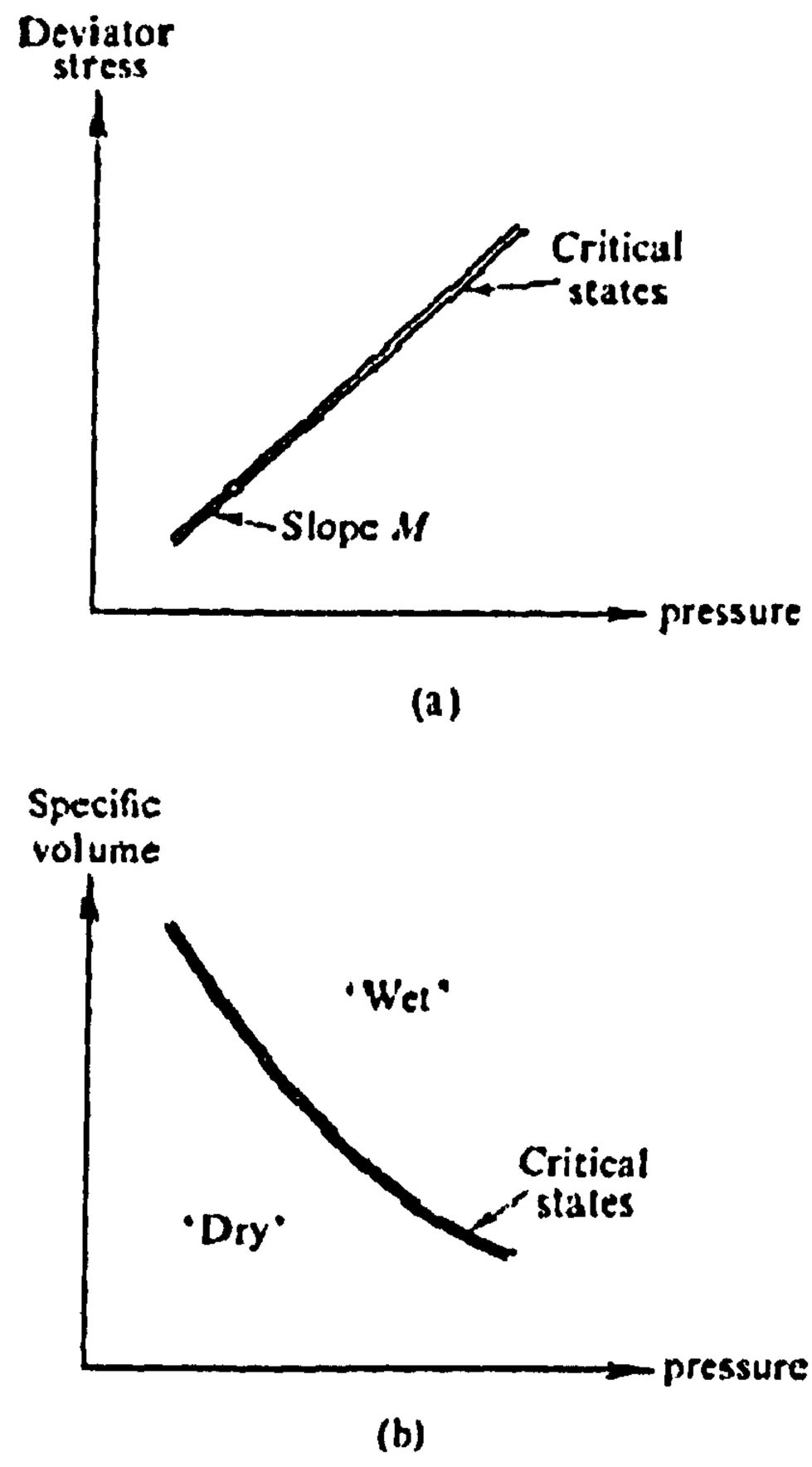

Figure 2. 10 Critical states (after Schofield and Wroth, 1968)

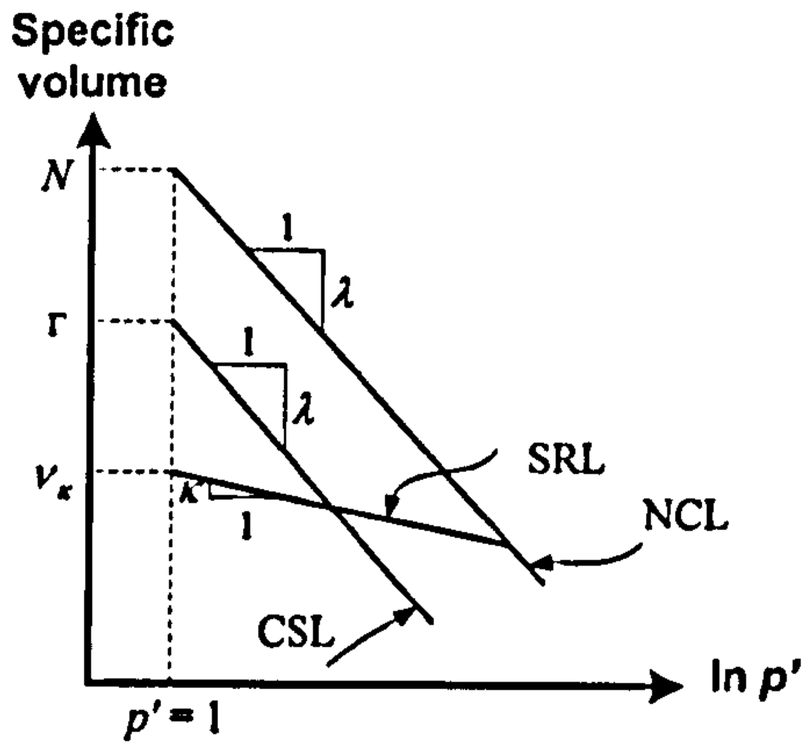

Figure 2. 11 Specific volume versus log of pressure

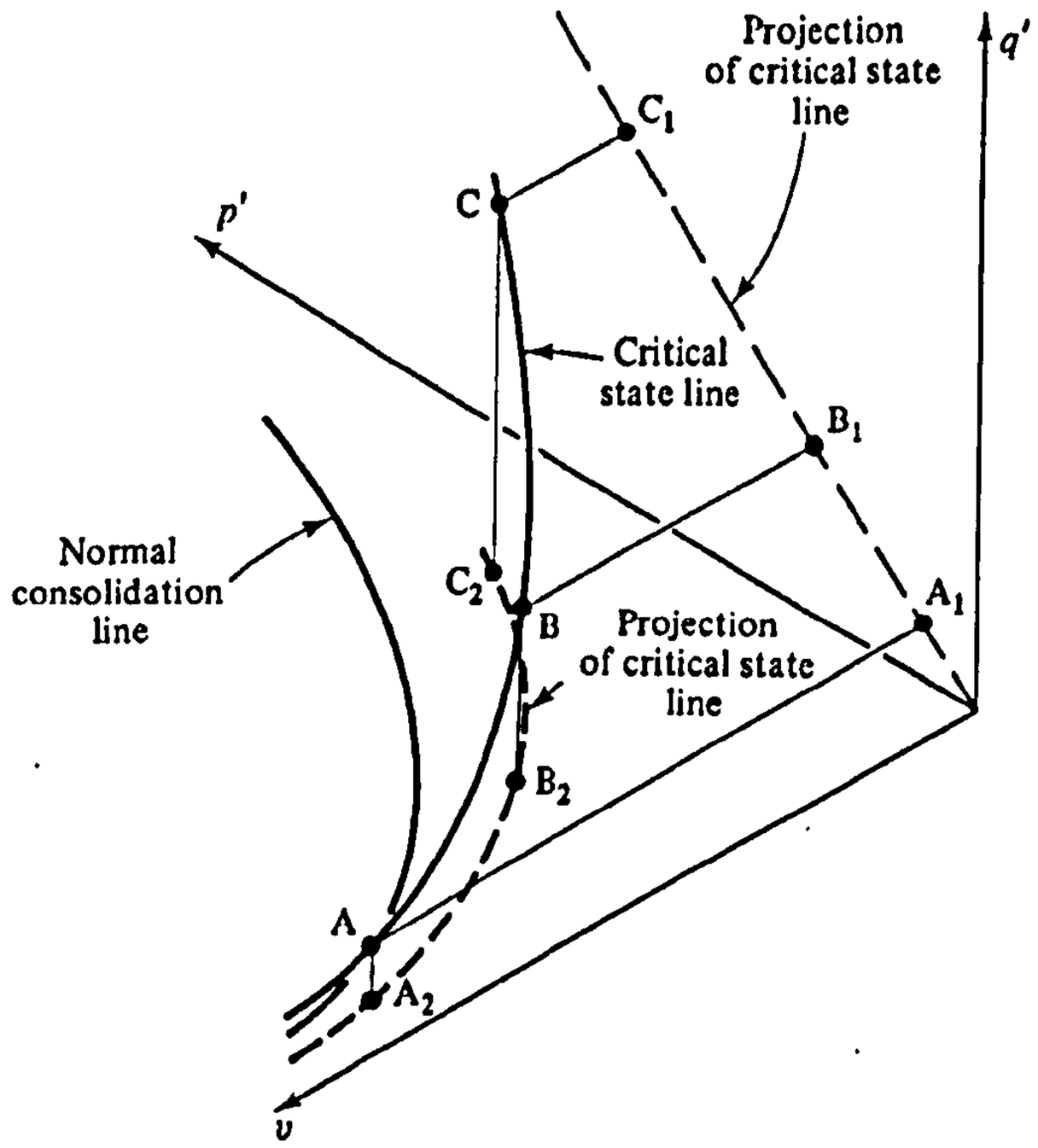

Figure 2. 12 The critical state line in $q' : p' : v$ space (after Atkinson and Bransby, 1978)

Schofield and Wroth (1968) claimed that Eq. 2.1 and Eq. 2.2 also make sense for both dry sand and saturated silty clay where low mean normal effective stresses result in large specific volumes.

There are also other critical state concepts. Casagrande (1940) stated that under undrained conditions, the critical state of soil is reached when the void ratio and the normal and shear stress remain constant under continued shearing. In sands, however, the critical state generally occurs only after effective stress failure at large strains (Yamamuro and Lade 1998). This concept and the critical state line are illustrated by Figure 2.13(a). At a given confining stress, loose sands contract and dense sands dilate during shearing, causing the void ratio to move from its initial value towards a unique critical state void ratio.

For a given sand, the unique critical state line is achieved (Figure 2.13(b)) by plotting the void ratio versus the log of confining stress. This diagram is called the critical- or steady-state diagram (Yamamuro and Lade 1998). If states of the soil lie above the critical state line, it is contractive soil. On the other hand, it is the dilative soil if it lies below the critical state line. It should be born in mind that this actually is the same as wet and dry states in critical state soil mechanics by Schofield and Wroth (1968). As such, Poorooshasb (1989) pointed out that the critical state and the steady state are in fact the same states.

The critical state by Seed and Lee (1967) is the combination of void ratio (after consolidation) and confining stress that produces zero total volume change at peak failure under drained conditions (Figure 2.13(a)). For undrained conditions, however, the critical state is the combination of current void ratio (the same value as that obtained after consolidation) and effective confining stress at the peak failure.

Therefore, the critical state of sand and clay should be clearly distinguished. The researchers on the critical state of sand always use the steady state concept instead of the critical state concept. In addition, the steady state concept is commonly used for liquefaction analysis because sandy soils are well known as most susceptible to the liquefaction.

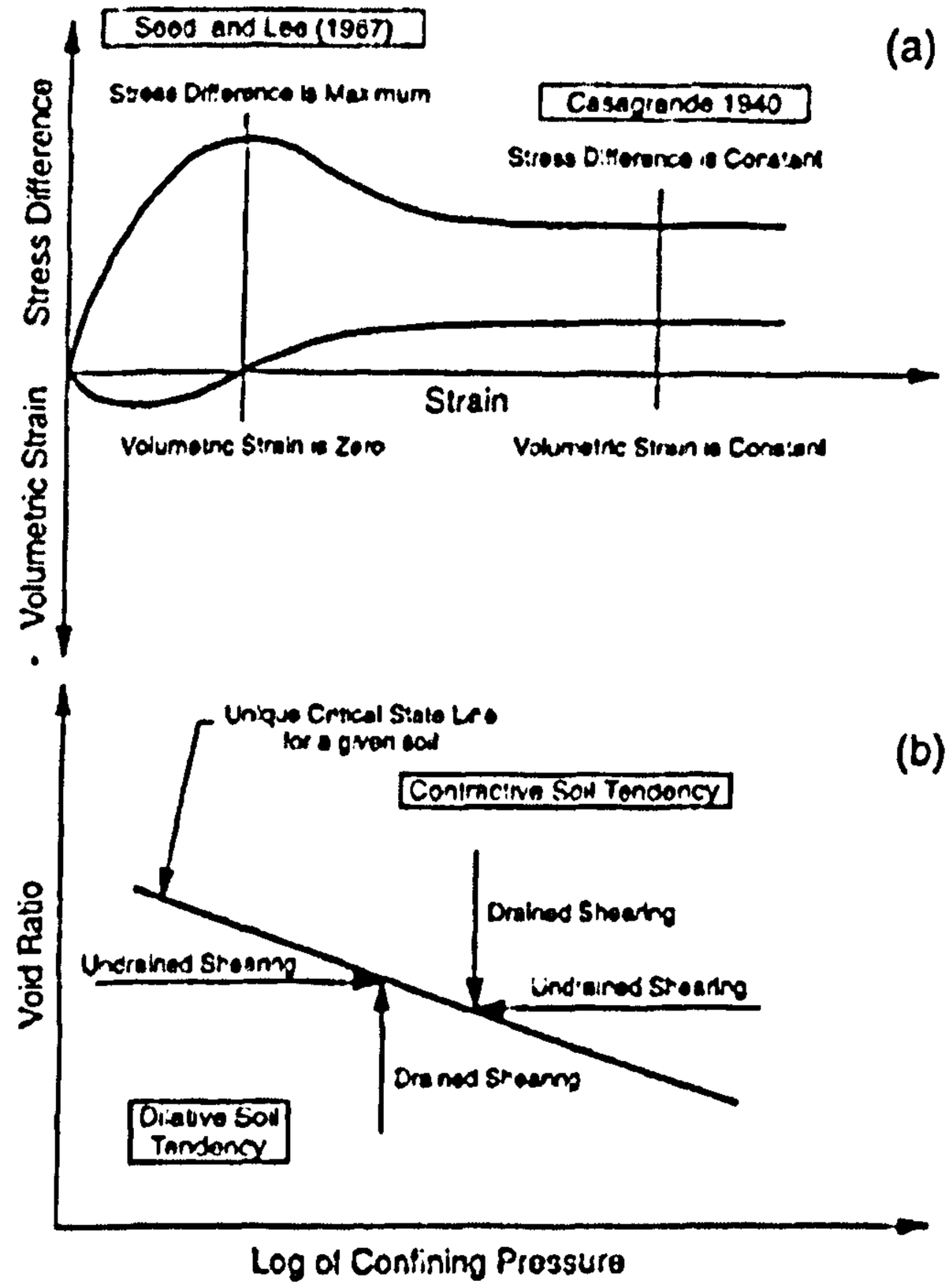

Figure 2. 13 Schematic diagram showing two definitions of critical state (after Yamamuro and Lade, 1998)

2.5 Assessment of Soil Liquefaction

2.5.1 Principles of Soil Liquefaction Determination

The basic principle of liquefaction potential determination is to compare the earthquake-induced shear stress to the liquefaction strength of a soil. In general, the most common approach for assessing the liquefaction potential is the concept of factor of safety. In this approach, the factor of safety against liquefaction F_L is defined as the ratio of the cyclic strength ratio of soil R to the maximum or equivalent cyclic shear stress ratio in the soil deposits induced by earthquakes L (Orense, 2005). The concept can be expressed by the equation:

$$F_L = \frac{R}{L} \qquad \textbf{(Eq. 2. 4)}$$

It should be noted that the cyclic strength ratio of soil R is commonly obtained from undrained cyclic triaxial test on either undisturbed or reconstituted specimens.

Also but less common, cyclic simple shear test and cyclic torsional test are employed for the task. If it is impossible to obtain samples from the desired location, the SPT-*N* value from standard penetration test and the resistance from cone penetration test can be employed for the assessment.

From Eq.2.4, if F_L is less than 1.0, it means that the earthquake-induced shear stress is greater than the liquefaction resistance of the soil; thus, the soil will essentially liquefy. On the other hand, if F_L is equal to or greater than 1.0, the soil will not liquefy.

Generally, the depth of a borehole for investigating the liquefaction potential of soil is up to 20m because the effective overburden pressure at a depth greater than those is very large. As a result, the earthquake-induced shear stress is relatively small compared to the cyclic strength ratio. For cyclic triaxial test, an effective confining stress of 100kPa is often applied which corresponds to normally consolidated state of soils in the field.

2.5.2 Simplified Procedure

In the evaluation of liquefaction potential of a soil, the commonly employed methods are the cyclic stress approach and the cyclic strain approach, either by laboratories or field tests (Sitharam *et al.*, 2004). For the cyclic stress approach, both earthquake loading and soil liquefaction resistance are characterised in terms of cyclic stresses. In the cyclic strain approach, however, earthquake-induced shear stress and liquefaction resistance of the soil are characterised by cyclic strains. Usually, the cyclic stress approach is called the cyclic stress controlled test while the cyclic strain approach is called cyclic strain controlled test.

After most of the modern structures were unexpectedly destroyed by earthquake-induced liquefaction at Niigata, it became essential to understand the behaviour of liquefied soils. Seismic zones containing soils that have a possibility of liquefaction must be identified in order to alert the engineer involving in a project. As a result, Seed and Idriss (1971) developed the so called simplified procedure for evaluating the susceptibility of in situ soil deposits to liquefaction. Since then the procedure has been improved and modified progressively by numerous researchers such as Seed (1979); Seed and Idriss (1982); and Seed *et al.*, (1985) (Youd *et al.*, 2001).

To evaluate the liquefaction resistance of the soil, the simplified procedure requires two variables: (1) the seismic demand on a soil layer, expressed in terms of *CSR*; and (2) the capacity of the soil to resist liquefaction, expressed in terms of *CRR*. It should be noted that the latter has also been called the cyclic stress ratio required to generate the liquefaction, and different researchers use different terms to express this.

The liquefaction potential of the soil can be evaluated by comparing those two variables using the following equation:

$$FS_L = \frac{CRR}{CSR} \qquad \textbf{(Eq. 2. 5)}$$

where,

FS_L = factor of safety against liquefaction,

CRR = cyclic resistance ratio, and

CSR = cyclic stress ratio.

The problem of selecting the ranges of value of factor of safety may arise for geotechnical engineers. However, this matter should depend on the size of projects, type of structures, soil and geology conditions, and cost of projects.

The earthquake induced stress ratio in the soil *CSR* can be estimated by employing the equation formulated by Seed and Idriss (1971), as shown below:

$$CSR = \frac{\tau_{av}}{\sigma'_{vo}} = 0.65\left(\frac{a_{max}}{g}\right)\left(\frac{\sigma_{vo}}{\sigma'_{vo}}\right)r_d \qquad \textbf{(Eq. 2. 6)}$$

where,

τ_{av} = average horizontal shear stress acting on soil layer during shaking generated by given earthquake,

a_{max} = peak horizontal acceleration at the ground surface generated by the earthquake,

g = acceleration of gravity,

σ_{vo} = total vertical overburden stress,

σ'_{vo} = effective vertical overburden stress, and

r_d = stress reduction coefficient.

For routine practice and non-critical projects, the value of r_d can be estimated using the following equations (Liao and Whitman, 1986):

$$r_d = 1.0 - 0.00765z \qquad \text{for } z \leq 9.15\text{m} \qquad \textbf{(Eq. 2. 7)}$$

$$r_d = 1.174 - 0.0267z \qquad \text{for } 9.15\text{m} < z \leq 23\text{m} \qquad \textbf{(Eq. 2. 8)}$$

where,

z = depth below ground surface.

Figure 2.14 shows the mean value of r_d from Eq. 2.7 and Eq. 2.8 along with the mean and range of values proposed by Seed and Idriss (1971). The evaluation procedures for cyclic resistance ratio *CRR* (or cyclic strength) both in the field and laboratory will be described in the following.

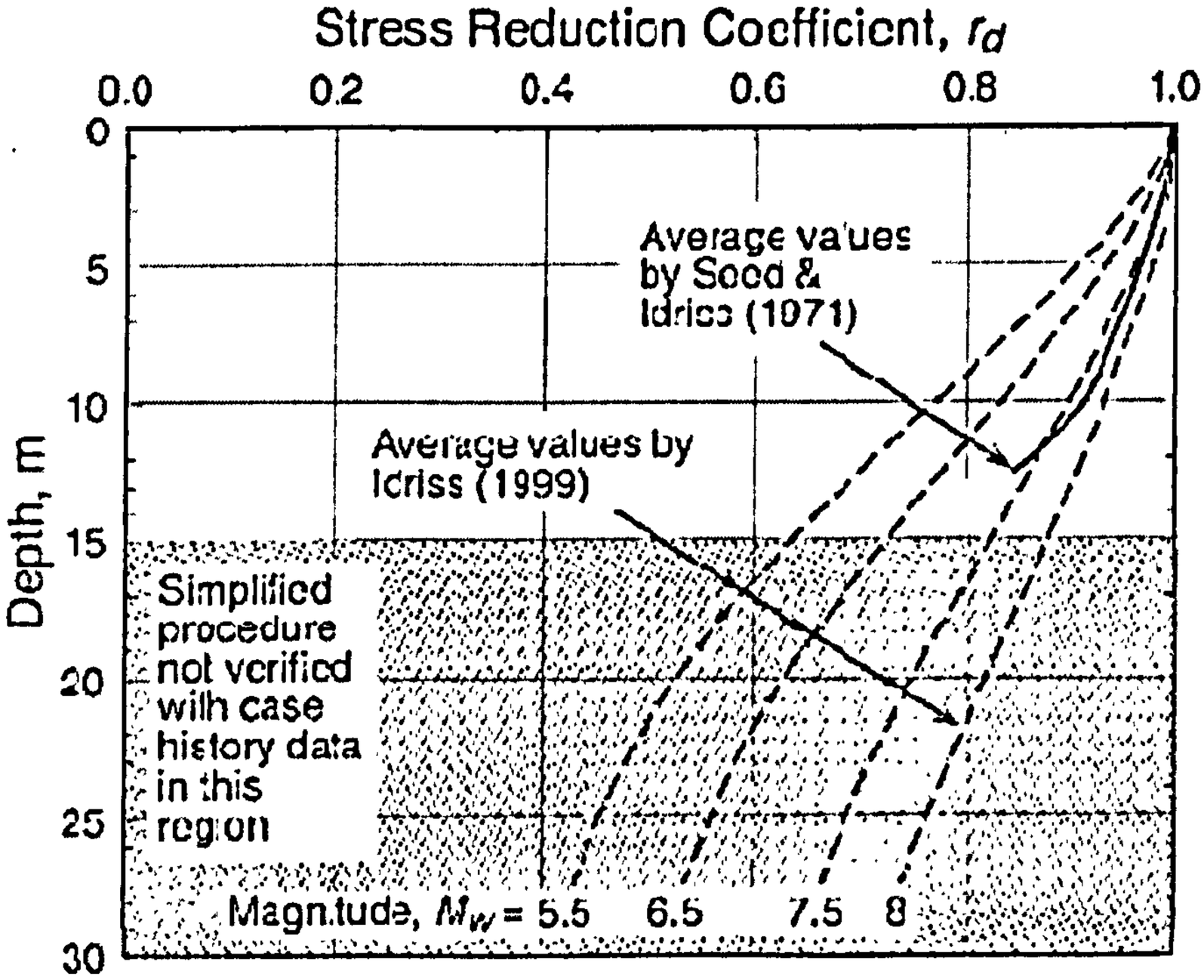

Figure 2. 14 Shear stress reduction factor used to adjust for flexibility in soil profiles during earthquake shaking (after Andrus and Stoke, 2000)

2.5.3 Field Determination of *CRR*

It has been widely accepted that the determination of liquefaction potential of a soil in laboratories essentially needs to be done on undisturbed samples for the sake of reliable results. However, obtaining high quality undisturbed samples is very difficult, expensive, and time consuming. Therefore, only large projects for which the consequence of liquefaction is very costly can afford this. Hence, simple, reliable, and economic procedures have been developed for estimating the liquefaction potential in the field for low-risk projects as well as for preliminary study.

The use of the Standard Penetration Test (SPT) was developed by Seed (1979) to estimate the possibility of liquefaction of soil deposits. Subsequently, Cone Penetration Test (CPT) was also used and is becoming more popular because of its greater repeatability and the continuous nature of its profile (Robertson and Wride, 1998).

Because there are several available methods for determining the liquefaction potential, it is essential to separate their features for the specific purpose of testing. They can be divided into two groups: (1) low strain methods; and (2) high strain methods. It should be noted that the small strain in soil testing is commonly referred to as a strain level of less than 10^{-3} %, and the strain at this level in particular is used in the dynamic analysis of soil. In this range of strain, the deformation is elastic and recoverable. In situ low strain tests include seismic reflection test, seismic refraction test, suspension logging test, Rayleigh wave test, spectral analysis of surface wave test, seismic cross-hole test, seismic down-hole test, and seismic cone test. The examples of large strain methods are SPT, CPT, dilatometer, and pressuremeter test.

(a) Low Strain Test

Unit weight, damping factor, and shear modulus are the soil constants needed for the analysis of seismic response. The shear modulus is significantly influenced by shear strain level and should be determined over the ranges of very small strain, i.e., 10^{-2} to 10^{-6}% (PHRI, 1997). The shear modulus at this strain level, however, can be measured by geophysical methods such as crosshole, uphole, downhole, and surface refraction (Hoar and Stokoe, 1978). Such methods measure the propagation speed of a compressive wave (P-wave) and shear wave (S-wave) by producing vibration, then the

receiver picks up the signal; subsequently, the shear wave velocity V_s can be determined from known distance l and travel time t as shown in the following equation:

$$V_s = \frac{l}{t} \qquad \textbf{(Eq. 2. 9)}$$

From the measurement, then, the small strain shear modulus G_{max} (is also symbolised as G_o and G_{dyn}) can be determined by the following equation:

$$G_{max} = \rho V_s^2 \qquad \textbf{(Eq. 2. 10)}$$

where,

ρ = mass density of soil, and

V_s = shear wave velocity.

To evaluate the liquefaction potential of soil using shear wave velocity requires three parameters: (1) cyclic stress ratio (*CSR*, caused by earthquake shaking); (2) stiffness of the soil (shear wave velocity); and (3) resistance of the soil to liquefaction (*CRR*).

Laboratory shear wave measurements by Roesler (1979), Stokoe *et al.*, (1985), and Belloti *et al.*, (1996) showed that they depend equally on principal stresses in the direction of wave propagation as well as particle motion (Andrus and Stokoe, 2000). Thus, the measured V_s in the vertical direction can also be related by the following equation:

$$V_s = A(\sigma'_v)^m(\sigma'_h)^m \qquad \textbf{(Eq. 2. 11)}$$

where,

A = parameter depending on soil structure,

σ'_v = initial effective vertical stress.

σ'_h = initial effective horizontal stress, and

m = stress exponent (about 0.125).

Similar to soil investigation by SPT and CPT, the effect of overburden pressure is also applied to the measurement of shear wave velocity. The following correction was proposed by Sykora (1987) and Robertson *et al.*, (1992):

$$V_{s1} = V_s C_v = V_s \left(\frac{P_a}{\sigma'_v}\right)^{0.25} \quad \textbf{(Eq. 2. 12)}$$

where,

V_{s1} = overburden stress-corrected shear wave velocity,

C_v = factor to correct measured shear wave velocity for overburden pressure,

P_a = reference stress of 100kPa or about atmospheric pressure, and

σ'_v = initial effective vertical stress.

A maximum value of 1.4 is commonly applied to C_v at shallow depths. Generally, the cyclic resistance ratio is based on an earthquake of magnitude 7.5 (Andrus and Stokoe, 2000), and the *CRR* at any magnitude of earthquakes can be obtained using the following equation:

$$CRR = \left\{a\left(\frac{V_{s1}}{100}\right)^2 + b\left(\frac{1}{V^*_{s1} - V_{s1}} - \frac{1}{V^*_{s1}}\right)\right\} MSF \quad \textbf{(Eq. 2. 13)}$$

where,

a = parameter for curve fitting (0.022),

b = parameter for curve fitting (2.8),

V^*_{s1} = upper limited value of V_{s1}, and

MSF = magnitude scaling factor for earthquake.

MSF is equal to 1.0 for earthquakes with a magnitude of 7.5. To determine the magnitude scaling factor for the earthquake of magnitude other than 7.5, the following equation can be applied:

$$MSF = \left(\frac{M_w}{7.5}\right)^n \quad \textbf{(Eq. 2. 14)}$$

where,

M_w = moment magnitude of earthquake, and

n = exponent (-2.56 to -3.3).

The upper limited value of V_s of sandy soil V^*_{s1} depends on percentage of fines content *FC* and can be expressed by the following equations:

$V_{s1}^{*} = 215$ (m/s) for sands with FC ≤ 5% **(Eq. 2. 15)**

$V_{s1}^{*} = 215 - 0.5(FC - 5)$ (m/s) for sands with 5% < FC ≤ 35% **(Eq. 2. 16)**

$V_{s1}^{*} = 200$ (m/s) for sands with FC ≥ 35% **(Eq. 2. 17)**

where,

FC = average fines content in percent by mass.

(b) High Strain Test

In situ investigation methods such as SPT and CPT were developed to determine the liquefaction potential of soils because it is impossible to obtain an undisturbed sample from the field (Ishihara, 1993). The test measures the number of blows, SPT-*N* value which represents the soil properties such as density and fabric. The SPT is popular because it has been used for investigating subsurface conditions for many years and many soil constants have been correlated to the SPT-*N* value. The resistance of soil to liquefaction can be simply obtained by employing the SPT-*N* value.

To determine the *CRR* of clean sand by employing the SPT, first after obtaining the standard measured SPT blow count (*N*), it must be corrected to a standardised SPT-*N* value $(N_1)_{60}$ using the factors (Youd *et al.*, 2001) calculated by the following equation:

$$(N_1)_{60} = N(C_N)(C_E)(C_B)(C_R)(C_S) \quad \textbf{(Eq. 2. 18)}$$

where,

C_N = correction for effective overburden pressure,

C_E = correction for hammer energy ratio,

C_B = correction for borehole diameter,

C_R = correction for rod length, and

C_S = correction for samplers (with or without liners).

All correction factors to the SPT shown in Eq. 2.18 are summarised in Table 2.3. Note that these correction values by Youd and Idriss (2001) were summarised from Skempton (1986) and Robertson and Wride (1998).

It has been reported worldwide that sand with some silt has a high liquefaction potential. As a result, it is essential to consider the effects of silt content on liquefaction. Seed *et al.*, (2003) proposed the equation to adjust the effects of fines content to the standardised value $(N_1)_{60}$ as:

$$(N_1)_{60,CS} = (N_1)_{60} \times C_{Fines} \qquad \textbf{(Eq. 2. 19)}$$

where C_{Fines} is the corrected value of $(N_1)_{60}$ due to percentage of fines content, and can be determined from the following equation:

$$C_{Fines} = (1 + 0.004FC) + 0.05\left[\frac{FC}{(N_1)_{60}}\right] \qquad \textbf{(Eq. 2. 20)}$$

The next step is to calculate the *CRR*. Recently, Rauch (1997) suggested the mathematical expression to determine the *CRR* for $(N_1)_{60} \leq 30$, as:

$$CRR = \left(\frac{95}{34-(N_1)_{60}} + \frac{(N_1)_{60}}{1.3} - \frac{1}{2}\right)\frac{MSF}{100} \qquad \textbf{(Eq. 2. 21)}$$

The magnitude scaling factor *MSF* is equal to 1.0 for the earthquake with a magnitude of 7.5. Otherwise, it can be determined from Eq. 2.14. However, Rauch (1997) also suggested that the *MSF* can be calculated from the following equations:

$$MSF = 10^{3.00} \times M_w^{-3.46} \qquad \text{for } M_w < 7.0 \qquad \textbf{(Eq. 2. 22)}$$

$$MSF = 10^{2.44} \times M_w^{-2.56} \qquad \text{for } M_w \geq 7.0 \qquad \textbf{(Eq. 2. 23)}$$

Liquefaction potential evaluation using CPT was described by Robertson and Wride (1998). The principle of employing the CPT for evaluating the liquefaction potential, similar to the SPT, is to measure the CPT penetration resistance of a soil, and then the *CRR* can be estimated. The CPT has advantages over the SPT in that it is less expensive if numerous boreholes are required and the result is more consistency. But, most important is the continuity of data with depth. However, it also has some disadvantages. For instance, the result may be uncertain if there is a thin layer between stiff layers. Such a condition may produce an incorrect tip resistance from the CPT (Seed *et al.*, 2003).

In addition to SPT and CPT, the Becker Penetration Test (BPT) has been widely used for liquefaction potential evaluation. The Becker penetration resistance is defined

as the number of blows to drive a large diameter casing though an increment of 300mm. However, it should be noted that the BPT has not been standardised, and there are several equipments and procedures. Thus, the BPT cannot be correlated directly with field behaviour, but rather through estimating equivalent SPT-*N* values from BPT data. Similar to the SPT and CPT, the equivalent SPT-*N* value converted from the BPT can be employed to evaluate the liquefaction potential (Youd and Idriss, 2001).

Table 2. 3 Correction factors to SPT (after Youd and Idriss, 2001)

Factor	Equipment Variable	Term	Correction
Overburden pressure	-	C_N	$(P_a/\sigma'_{vo})^{0.5}$
Overburden pressure	-	C_N	$C_N \leq 1.7$
Energy ratio	Donut hammer	C_E	0.5 – 1.0
Energy ratio	Safety hammer	C_E	0.7 – 1.2
Energy ratio	Automatic-trip Donut-type hammer	C_E	0.8 – 1.3
Borehole diameter	65 – 115 mm	C_B	1.0
Borehole diameter	150 mm	C_B	1.05
Borehole diameter	200 mm	C_B	1.15
Rod length	< 3 m	C_R	0.75
Rod length	3 – 4 m	C_R	0.80
Rod length	4 – 6 m	C_R	0.85
Rod length	6 – 10 m	C_R	0.95
Rod length	10 – 30 m	C_R	1.0
Sampling method	Standard sampler	C_S	1.0
Sampling method	Sampler without liners	C_S	1.1 – 1.3

2.5.4 Laboratory Determination of *CRR*

In early work, liquefaction characteristics of a soil were studied by means of laboratory testing using reconstituted samples. The principle is to apply cyclic loading using a modified triaxial apparatus; subsequently, cyclic simple shear tests and cyclic torsional tests were introduced. In the mean time, the wave propagation theory had also been used for investigating subsurface conditions both in soils and rocks. Later on, the technique was developed and used in laboratories.

Nowadays, there are many techniques and devices available for studying the liquefaction of a soil. Similarly to the field determination, the laboratory determination of *CRR* can be divided into two groups following ranges of applicable strain; (1) low strain, and (2) high strain. Cyclic triaxial tests, cyclic simple shear tests, and cyclic torsional tests clearly fall into the high strain method. The high strain method also

includes shaking table tests, centrifuge tests, and hydraulic gradient similitude tests. Whereas the small strain method includes resonant column tests, ultrasonic pulse tests, and bender element tests.

The important matter of estimation of soil liquefaction in laboratories is that a soil specimen must be fully saturated and should be brought to the same state as in the field. For the saturation, it has been found that using CO_2 is very helpful in bringing a sand specimen to fully saturation. The stress state of a soil can be accomplished by the consolidation either isotropically or an-isotropically.

(a) Low Strain Test

The resonant column test has been used for measuring the modulus and damping of soil by means of employing wave propagation through cylindrical specimens. The wave is produced by exciting the vibration device attached to the specimen. The specimen may also be subjected to other controlled conditions such as degree of saturation and pore water pressure. This method is considered non-destructive because the strain amplitudes of vibration are less than 10^{-4}radian (Drnevich *et al.*, 1978).

The theory of ultrasound has been introduced to geotechnical investigation for many years. To determine the velocity of compression wave and shear wave, at least two ultrasonic probes are used (Stephenson, 1978). One probe is used to generate a pulse from one side of a specimen, and the other probe attached to the opposite side is used for receiving the signal. Then, the velocity of waves can be determined and the shear modulus can be obtained. This method is also referred to as non-destructive testing because the strain produced is less than 10^{-4}%.

Shear wave measurements using piezoceramic bender elements in a laboratory were first used by Shirley (1978) and Shirley and Hampton (1978). The bender element is a plate which protrudes cantilevered into a soil specimen and produces a shear wave from a function generator which propagates perpendicularly to the soil particle (Lacasse and Berre, 1988). The shear wave signal then is received by a receiving bender and is amplified and filtered by an oscilloscope. A computer is now used for data processing. Because the distance between the driving bender and the receiving bender is known, the shear wave velocity V_s can be obtained using Eq. 2.9. Huang *et al.*, (2000) successfully performed the bender element test using existing dynamic triaxial testing system for the

determination of G_{max}. In addition, Zeng and Grolewski (2005) measured G_{max} of saturated clay using the bender elements by accommodating them in an oedometer cell.

The operation and interpretation of the bender element test have been described in detail by Viggiani and Atkinson (1995); Blewett *et al.*, (2000); and Lee and Santamarina (2005). The modification of the bender element by wiring configuration, called bender/extender (Lings and Greening, 2001; Dano *et al.*, 2003), can also be used for determining the shear wave velocity.

Ismail and Rammah (2005) studied the use of a shear plate as a possible alternative to bender elements for measuring G_{max} because the bender elements have some physical disadvantages, i.e., they must be penetrated into a specimen and this process may disturb the soil fabric. They employed the shear plate alongside the bender elements to measure G_{max} on soft clay, un-cemented silica sand, and strongly cemented calcareous sand. The shear plate was made by cutting piezoelectric materials to the dimensions of 7 x 7 x 7mm and coating them with non-conductive epoxy. Then, to accommodate the shear plate, it was cased with stainless steel having the diameter of 15mm, 18mm long, and 1mm thick, and glued to a 1mm thick titanium disc. The result showed that the shear wave velocity measured by the shear plate is the same as measured by the bender elements, except for clay samples in which the bender element yields better results.

Employing G_{max} from measured travel time of shear wave velocity tested in laboratories in any geotechnical design must be done with caution because of the effects of sample size. To avoid unreliable results, ASTM D2845 (1997) recommends that the ratio of the length to diameter L/D of the specimen should not exceed 5 to obtain reliable shear wave velocities. However, the routine tests in geotechnical laboratory always use a specimen with L/D ratio ranging from 0.3 to 2.5 (Leong *et al.*, 2005).

ASTM D2485 (1997) assumes that the specimen is an infinite medium. To eliminate wave dispersion for compression waves, the diameter of a specimen D should be greater than five times the wave length λ (Eq. 2.24 and Eq. 2.25). Dispersions arise when the wave interacts with the boundary of the specimen causing continual partial conversion of shear wave to compression wave. ASTM also recommends that the wavelength shall be at least three times the average grain size (Eq.2.26). Wave length

and recommendations from ASTM (1997) can be determined by the following equations:

$$\lambda \approx \frac{V_s}{f} \quad \textbf{(Eq. 2. 24)}$$

$$D \geq 5\lambda \quad \textbf{(Eq. 2. 25)}$$

$$\lambda \geq 3d \quad \textbf{(Eq. 2. 26)}$$

where,

λ = wave length,

V_s = pulse propagation velocity,

f = natural resonance frequency of transducers,

D = minimum lateral dimension of test specimen, and

d = average grain size.

(b) High Strain Test

Since the beginning of liquefaction studies, cyclic triaxial tests have been used routinely for determining the cyclic strength of sand by which triaxial compression and extension are repeatedly applied to a specimen (Hosono and Yoshimine, 2004). However, the behaviour of the ground during earthquake shaking is far different from that in the cyclic triaxial test. The cyclic simple shear test was later introduced because it is believed that the apparatus gives strain conditions more representative of in situ ground during earthquake shaking. However, the cyclic simple shear has a problem of applying precise undrained and constant volume conditions because of the shorter height of the specimen as well as the boundary confinement condition. Using hollow cylindrical specimens for the cyclic simple shear test appears to overcome these difficulties because the height of the specimen is fixed, and the saturated specimen and inner hollow space are kept undrained.

Despite some disadvantages, the stress controlled cyclic triaxial test has mostly been used for liquefaction studies because it is easy to conduct and inexpensive. Moreover, wide ranges of strains and strain rates can be employed, and a larger specimen can be tested with small modifications. In addition, because it has been used for many years with different soil types, the data obtained can be compared to others.

The typical procedures for a cyclic triaxial test are: saturation, consolidation (either isotropically or anisotropically), and applying cyclic shear stress at a given frequency. Generally, to interpret the result, four values are plotted against the number of load cycles N which are: deviator stress q, axial strain ε_a, excess pore pressure ratio $\Delta u/\sigma'_{3c}$, and deviator stress ratio q/p'. The deviator stress q against axial strain ε_a and deviator stress q against mean normal effective stress p' diagrams are also plotted for the interpretation.

The cyclic direct simple shear test (Song *et al.*, 2004) can be divided into two types: (1) SGI and NGI type, and (2) the Cambridge type. It should be noted that they are designed to be able to conduct the testing under constant volume conditions which reasonably simulate undrained and pure shear stress conditions which cannot be achieved in cyclic triaxial tests. In the torsional simple shear test, a hollow cylindrical specimen is consolidated at constant vertical and lateral stress (σ'_v and σ'_h), and then subjected to cyclic torsional forces in order to produce shear stress τ on the horizontal planes of the specimen (JGS, 1998).

It can be said that the most widely used apparatus in laboratories for determination of liquefaction potential of the soil is cyclic triaxial systems. Typically, the apparatus includes an actuator controlled by either computer- stress-controlled or strain-controlled loading. The system is designed to axially load cylindrical specimens which are sealed within a triaxial cell, and provide independent control of the pore water pressure within the specimen. For more accurate measurements an internal or submersible load cell can be used to overcome the friction of piston and effects of cell pressure, and displacement transducers are the standard. However, better testing results can be achieved by using local deformation transducers (Local LVDT) directly attached on the specimen. All the procedures can be controlled by a central data acquisition system connected between the computer and the triaxial system (Riemer, 2004).

2.6 Mitigation of Liquefaction

2.6.1 Principles of Liquefaction Mitigation

If foundation soils, backfills, and fill materials are likely to liquefy during earthquakes, it may lead to disastrous consequences. Mitigation of the hazard must be considered carefully. For foundation soils and fill materials, structures may sink or float, depending

on the unit weight of the structure compared to the unit weight of liquefied soil, and large settlement after liquefaction is to be foreseen. For backfills behind retaining walls, the excess horizontal pressures from liquefied soils may damage the structures. Lateral spread also damages many structures by moving the buildings and bending piled foundations.

Generally, if liquefaction is likely to occur, and the deformation and displacement are not acceptable, i.e., structures will damage or collapse if the soil is liquefied; further actions are needed. For example, either using more sophisticated theories and tools to validate the liquefaction potential or considering remediation and mitigation techniques should be examined. Other options are designing the structure to resist the anticipated deformations and choosing other sites.

The basic principles of reducing the risk are increasing the shear strength and stiffness of the soil expected to liquefy. The other alternatives are improving the drainage condition and replacement.

Many techniques have been used for mitigating the liquefaction. They are replacement of new fills, removal of water, soil compaction, chemical grouting and deep mixing, and thermal treatment (Sitharam, 2003). Among these, the ground improvement by compaction of potentially liquefiable soils has commonly been used. Recently, soil reinforced with geosynthetics has shown that it can be an alternative for the mitigation.

When bridges, buildings, retaining walls, ports and harbours, and buried structures are being constructed in seismic zones, civil and geotechnical engineers must achieve the processes illustrated in Figure 2.15. For the first step, assessment of triggering of initiation of soil liquefaction, there have been some advances in recent years because of extensive studies and case histories. Several methods and techniques, both in the laboratory and in the field, have been developed and the findings are well agreed from many case studies.

Once, if the liquefaction will occur, the next step is to assess the consequences of the potential liquefaction. If the post liquefaction strength and overall stability are not acceptable, then the next step is needed. The analysed deformation and displacement from step 3 are used to assess the consequences to structures. Finally, if all clues

indicate that satisfactory performance of structures cannot be counted on, mitigation techniques must be employed to minimise the hazards (Seed *et al.*, 2003).

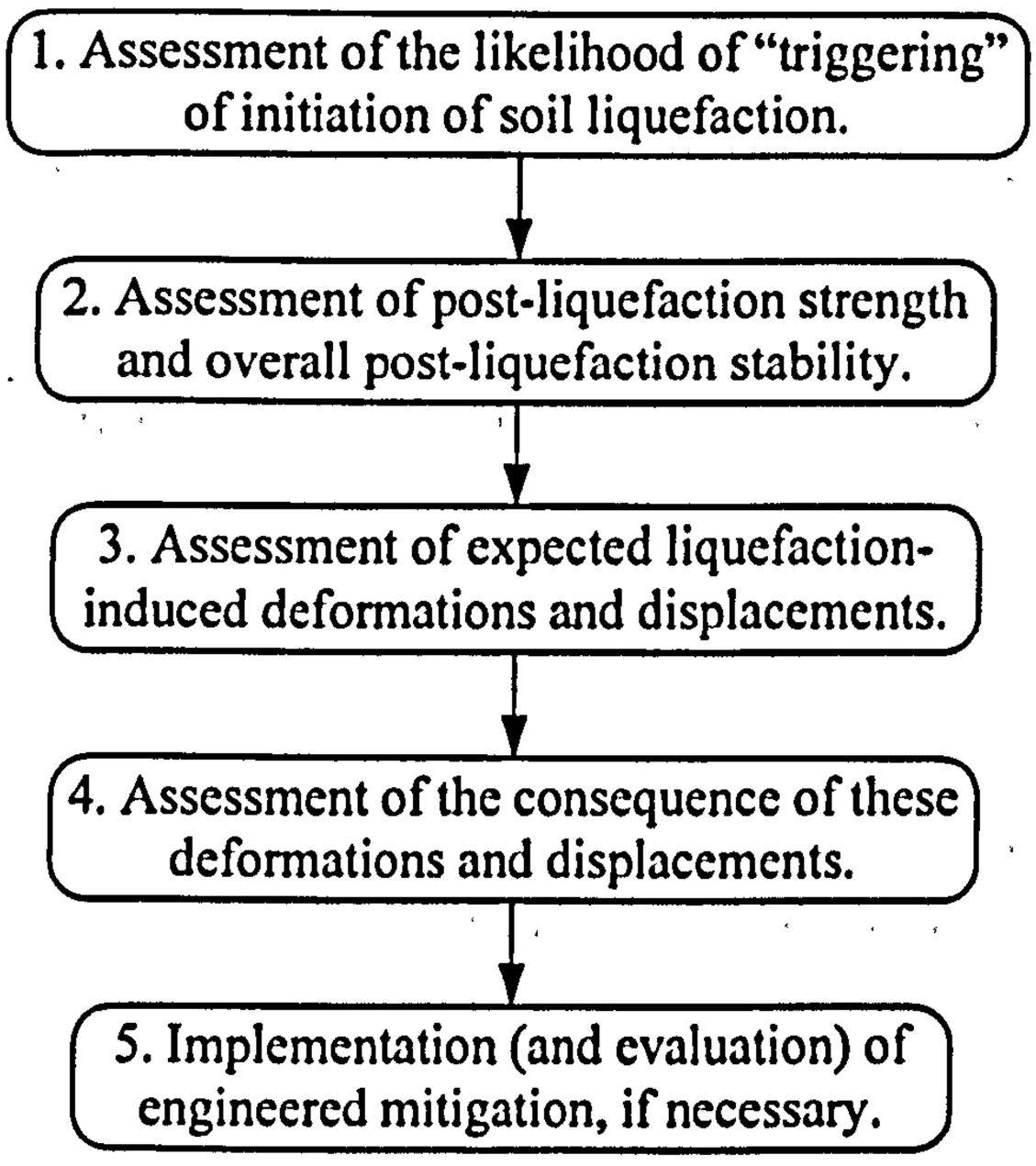

Figure 2. 15 Key elements of soil liquefaction engineering (after Seed *et al.*, 2003)

2.6.2 Mitigation Methods

Methods and techniques for mitigating the liquefaction of soils have been systematically classified by JGS (1998). They can be divided into 6 groups: (1) densification, (2) solidification and replacement, (3) lowering of the groundwater table, (4) dissipation of pore water pressure, (5) restraining shear strain, and (6) strengthening structures. Ground modification techniques and details can be found in Hausmann (1990).

The principle of densification methods for increasing the resistance against liquefaction is to reduce the volume of voids between soil particles. As a result, the void ratio is decreased and the stress state of deposits is changed. Soil stabilisation by chemical substances is in the solidification and replacement methods. Soil liquefaction resistance can be increased by mixing cement with sand. JGS (1998) reported that Akita Port sand with 5% of added cement shows up to four times increased liquefaction resistance.

Lowering of the groundwater table will have three effects: (1) soil above the ground water table will not be saturated, thus, it will not liquefy, (2) the effective confining stress of a target layer will increase, therefore, the liquefaction resistance will increase, and (3) the non-liquefiable layer increases, thus the influence from an underlying liquefied layer is reduced (JGS, 1998). During earthquakes the liquefiable soil might not liquefy if the excess pore water pressure dissipates simultaneously. This can be done by installing drains in sand deposits. As a result, the accumulation of pore water pressure may be delayed and soil will not liquefy. Restraining shear strain can be accomplished by using diaphragm walls and sheet piles. They will prevent the occurrence of liquefaction by surrounding the ground underneath a structure.

Soil improvement methods are to prevent the occurrence of liquefaction while strengthening a structure is a means of minimising damages to structures in case of soil liquefaction. Examples of the structural strengthening are increasing the size of piled foundations and replacement with stronger materials.

Recently, reinforcement techniques using geosynthetics have shown to reduce the liquefaction potential of soil (Vercueil *et al.*, 1997). Krishnaswamy and Isaac (1995) analytically and experimentally evaluated the liquefaction behaviour of sand reinforced with woven geotextile, nonwoven geotextile, and coir, under triaxial stress conditions. The specimens were tested using stress-controlled cyclic triaxial with 1 Hz frequency. They concluded that the deployment of reinforcement significantly increases the liquefaction resistance of the sand. Such a result will be of benefit to liquefiable foundation soils, embankments, hydraulic fills, and retaining walls.

2.7 Sand-Tyre Chip Mixtures

2.7.1 Waste Tyres

Discarded tyres, a kind of solid waste from industrial development are becoming increasingly problematic. In 1996, the scrap tyres generated by the United States were 260 million while Great Britain generated 23.4 million (North Carolina Department of Environment and Natural Resources). In Western Europe, the EU estimated that more than 2.5 million tonnes of post-consumer tyre material were produced annually (Khalid and Artamendi, 2004). As such, stockpiling and destroying this many are very difficult and would cause associated pollutions. Disposing of the whole used tyre into landfill

was prohibited by the new EU Landfill Directive in July 2003. In July 2006, the prohibition also included shredded tyres (Khalid and Artamendi, 2004).

Because recycling waste tyres may cause consequent effects. Making use of them needs to be considered, and the solution must be sustainable. The solution should cover social, environmental, and economic sustainability. Details of sustainable development were given by Parkin *et al.*, (2003). They use five capital frameworks to achieve sustainable development, which are: (1) natural capital, including soil, sea, air, and ecological systems, (2) human capital, including health, knowledge, motivation, and spiritual ease, (3) social capital, including governance systems, families, communities, and organisations, (4) manufactured capital, including existing tools, infrastructure, and buildings, and (5) financial capital, including money, stock, and bonds.

2.7.2 Classification and Properties of Recycled Tyres

Countries around the world are beginning to use shredded recycled tyres because of the availability of vast quantities and stockpiling causes environmental problems (Foose *et al.*, 1996). To make use of these waste tyres, shredders and cutters are needed to make them smaller, depending on the application. However, each country has different machines and different measurement systems. Therefore, it is essential to have a standard for classification of recycled tyres.

For civil engineering purpose, the American Society of Testing and Materials (ASTM) published ASTM D6270-98, Standard Practice for Use of Scrap Tires in Civil Engineering Applications (ASTM, 1998). This document gives a guideline for civil engineering application of waste tyres. Table 2.4 shows names of different size in accordance with ASTM D 6270-98.

The bulk and apparent specific gravity values of tyre shreds are 0.98 -1.06 and 1.02 - 1.27 respectively (ASTM, 1998), compared to 1.13 to 1.36 by Edil and Bosscher (1994). It should be noted that the value varies depending on materials and manufacturing processes. If a larger size of tyre shred is to be used, materials belted in the used tyres should be considered in the determination of the specific gravity. The belt mostly used for reinforcing the tyre is steel, but glass fibre is also used.

Another important property of engineering materials is density. The dry density of tyre shreds depends on the compaction methods used. In a loose state in with no compaction, its density ranges from 341 to 489kg/m^3. Compaction by vibration gives a density of 473 to 496kg/m^3. At standard compaction and modified compaction, the densities are from 560 to 640kg/m^3 and 660 to 685kg/m^3, respectively (ASTM, 1998).

The compressibility of material is important in geotechnical engineering in that it is used for the analysis of settlement. For tyre shreds, the compressibility on initial loading ranges from 7 to 20kPa and from 8 to 28kPa at 10% and 25% vertical strains, respectively (ASTM, 1998). However, it should be determined material by material because shape and size of shredded tyres play an important role in this property. Moreover, the type of machine used for recycling the tyre is not negligible.

An important material property used in geotechnical engineering is shear strength. The shear strength of tyre shreds, in recent years, reported from several papers, indicates that the value varies widely. This is because each part of the world uses different base material for producing the tyre. However, almost every standard device in geotechnical laboratory can be used for determination of the shear strength; but, the engineer should be aware of size and boundary effects if large size of shredded tyres will be tested. Note that the larger specimen is often used for the purpose.

Table 2. 4 Size of recycled tyres (summarised from ASTM D6270-98, 1998)

Name	Size	Note
Granulated Rubber	below 425 μm to 12 mm	also refer to particulate rubber
Ground Rubber	below 425 μm to 2 mm	also refer to particulate rubber
Powered Rubber	below 425 μm	
Rough Shred	between 50 x 50 x 50 mm to 762 x 50 x 100 mm	
Tyre Chips	12 mm to 50 mm	most wire removed
Tyre Shreds	50 mm to 305 mm	

2.7.3 Shear Strength of Mixtures

To determine the shear strength of the mixtures, there are two methods for mixing: by weight and by volume. It should be noted that in the field, the construction of road embankments always use the proportions of mixtures by volume. The reason is that the capacity of a tray is known. In laboratories, however, both methods have been used.

All conventional geotechnical laboratory devices can be used to determine the shear strength and deformation characteristics of sand mixed with tyre chips; e.g., standard triaxial tests, cyclic triaxial tests, direct shear tests, and direct simple shear tests. However, engineers should be aware of the effect of size of tyre chips compared to the size of specimens (Zornberg *et al.*, 2004). For example, the largest size of samples compared to the diameter of specimens should not exceed one-sixth. To overcome this limitation, larger diameter may be used if tested on sand-tyre chip mixtures.

Unlike sands, the shape of the tyre chip varies widely depending on types of cutting machine. Tyre chips may have a shape which is square, parallelogram, cubic, or elongated. This cannot be neglected because the shape of tyre chips strongly influences the strength of the mixtures (Bergado *et al.*, 2005). Therefore, the aspect ratio, η is used to demonstrate the shape of recycled tyre as:

$$\eta = \frac{l_{rb}}{w_{rb}} \qquad \textbf{(Eq. 2. 27)}$$

where,

l_{rb} = length of individual rubber, and

w_{rb} = width of individual rubber.

Youwai and Bergado (2003) performed triaxial tests on compacted shredded rubber tyres having a D_{10} of 5mm mixed with sands using a different ratio of mixtures. The size of specimens was 100mm in diameter and 200mm high. The average specific gravity of tyre chips was 1.22, which is 57% of that of sand (2.67). The ratios of tyre chips to sand were 20:80, 30:70, 40:60, and 50:50, by weight. The results showed that the peak internal friction angle varied from 30 to 34° with increasing proportions of sand in the mix. At vertical strain less than 10%, the relationship between deviator stress and strain was linear. At high confining pressure, no failures occurred even at a

strain greater than 20%. When the sand in the mixtures is greater than 30%, the deformation is significantly reduced. Mixing sand with granular rubber by weight was also studied by Ghazavi (2004) to determine the shear strength characteristics of the mixtures.

Wu *et al.*, (1997) carried out triaxial compression tests on 5 different shapes and sizes of tyre chips. The shapes of tyre chips were flat, granular, elongated, and powder. The sizes of tyre chips were 2, 9.5, 9.5, 19, and 38mm for the particles having shape of powder, granular, elongated, granular, and flat. The specific gravity and density ranges from 1.08 to 1.18 and 505 to 600kg/m^3. The friction angle from triaxial compression tests ranges from 45° to 60°. The maximum friction angle of 60° is obtained from elongated particles. Modulus of elasticity is from 350 to 820kPa. Similar parameters were also studied by Ghazavi and Sakhi (2005).

Moo-Young *et al.*, (2003) determined the physical and chemical properties of tyre shreds having particle sizes of 50 to 300mm using large scale direct shear apparatus. They found that the average specific gravity of tyre shreds ranged from 1.06 to 1.10; the angles of friction and densities ranged from 15° to 32° and 349 to 394kPa, respectively. They concluded that compressibility increased as tyre shred size increased.

The mechanical properties of tyre chips with sizes from 2 to 10mm were studied by Yang *et al.*, (2002) using confined compression, direct shear, and triaxial tests. The average specific gravity of tyre chips is 1.15 (compared to ASTM 1.02-1.27). The friction angle from direct shear tests was found to be 32° at 10% displacement. In addition, the compressibility of tyre chips was quite lower than that of tyre shreds, which is similar to the studies by Moo-Young *et al.*, (2003). This is because the initial void ratio of large-sized tyre shreds was 3, while the initial void ratio of small tyre chips is only 0.98.

A torsional resonant column was used to study the shear modulus and damping ratio of sand mixed with granulated rubber by Feng and Sutter (2000). The proportions of rubber mixed with sand were 29, 49, 76, and 100%, by volume. The specific gravity of tyre chips and Ottawa sand from this study was 1.11 and 2.67, respectively. The specimen for resonant column test was 7cm in diameter and 15cm high. Shear modulus of the mixtures decreases insignificantly with increasing shear strain for 49% and 76%

rubber samples because of the high elasticity of the rubber. In 100% rubber samples, as confining pressures increased, the damping ratio slightly increased, which is the opposite to typical soils. The study shows that the shear modulus of the mixtures is mainly influenced by the percentage of the rubber inclusion.

Due to the comparatively large size of tyre shreds, large scale triaxial specimens were used to determine the mechanical behaviour of tyre shreds-soil composites by Zornberg *et al.*, (2004) to minimise potential boundary effects. The sizes of tyre shreds were from 12.7 to 25.4mm with aspect ratios η of 1, 2, 4, and 8. The specific gravity of tyre shreds was 1.15 while the unit weight under unconfined conditions ranged from 5.97 - 6.76kN/m^3 and the approximate value of void ratio was 0.79. The specimens were scaled up to 153mm in diameter and 305mm in height. The percentage of tyre shreds varied from 0 to 100%, by weight. The maximum shear strength of the mixtures was found at 35% of tyre shreds. At a given tyre shred content, increasing the tyre shred aspect ratio leads to an increase of overall shear strength, particularly, when the aspect ratio is increased from 4 to 8.

The influence of aspect ratios of recycled rubber on the shear strength of sand-tyre chips mixtures is also found in a study by Ghazavi and Sakhi (2005). They showed that the friction angle of the mixtures increases about 25% when the aspect ratio is increased.

2.7.4 Cyclic Strength of Mixtures

Recycled tyres have been employed in civil engineering projects for many years, for example, road and embankment construction and backfilling for retaining walls. Most research involving the use of recycled tyres has been conducted under static loading conditions such as the standard triaxial test (Lee *et al.*, 1999; Bergado *et al.*, 2005) and direct shear test (Edil and Bosscher, 1994; Ghazavi and Sakhi, 2005). The dynamic behaviour of soil mixed with recycled tyres has recently attracted the attention of researchers, especially in Japan. There are two reasons: first Japan has increasingly seen the problem of growing numbers of waste tyres, and secondly it is located on the most severe earthquake-prone area.

For example, Hyodo *et al.*, (2008) reported that compound sand with tyre chips increases the undrained cyclic shear strength. From the test results obtained from undrained cyclic triaxial tests, they concluded that when the sand fraction in sand-rubber mixtures was greater than 0.5 liquefaction was observed. However, when the sand fraction was less that 0.5, liquefaction was not clearly observed. They pointed out that the rubber in the mixtures controls the generation of pore water pressure.

Uchimura *et al.*, (2008) studied the liquefaction characteristics and the uplift of buried pipes by means of a series of shaking table tests and undrained cyclic loading tests. The study compared the behaviour of buried pipes under seismic loading with various mixtures of Toyoura sand and tyre chips. The results showed that the backfill with sand mixed with tyre chips has significantly higher cyclic strength than pure Toyoura sand. Moreover, the results from undrained cyclic loading tests showed the improvement of the liquefaction resistance of the backfill using sand-tyre chip mixtures, compared to pure Toyoura sand.

2.7.5 Applications of Mixtures in Civil Engineering

Once, used tyres were thought of as a waste material. Nowadays, they are increasingly being considered as a construction material. This is because they have basic properties that meet civil engineer's needs. The most important property of shredded tyres is that they are lighter compared to other fill materials, usually soils. Such a property aids geotechnical engineers to overcome the settlement and stability problems of embankments constructed on very soft clay. Another benefit is that they are very free draining. Moreover, obtaining them is totally free if one excludes the cost of the recycling process. As a result, the cost of construction can significantly decrease. The disadvantages are high compressibility and potential for exothermic reactions (Zornberg *et al.*, 2004). Another drawback is that they may generate ground water contamination if improperly used. However, a study by Humphrey (1998) showed that uses of tyre shreds in construction have a negligible environmental impact under normal conditions. Another disadvantage is that they easily catch fire, but, this can be prevented by mixing with other materials or using soil embankment caps. To make use of recycled tyres, they are usually mixed with other materials such as soils, asphalt, or concrete (Feng and Sutter, 2000).

Ghazavi (2004) summarised the studies from others and showed that recycled waste tyres can be used in road construction, to control ground erosion, for stabilising slopes, for backfilling retaining structures, as aggregates in leachate beds for landfills, as an additive material to asphalt, as sound barriers, as a limiter for freezing depth, as a source for creating heat, as a fuel-supplement in coal-fired boilers, for vibration isolation, as cushioning foams, and for low strength but ductile concrete. The greatest use of waste tyres, however, is in highway applications; i.e., as a fill material. It is also suitable as a lightweight backfill where the horizontal pressure behind a wall will also be reduced due to the free draining properties. It has also been observed that if the ratio of sand to tyre chips is low, typically less than 30% by volume, the segregation of mixtures tends to occur.

There is also a possibility of using rubber-soil mixtures as a seismic isolation as reported by Tsang (2008). A numerical analysis using finite element modelling showed that mixing soil with recycled tyres could reduce the level of shaking in the horizontal direction. However, the more significant advantage was the reduction of shaking level of vertical ground motion, which has increasingly attracted the attention of the earthquake engineering community.

CHAPTER 3

MATERIALS AND TEST PROGRAMMES

3.1 Introduction

When an artificial island is to be reclaimed from the sea, the sand dredged from the nearby seabed is often considered first as a fill material because it is a cheap alternative owing to the abundant quantities and especially the transportation cost. The reclaimed land is then generally constructed by just simply dumping the fill materials without any compaction effort. This will result in the ground being deposited in a loose to medium dense state. If a strong earthquake were to strike whilst the ground was fully saturated, the probability of liquefaction would thus be higher.

Leighton Buzzard 16/30 sand having a mean particle size of about 0.7mm was mixed with various sizes of tyre chips to investigate the liquefaction characteristics under simulated earthquake loading. The sand was chosen as a base material because, during the initial investigation, it was liquefiable even when prepared in medium to dense state. The sizes of the tyre chips were carefully considered to ensure that the effects of varying size relative to the sand were investigated. This was constrained by the principle that the maximum particle size should not exceed 1/10 the diameter of a cylindrical triaxial specimen, so that the boundary problems were not encountered.

This chapter presents the materials and their basic properties. Also included are the ratios of sand to tyre chips that were used for the test programmes, including undrained monotonic triaxial tests, undrained cyclic triaxial tests, and bender element tests.

3.2 Test Materials

The test sand, Leighton Buzzard 16/30 sand, obtained from WBB Minerals, UK, is a silica sand having brown colour, medium sphericity, and sub-rounded to sub-angular grains. According to WBB Minerals, it comprises 97% of SiO_2, 1.73% of Fe_2O_3, 0.32% of Al2O3, 0.05% of K_2O, and 0.46% of LOI.

Recycled tyre chips were obtained commercially from Charles Lawrence International. Four tyre chips were chosen in order that the effects of mixing the sand with various sizes of the tyre chips could be investigated. They were tyre chips CT0515, CT1030, CT2060, and CT4010, which correspond to the ranges of particle sizes of 0.5 – 1.5mm, 1 – 3mm, 2 – 6mm, and 4 – 10mm, respectively. The true scale pictures of the test sand as well as the tyre chips are illustrated by Figure 3.1. According to Charles Lawrence International the tyre chips were produced by using a shredder. This resulted in the tyre chips having an irregular shape, as is evident in Figure 3.1(b), (c), (d), and (e). For further references in this research the sand was symbolised as "S". For the tyre chips CT0515, CT1030, CT2060, and CT4010, the symbols "A", "B", "C", and "D" were assigned, respectively.

It has been recognised that the aspect ratio of recycled rubber influences the characteristics of soil mixed with the rubber (e.g., Wu *et al.*, 1997; Bergado *et al.*, 2005). Therefore, it is vital to include this in the analysis of the test results. However, as evident in Figure 3.1 that all tyre chips have a highly irregular shape; thus, it would be very difficult and cumbersome to determine the aspect ratio. Instead, the analysis of the effects of different sizes of tyre chips when mixed with the sand will be based on the mean particle size.

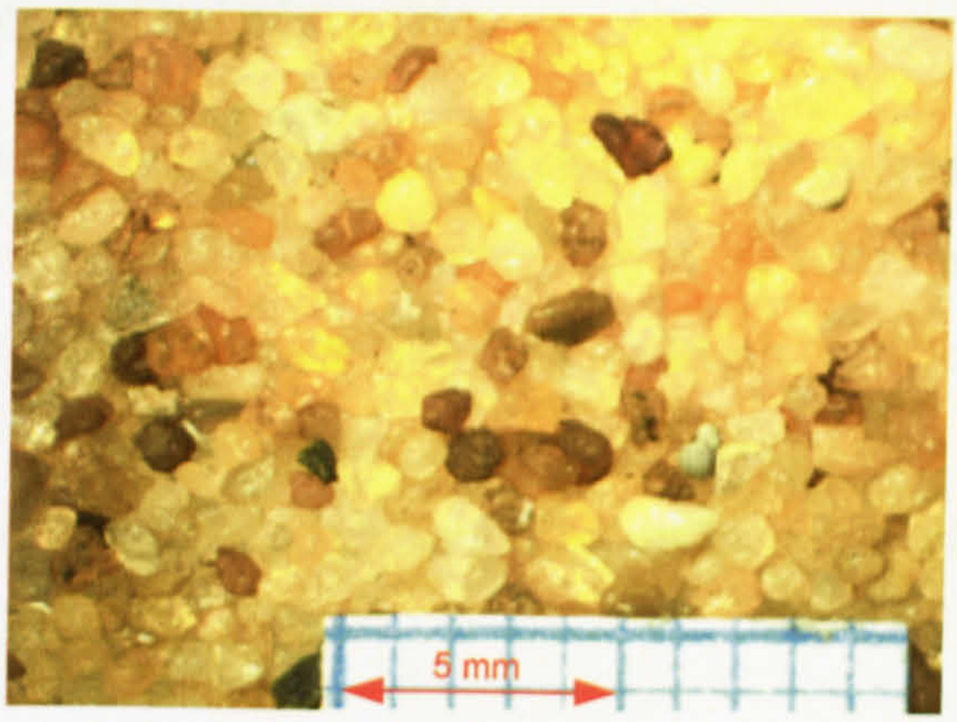

(a) Leighton Buzzard 16/30 Sand, S

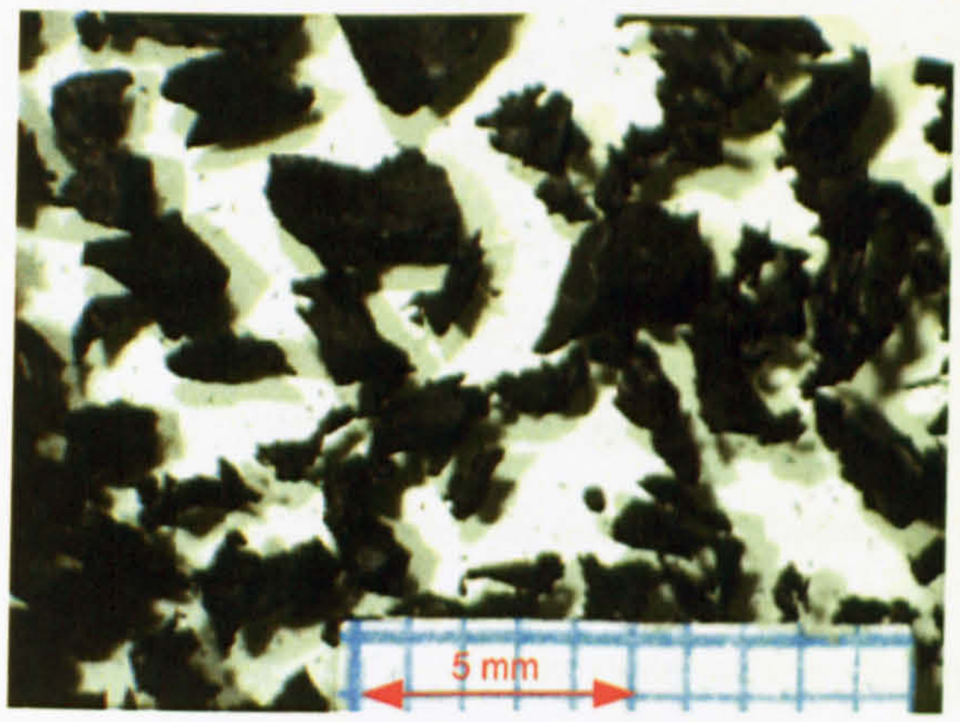

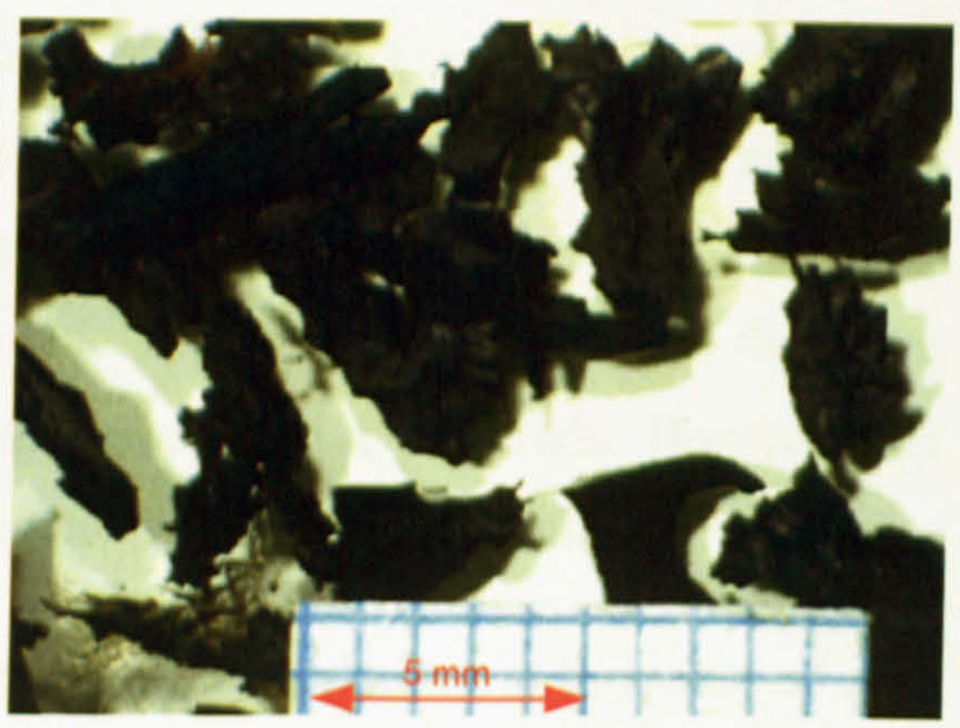

(b) Tyre Chips CT0515, A

(c) Tyre Chips CT1030, B

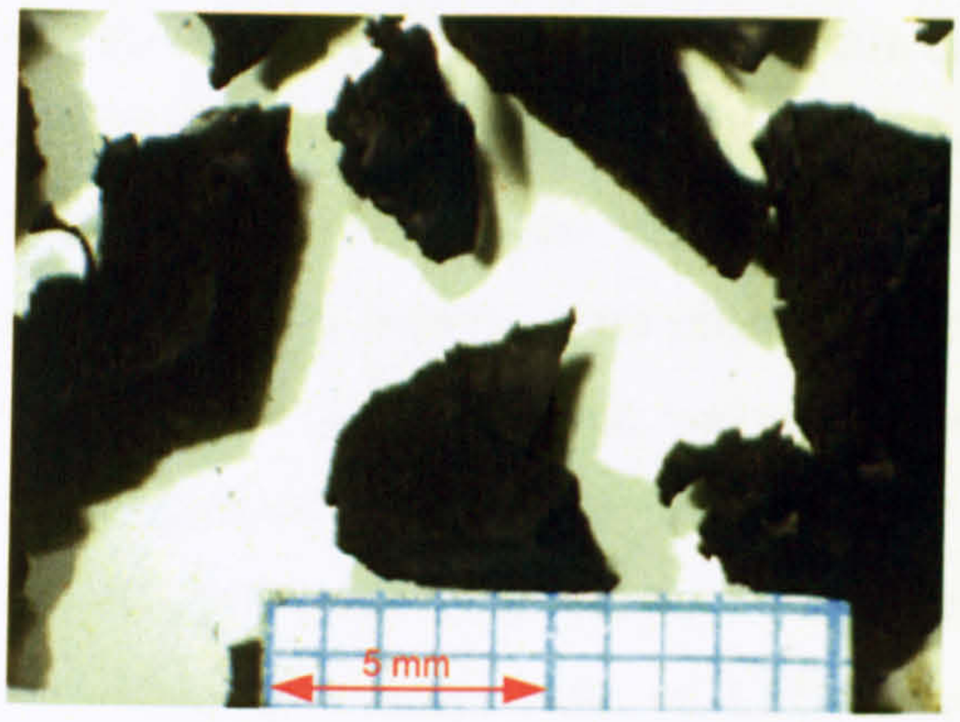

(d) Tyre Chips CT2060, C

(e) Tyre Chips CT4010, D

Figure 3. 1 True scale pictures of tested materials

3.3 Basic Properties of Test Materials

The grading curves for the sand and the tyre chips are illustrated by Figure 3.2. It was observed that the characteristics of the grading curves for both sand and tyre chips were quite similar. However, the sizes were different; the mean particle sizes D_{50} for S, A, B, C, and D were 0.7, 1.2, 2.3, 4, and 8mm, respectively. It can also be seen that all curves had a uniform grading, which was confirmed by all having coefficients of uniformity below 3, as shown in Table 3.1.

To compare the influence of the size of tyre chips mixed with the sand in the chapters reporting and discussing the test results, the particle size ratios D_r/D_s (Kim and Santamarina, 2008) were also included in Table 3.1, where D_r and D_s denote the mean particle sizes for the rubber and the sand, respectively. It should be noted that according to ASTM D 6270-98 (1998), recycled rubber having a particle size ranging from 12 to 50mm is classified as "tyre chips". If the size is smaller or bigger than that, it is otherwise called, granulated rubber, ground rubber, and tyre shreds. However, for convenience, all recycled rubbers employed in this research were labelled as tyre chips.

The vital parameter used in the design of soil-rubber mixtures by means of solid volume is the specific gravity. It should be noted that the calculation of the sand and tyre chips portions used in a particular mixture was by means of solid volume in order that the void ratio could be controlled. For the sand, according to BS 1377-2 (1990), the specific gravity was 2.66, which is within the range for most mineral grains of 2.65 and 2.75 (Atkinson and Bransby, 1995). For the tyre chips, regardless of their size, it was found that their irregular shape made the determination of the specific gravity problematic: air bubbles were observed to be trapped around the edge causing the tyre chips to float. This, however, was overcome by boiling the water until the air bubbles were eliminated. The values for the specific gravity for the tyre chips were found to be between 1.13 and 1.16. However, for the sake of the consistency of the mixture calculation, an average value of 1.15 was used throughout, which is comparable with the values of 1.13 to 1.36 reported by Edil and Bosscher (1994). In addition, the specific gravity for the tyre chips is exactly the same as the shredded rubber tyres studied by Youwai and Bergado (2003).

It can be seen that both sand and tyre chips had a great difference in their specific gravities. Thus, it was interesting to examine the density of the sand mixed with various rubber contents. The minimum and maximum densities of S, A, B, C, and D, as well as the mixtures SA, SB, SC, and SD, were investigated in accordance with BS 1377-2 (1990), and are shown in Table 3.2. Note that the sand to rubber ratios employed in the density determination and also subsequently used for the undrained monotonic and cyclic triaxial tests as well as the bender element tests, were based on the initial investigation of the liquefaction characteristics of the mixtures.

It was found that, during the compaction of a mixture underwater the tyre chips floated which caused the determination of maximum density impossible. Thus, the maximum density was determined in dry conditions. The minimum and maximum densities in Mg/m^3 for S, A, B, C, and D are illustrated by Figure 3.3. For the mixtures SA, SB, SC, and SD, they were illustrated by Figure 3.4(a), (b), (c), and (d), respectively. Figure 3.5(a) and (b) depicts the minimum and maximum densities for SA, SB, SC, and SD together, so that a particular mixture but with different sizes of rubber added could be observed.

The minimum and maximum densities of Leighton Buzzard 16/30 sand were 1.509 and 1.839Mg/m^3, respectively. For the tyre chips CT0515, CT1030, CT2060, and CT4010, they were 0.361 and 0.521; 0.380 and 0.553; 0.418 and 0.598; and 0.397 and 0.577Mg/m^3, respectively. It was observed that, regardless of the particle size, all tyre chips had quite a similar range of densities. However, the tyre chips having the smallest size – CT0515, A – had the lowest minimum density. Also, it was observed that the bigger the size of tyre chips the greater the density. When considering the differences between the minimum and maximum densities, it can be seen that the size of tyre chips had little effect, as can be observed in Figure 3.3.

For the mixtures SA, SB, SC, and SD, having sand to rubber ratios of 95:5, 90:10, 80:20, 70:30, 60:40, and 50:50 (see Figure 3.4), it was observed that the higher the percentage of rubber added the lower the minimum and maximum densities. This, however, was anticipated because the specific gravity of the tyre chips was much lower than that of the sand.

Furthermore, it was found that regardless of the size of the rubber mixed, when the mixtures contained the smaller rubber contents of 5% and 10%, only slight differences between the minimum and maximum densities were observed. However, when the rubber portion was increased to 30% and higher, the effect of the size of tyre chips on the minimum and maximum densities of the mixtures was pronounced, especially for the mixtures containing 40% and 50% rubber contents (see Figure 3.5).

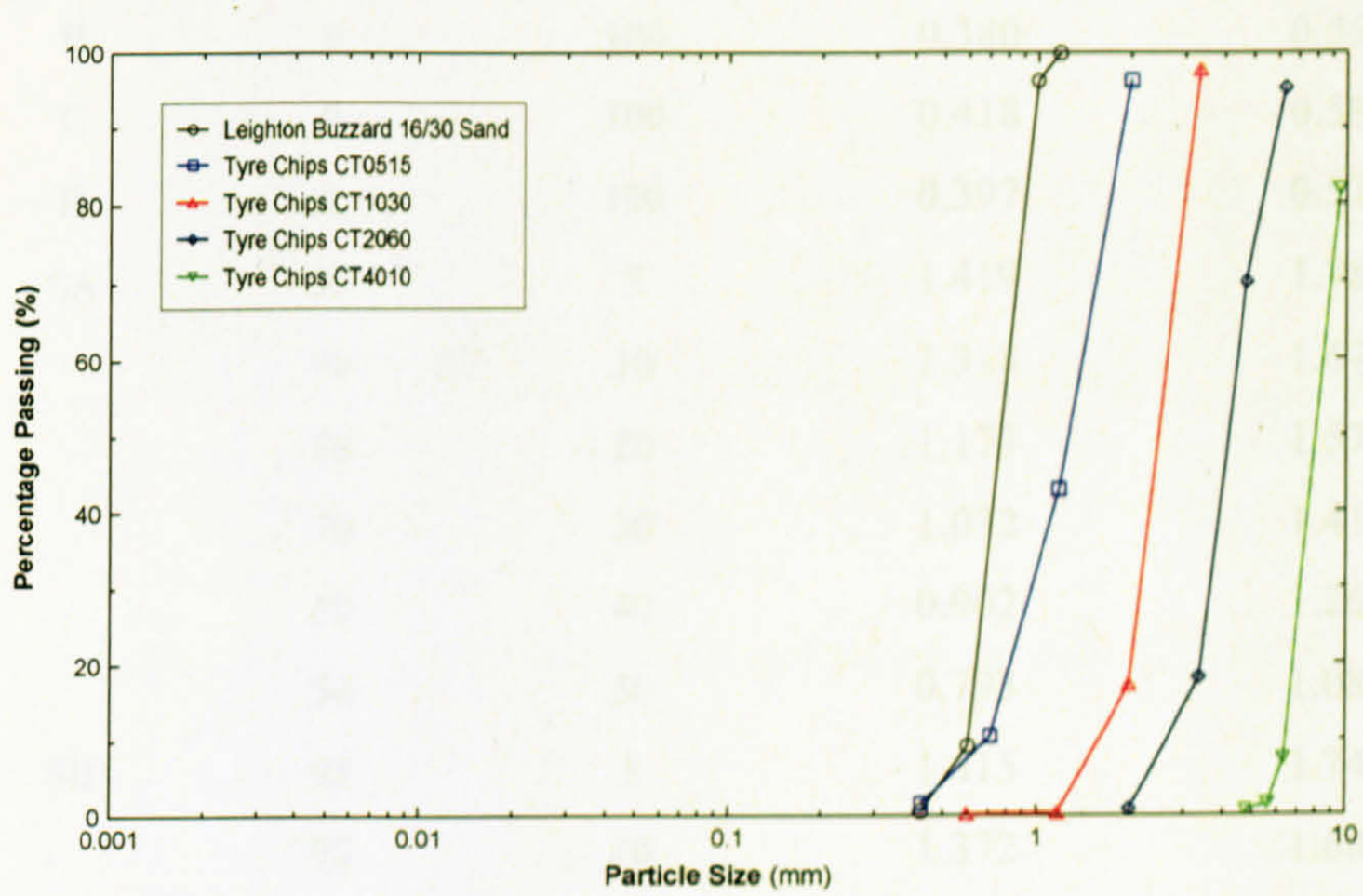

Figure 3. 2 Grain size distribution curves for the tested materials

Table 3. 1 Basic properties of the tested materials

Material	Symbol	Specific Gravity	D_{10} (mm)	D_{30} (mm)	D_{50} (mm)	D_{60} (mm)	Coefficient of Uniformity, Cu	Coefficient of Curvature, Cc	Particle Size Ratio D_r/D_s
Leighton Buzzard 16/30 Sand	S	2.66	0.60	0.66	0.70	0.82	1.37	0.89	-
Tyre Chips CT0515	A	1.15*	0.70	0.95	1.20	1.30	1.86	0.99	1.7
Tyre Chips CT1030	B	1.15*	1.40	2.00	2.30	2.60	1.86	1.10	3.3
Tyre Chips CT2060	C	1.15*	2.00	2.50	4.00	4.20	2.10	0.74	5.7
Tyre Chips CT4010	D	1.15*	5.10	7.00	8.00	8.20	1.61	1.17	11.4

Table 3. 2 Minimum and maximum densities of pure sand, tyre chips, and sand mixed with tyre chips

Group	Mixture (by Solid Volume)		Minimum Dry Density (Mg/cu.m)	Maximum Dry Density (Mg/cu.m)
	Sand (%)	Rubber (%)		
S	100	0	1.509	1.839
A	0	100	0.361	0.521
B	0	100	0.380	0.553
C	0	100	0.418	0.598
D	0	100	0.397	0.577
SA	95	5	1.419	1.787
	90	10	1.318	1.679
	80	20	1.173	1.575
	70	30	1.032	1.412
	60	40	0.902	1.267
	50	50	0.793	1.083
SB	95	5	1.415	1.746
	90	10	1.372	1.689
	80	20	1.229	1.587
	70	30	1.118	1.492
	60	40	0.979	1.341
	50	50	0.858	1.211
SC	95	5	1.448	1.777
	90	10	1.419	1.747
	80	20	1.341	1.655
	70	30	1.256	1.562
	60	40	1.124	1.437
	50	50	1.005	1.320
SD	95	5	1.458	1.767
	90	10	1.432	1.742
	80	20	1.381	1.668
	70	30	1.351	1.589
	60	40	1.269	1.506
	50	50	1.100	1.377

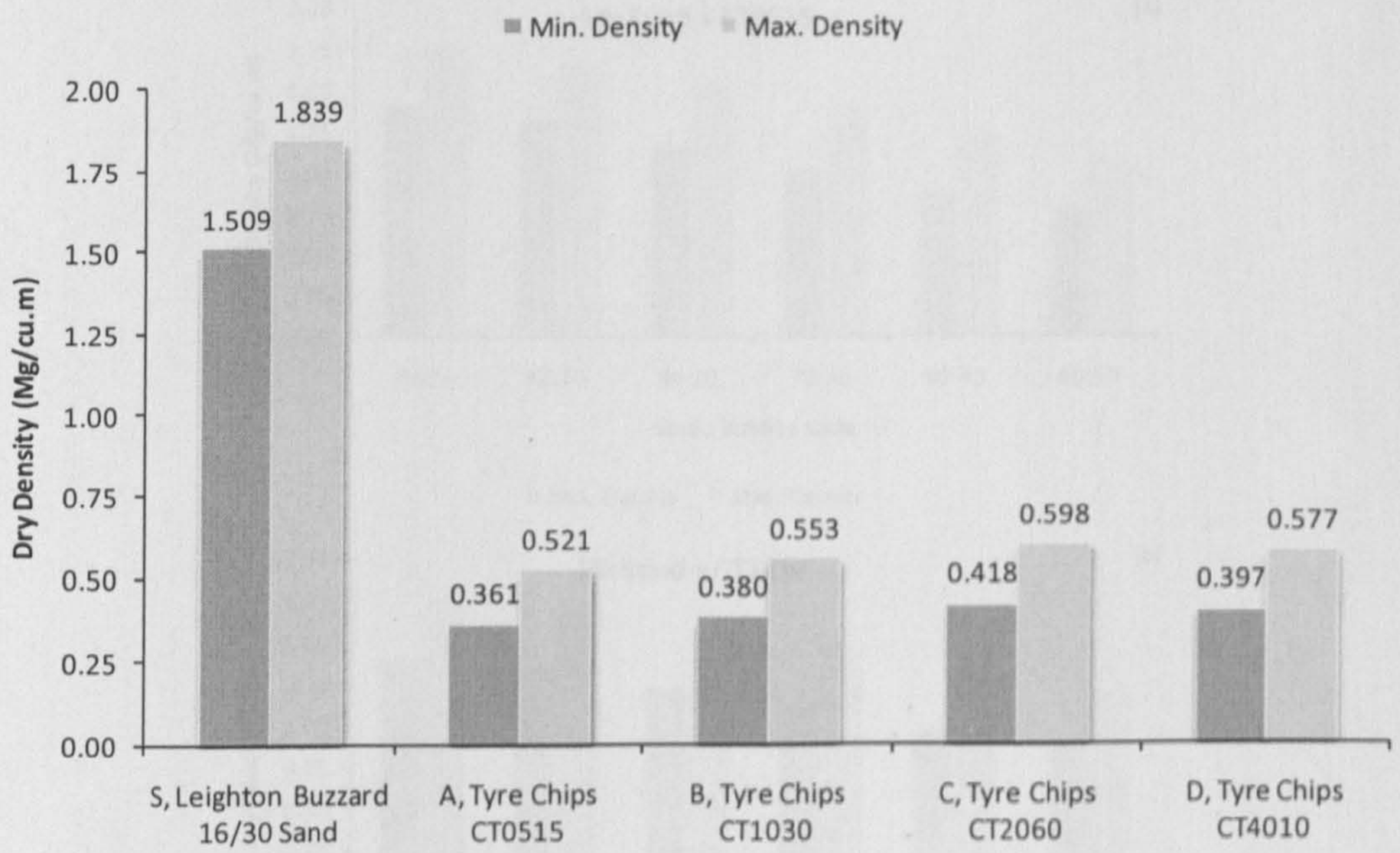

Figure 3. 3 Minimum and maximum densities for S, A, B, C, and D

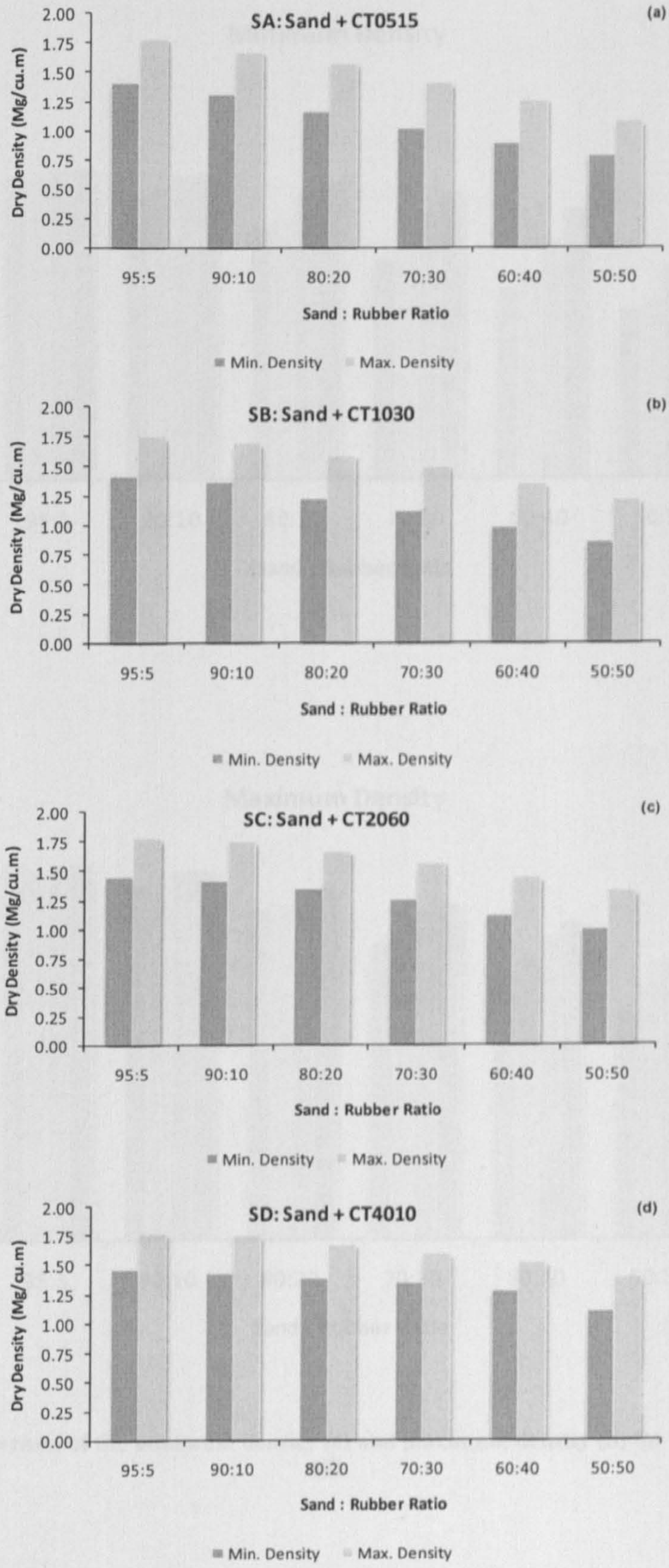

Figure 3. 4 Minimum and maximum densities for SA (a), SB (b), SC (c), and SD (d)

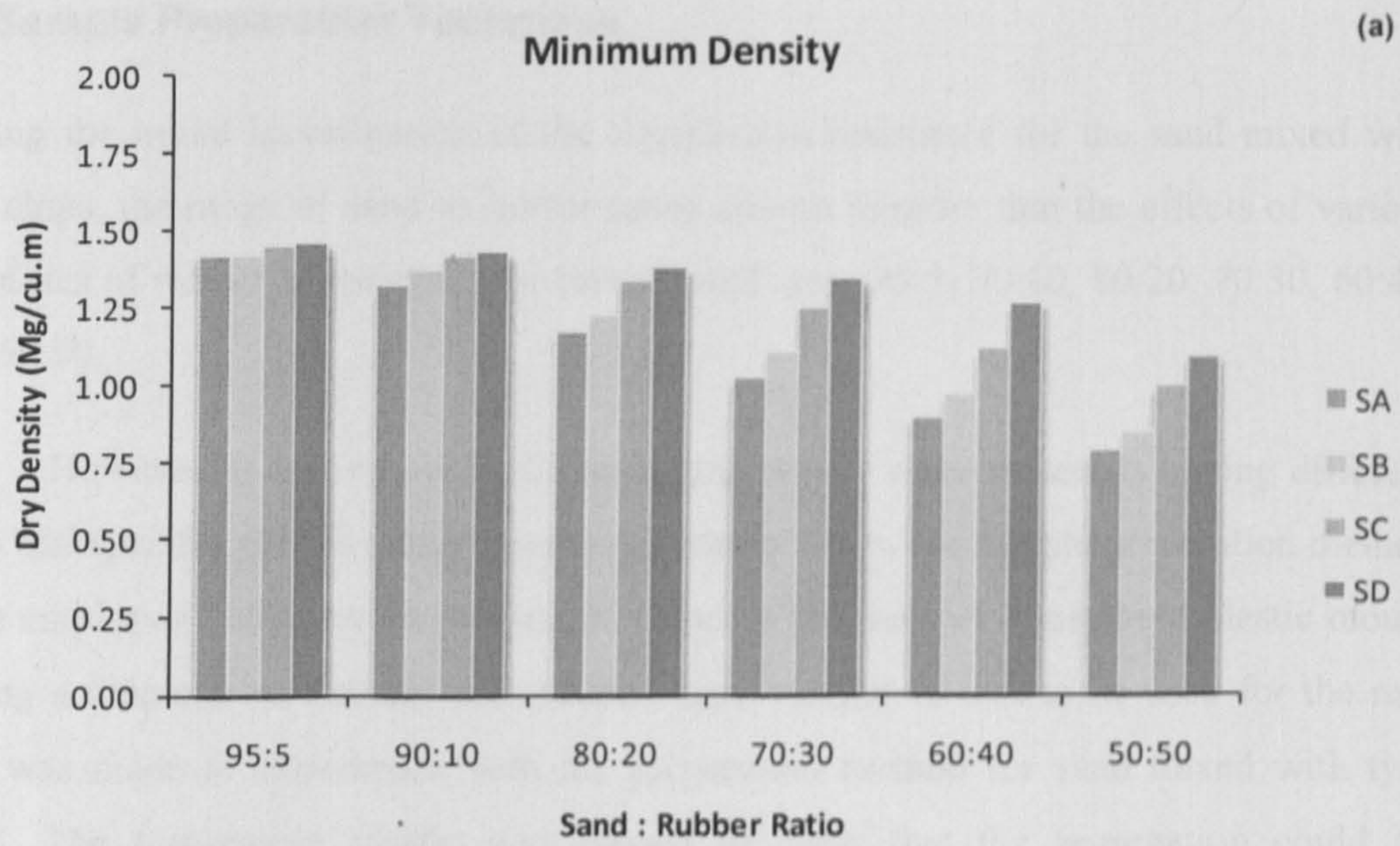

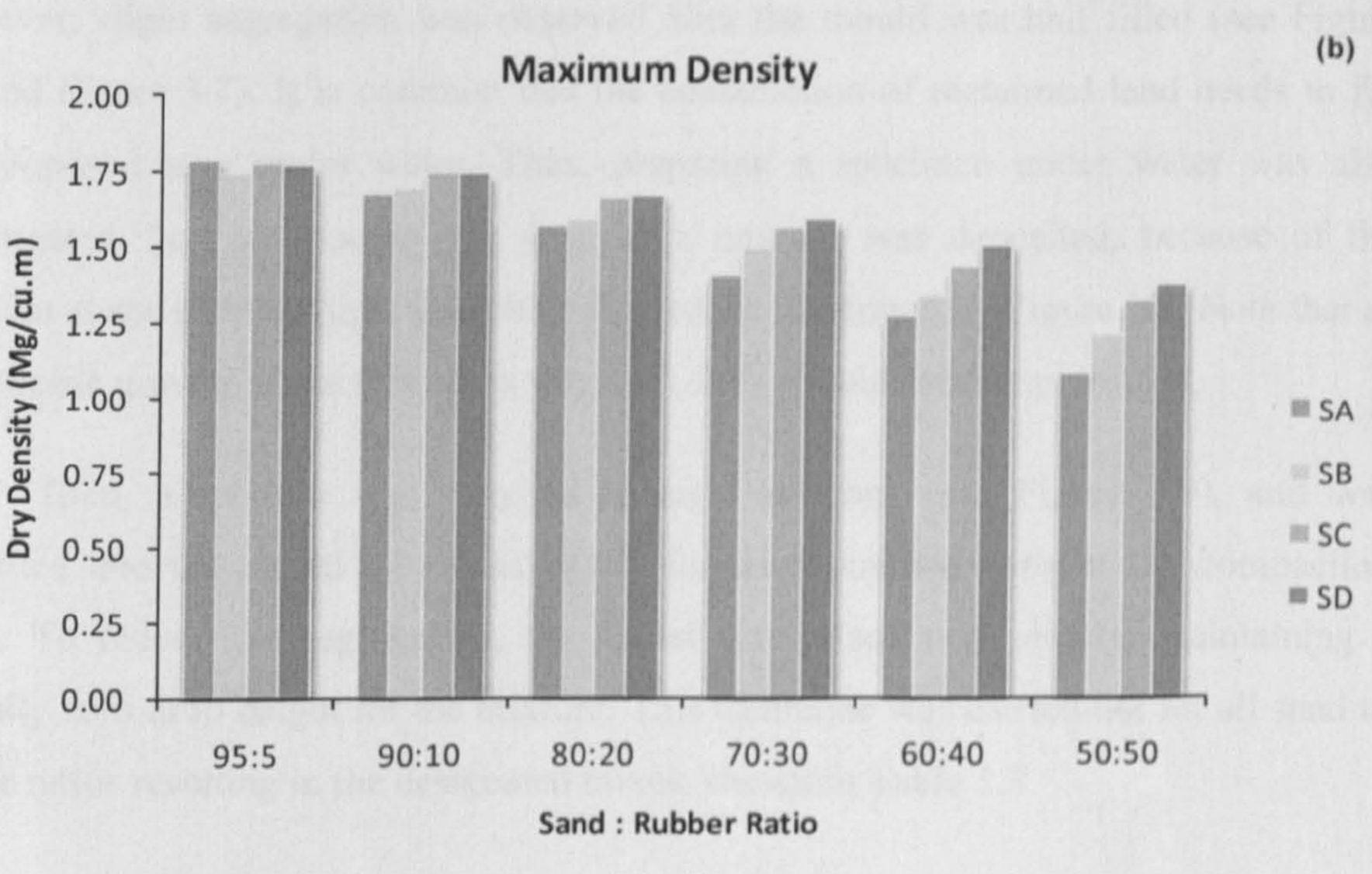

Figure 3. 5 Comparison of the minimum density (a) and maximum density (b) for SA, SB, SC, and SD

3.4 Sample Preparation Technique

During the initial investigation of the liquefaction resistance for the sand mixed with tyre chips, the range of sand to rubber ratios chosen in order that the effects of various quantities of rubber added could be investigated were 95:5, 90:10, 80:20, 70:30, 60:40, and 50:50.

However, it was recognised that mixing two or more materials having different sizes and specific gravities may cause segregation. Thus, the sample preparation method to be employed had to avoid causing this kind of problem. A transparent plastic mould having a diameter of 100mm and 200mm high, similar to that to be used for the real test, was made to experiment with the preparation method for sand mixed with tyre chips. The transparent plastic was chosen in order that the segregation could be observed from the sides as well.

First, a funnel was mounted at a certain level, and a mixture was poured through. However, slight segregation was observed after the mould was half filled (see Figure 3.6 and Figure 3.7). It is common that the construction of reclaimed land needs to fill the proposed area under water. Thus, preparing a specimen under water was also investigated. Not surprisingly, as soon as a mixture was deposited, because of the irregular shape of tyre chips, the rubber floated, as illustrated by Figure 3.8. Note that as the specific gravity of the tyre chips was 1.15, they should submerge instead.

Then, a mixture was weighed in eight portions (see Figure 3.9), and was deposited into the mould by means of dry funnel deposition without any compaction effort. To reduce the segregation, the funnel was raised very slowly, maintaining a virtually zero drop height for the mixture. This technique was carried out for all sand to rubber ratios resulting in the designated mixes, shown in Table 3.3

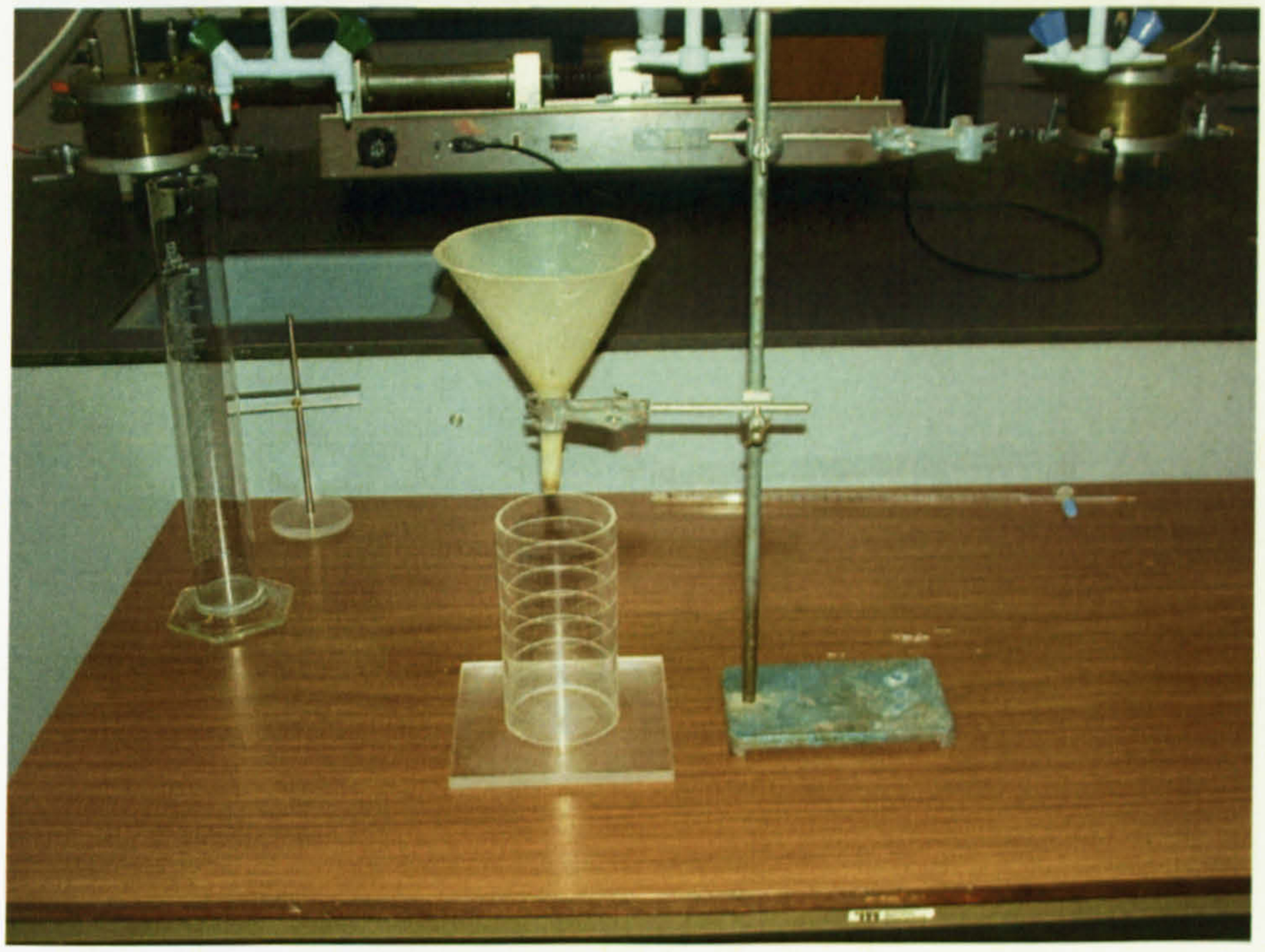

Figure 3. 6 Set up for segregation test of sand-rubber mixtures

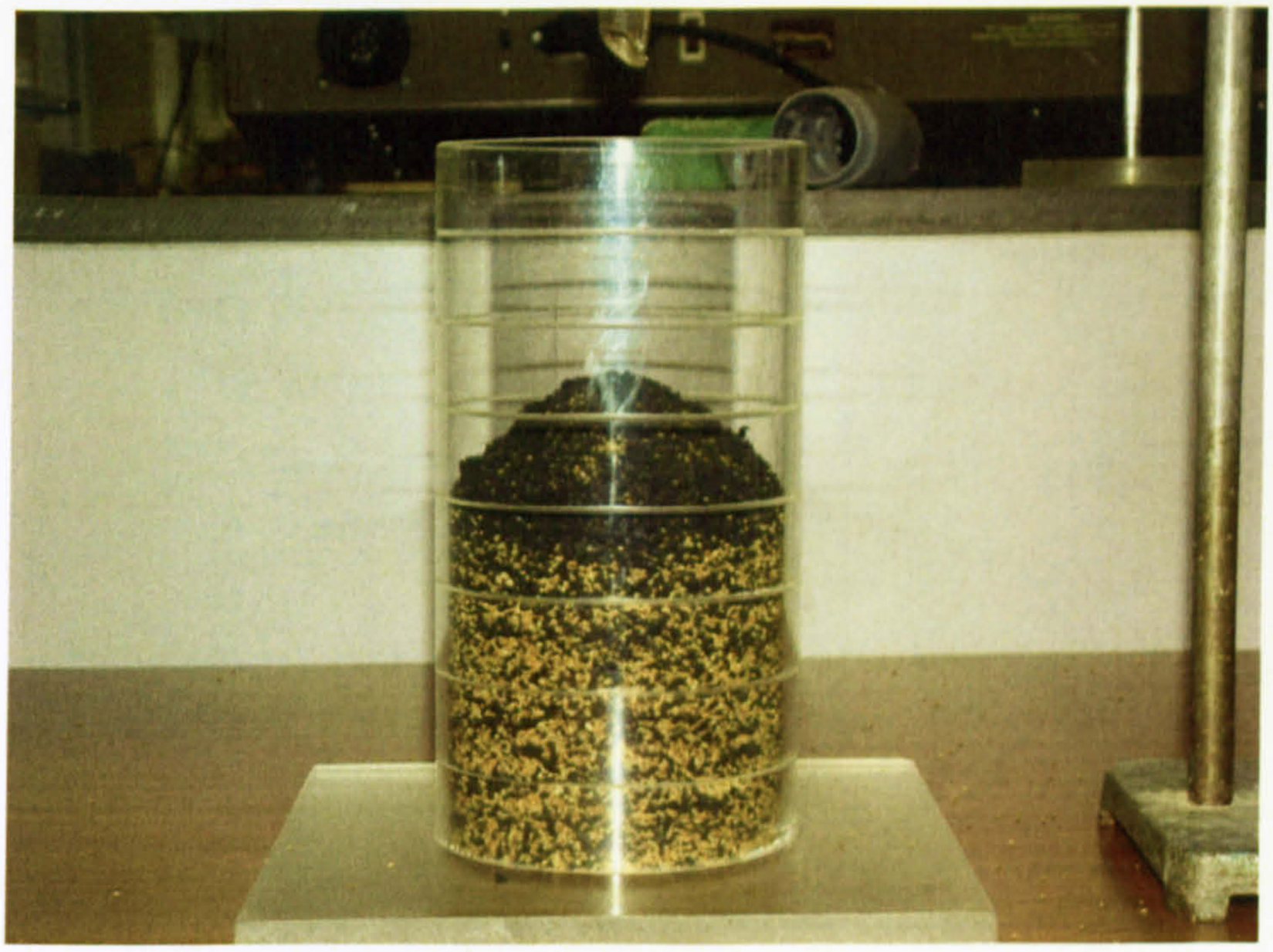

Figure 3. 7 Segregation of sand mixed with tyre chips

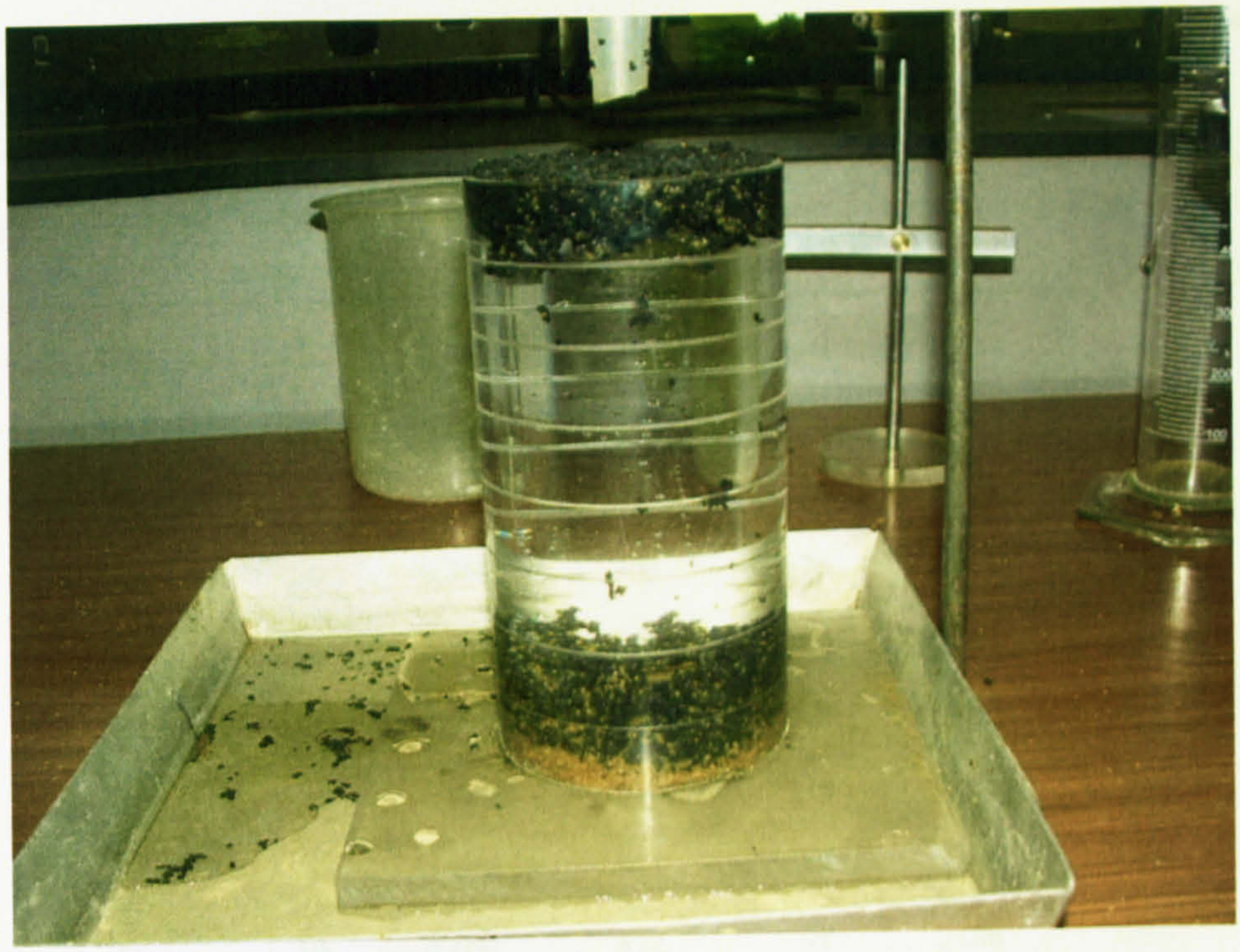

Figure 3. 8 Tyre chips floating due to air trapped around their edges

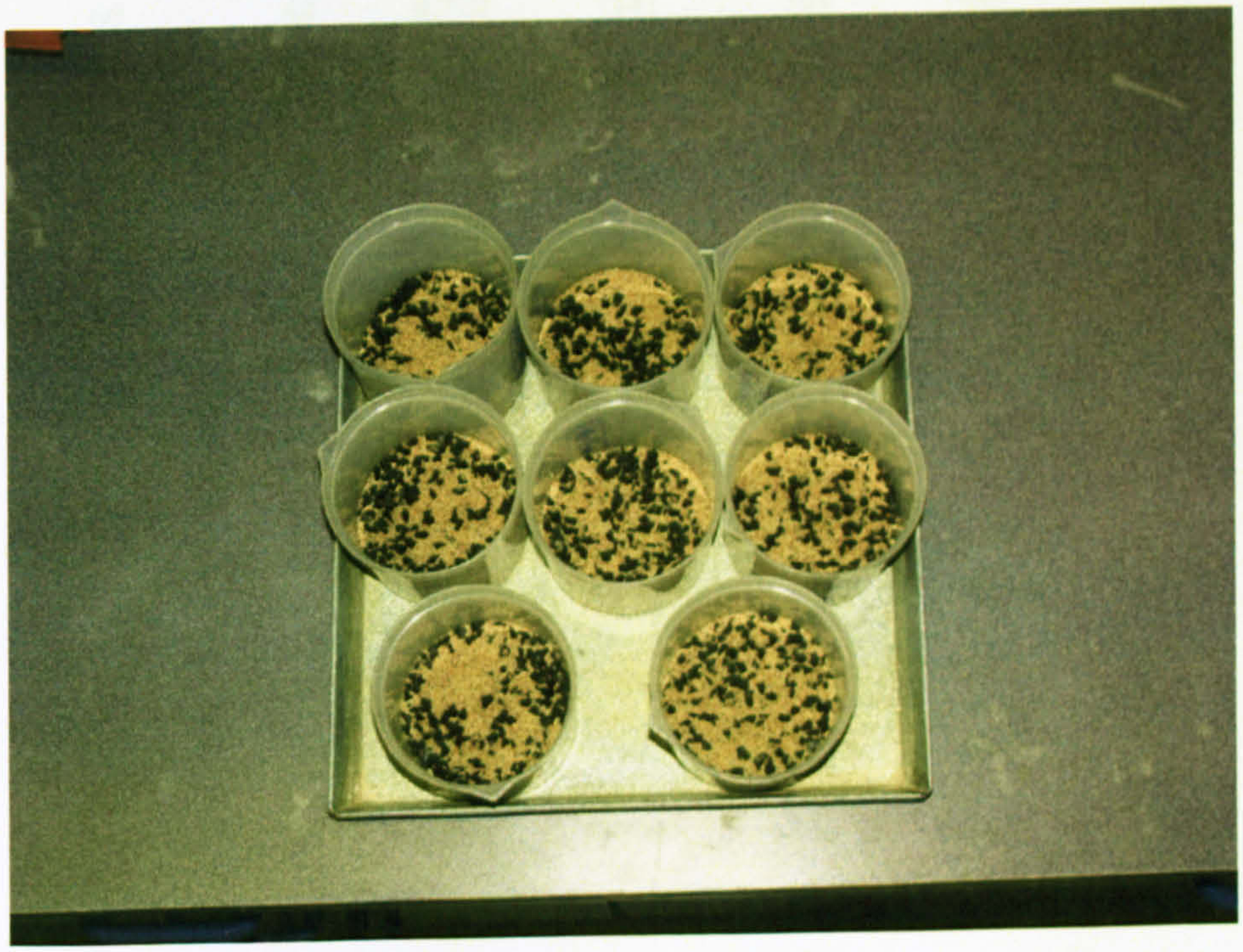

Figure 3. 9 Eight weighed portions of sand-rubber mixture

Table 3. 3 Designated sand-tyre chip mixtures for the undrained monotonic triaxial and undrained cyclic triaxial tests

Group	Mixture (by Solid Volume)		e_o	Vol. of Sand	Vol. of Rubber	Wt. of Sand	Wt. of Rubber	Global Wt.
	Sand (%)	Rubber (%)		(cu.cm)	(cu.cm)	(g)	(g)	(g)
S	100	0	0.690	918	0	2443	0	2443
SA	95	5	0.700	867	46	2307	52	2360
	90	10	0.708	818	91	2176	105	2280
	80	20	0.766	703	176	1870	202	2072
	70	30	0.844	589	252	1567	290	1858
	60	40	0.908	488	325	1298	374	1672
	50	50	0.945	399	399	1061	459	1520
SB	95	5	0.700	867	46	2307	52	2360
	90	10	0.700	822	91	2186	105	2291
	80	20	0.700	730	183	1943	210	2153
	70	30	0.710	635	272	1690	313	2003
	60	40	0.720	541	361	1440	415	1855
	50	50	0.810	429	429	1140	493	1633
SC	95	5	0.676	880	46	2340	53	2393
	90	10	0.644	850	94	2260	109	2369
	80	20	0.615	769	192	2045	221	2266
	70	30	0.591	683	293	1817	337	2154
	60	40	0.566	595	396	1582	456	2038
	50	50	0.570	494	494	1315	568	1883
SD	95	5	0.671	882	46	2347	53	2400
	90	10	0.641	851	95	2264	109	2373
	80	20	0.604	774	193	2059	223	2281
	70	30	0.552	700	300	1862	345	2207
	60	40	0.528	609	406	1621	467	2088
	50	50	0.470	528	528	1404	607	2011

3.5 Test Programmes

Three types of test were conducted, namely undrained monotonic triaxial compression and extension tests, undrained cyclic triaxial tests, and bender element tests. The undrained monotonic shearing test was performed to provide the stress-strain and pore water pressure characteristics of the sand as well as sand mixed with tyre chips. The cyclic strength was determined by employing a computer-controlled cyclic triaxial testing system. Cyclic loading specimens were subjected to bender element tests after consolidation but before the cyclic loading was applied.

3.5.1 Undrained Monotonic Triaxial Tests

A total of 25 undrained triaxial compression tests and 25 undrained triaxial extension tests were performed. Each series of the compression and extension tests comprised one pure sand specimen, six SA mixtures, six SB mixtures, six SC mixtures, and six SD mixtures. The name of a test was designed to designate the type of testing, type of tyre chips mixed, and amount of tyre chips added. For example, for the test number TC95A; TC denotes the undrained triaxial compression test (TE denotes the undrained triaxial extension test); 95 tells the percentage of the sand (the remaining content is the rubber; which is, for this case, 5%); and A indicates the type of tyre chips mixed. All test numbers are shown in Table 3.4.

Table 3. 4 List of undrained monotonic triaxial compression and extension tests

Group	Mixture (by Solid Volume)		Test Number	
	Sand (%)	Rubber (%)	Undrained Triaxial Compression Test	Undrained Triaxial Extension Test
S	100	0	TC100S	TE100S
SA	95	5	TC95SA	TE95SA
	90	10	TC90SA	TE90SA
	80	20	TC80SA	TE80SA
	70	30	TC70SA	TE70SA
	60	40	TC60SA	TE60SA
	50	50	TC50SA	TE50SA
SB	95	5	TC95SB	TE95SB
	90	10	TC90SB	TE90SB
	80	20	TC80SB	TE80SB
	70	30	TC70SB	TE70SB
	60	40	TC60SB	TE60SB
	50	50	TC50SB	TE50SB
SC	95	5	TC95SC	TE95SC
	90	10	TC90SC	TE90SC
	80	20	TC80SC	TE80SC
	70	30	TC70SC	TE70SC
	60	40	TC60SC	TE60SC
	50	50	TC50SC	TE50SC
SD	95	5	TC95SD	TE95SD
	90	10	TC90SD	TE90SD
	80	20	TC80SD	TE80SD
	70	30	TC70SD	TE70SD
	60	40	TC60SD	TE60SD
	50	50	TC50SD	TE50SD

3.5.2 Undrained Cyclic Triaxial Tests and Bender Element Tests

The undrained cyclic triaxial tests comprised 106 tests; including five pure sand specimens, 25 SA mixtures, 25 SB mixtures, 26 SC mixtures, and 25 SD mixtures. Each of these was also subjected to a bender element test. The test number for both undrained cyclic triaxial tests and bender element tests was designed so that, similar to the undrained monotonic triaxial tests, it gave full information for a mixture. For example, test number CT95A365; first two letters CT indicates the cyclic triaxial test (BE is for the bender element test), 95 indicates that the mixture contains 95% sand and 5% tyre chips, A indicates the type of tyre chips mixed, and the last three numbers 365 denotes the applied single-amplitude cyclic deviator stress (in kPa) multiplied by 10 (36.5 kPa for this case). The list for both undrained cyclic triaxial tests and bender element tests for pure sand S is shown in Table 3.5. Tables 3.6 – 3.9 show the lists of test numbers for SA, SB, SC, and SD, respectively.

Table 3. 5 List of undrained cyclic triaxial tests and bender element tests for S

Group	Mixture (by Solid Volume)		Test Number	
	Sand (%)	Rubber (%)	Undrained Cyclic Triaxial Test	Bender Elements Test
S	100	0	CT100S430	BE100S430
			CT100S370	BE100S370
			CT100S320	BE100S320
			CT100S290	BE100S290
			CT100S250	BE100S250

Table 3. 6 List of undrained cyclic triaxial tests and bender element tests for SA

Group	Mixture (by Solid Volume)		Test Number	
	Sand (%)	Rubber (%)	Undrained Cyclic Triaxial Test	Bender Elements Test
SA	95	5	CT95SA365	BE95SA365
			CT95SA296	BE95SA296
			CT95SA240	BE95SA240
			CT95SA225	BE95SA225
			CT95SA205	BE95SA205
	90	10	CT90SA285	BE90SA285
			CT90SA220	BE90SA220
			CT90SA185	BE90SA185
			CT90SA165	BE90SA165
	80	20	CT80SA280	BE80SA280
			CT80SA230	BE80SA230
			CT80SA195	BE80SA195
			CT80SA160	BE80SA160
	70	30	CT70SA350	BE70SA350
			CT70SA270	BE70SA270
			CT70SA245	BE70SA245
			CT70SA230	BE70SA230
	60	40	CT60SA420	BE60SA420
			CT60SA370	BE60SA370
			CT60SA340	BE60SA340
			CT60SA310	BE60SA310
	50	50	CT50SA515	BE50SA515
			CT50SA465	BE50SA465
			CT50SA420	BE50SA420
			CT50SA370	BE50SA370

Table 3. 7 List of undrained cyclic triaxial tests and bender element tests for SB

Group	Mixture (by Solid Volume)		Test Number	
	Sand (%)	Rubber (%)	Undrained Cyclic Triaxial Test	Bender Elements Test
SB	95	5	CT95SB270	BE95SB270
			CT95SB245	BE95SB245
			CT95SB225	BE95SB225
			CT95SB210	BE95SB210
	90	10	CT90SB260	BE90SB260
			CT90SB235	BE90SB235
			CT90SB213	BE90SB213
			CT90SB190	BE90SB190
	80	20	CT80SB256	BE80SB256
			CT80SB217	BE80SB217
			CT80SB195	BE80SB195
			CT80SB170	BE80SB170
	70	30	CT70SB340	BE70SB340
			CT70SB300	BE70SB300
			CT70SB260	BE70SB260
			CT70SB200	BE70SB200
	60	40	CT60SB550	BE60SB550
			CT60SB435	BE60SB435
			CT60SB350	BE60SB350
			CT60SB310	BE60SB310
	50	50	CT50SB540	BE50SB540
			CT50SB455	BE50SB455
			CT50SB445	BE50SB445
			CT50SB405	BE50SB405
			CT50SB350	BE50SB350

Table 3. 8 List of undrained cyclic triaxial tests and bender element tests for SC

Group	Mixture (by Solid Volume)		Test Number	
	Sand (%)	Rubber (%)	Undrained Cyclic Triaxial Test	Bender Elements Test
SC	95	5	CT95SC380	BE95SC380
			CT95SC360	BE95SC360
			CT95SC300	BE95SC300
			CT95SC250	BE95SC250
			CT95SC230	BE95SC230
	90	10	CT90SC365	BE90SC365
			CT90SC310	BE90SC310
			CT90SC260	BE90SC260
			CT90SC210	BE90SC210
	80	20	CT80SC320	BE80SC320
			CT80SC300	BE80SC300
			CT80SC250	BE80SC250
			CT80SC230	BE80SC230
			CT80SC212	BE80SC212
	70	30	CT70SC430	BE70SC430
			CT70SC350	BE70SC350
			CT70SC320	BE70SC320
			CT70SC280	BE70SC280
	60	40	CT60SC550	BE60SC550
			CT60SC440	BE60SC440
			CT60SC370	BE60SC370
			CT60SC300	BE60SC300
	50	50	CT50SC560	BE50SC560
			CT50SC495	BE50SC495
			CT50SC430	BE50SC430
			CT50SC345	BE50SC345

Table 3. 9 List of undrained cyclic triaxial tests and bender element tests for SD

Group	Mixture (by Solid Volume)		Test Number	
	Sand (%)	Rubber (%)	Undrained Cyclic Triaxial Test	Bender Elements Test
SD	95	5	CT95SD350	BE95SD350
			CT95SD325	BE95SD325
			CT95SD280	BE95SD280
			CT95SD240	BE95SD240
	90	10	CT90SD360	BE90SD360
			CT90SD305	BE90SD305
			CT90SD270	BE90SD270
			CT90SD225	BE90SD225
	80	20	CT80SD322	BE80SD322
			CT80SD240	BE80SD240
			CT80SD220	BE80SD220
			CT80SD205	BE80SD205
	70	30	CT70SD420	BE70SD420
			CT70SD330	BE70SD330
			CT70SD300	BE70SD300
			CT70SD250	BE70SD250
			CT70SD210	BE70SD210
	60	40	CT60SD555	BE60SD555
			CT60SD445	BE60SD445
			CT60SD340	BE60SD340
			CT60SD305	BE60SD305
	50	50	CT50SD550	BE50SD550
			CT50SD400	BE50SD400
			CT50SD365	BE50SD365
			CT50SD300	BE50SD300

CHAPTER 4

EQUIPMENT AND TESTING METHODS

4.1 Introduction

To achieve the aims of the research, three testing systems were proposed: (1) a standard triaxial testing system, (2) a computer-controlled cyclic triaxial testing system, and (3) bender elements. The cyclic triaxial testing system was employed to determine the cyclic strength of the sand as well as sand mixed with tyre chips. It was conducted under undrained conditions such that the behaviour of pore water pressure generated by seismic loading could be studied. The monotonic triaxial test was therefore also performed under undrained conditions. The bender element test was accomplished using the same specimens used for the cyclic triaxial test. The aim of the bender element test was to determine the shear wave velocity and hence the small-strain shear modulus. The bender element test was performed for a range of frequencies after the consolidation had been finished, and just before the cyclic loading was applied.

4.2 Undrained Monotonic Triaxial Test

4.2.1 Equipment and Principles of Undrained Monotonic Triaxial Test

One critical feature of the triaxial test is that the drainage of a soil under test can be controlled. This was accomplished by a drainage connection through the base pedestal. To prevent the soil particles migrating through this connection, a porous disc was placed on the top of the pedestal. Typical details of a triaxial cell accommodating a drainage line and pressure lines are schematically illustrated by Figure 4.1.

The standard triaxial testing system employed in this research basically comprised a conventional loading frame manufactured by Wykeham Farrance; a pressure system and pressure gauges; a water/paraffin volume change unit; a 7-Bar

Druck pore water pressure transducer and a transducer indicator; and a de-aired water cell. The loading frame was fitted with a proving ring and a dial gauge providing the measurement of axial load and axial strain, respectively. Attached to a column of the frame was a control box used for lowering/raising the triaxial base as well as controlling the strain rate. The CO_2 facility was added into the system to accelerate the saturation process by flushing specimens to displace air from the voids and replace it by CO_2. This process aids saturation as CO_2 can be more easily displaced or dissolved by the water during the saturation process.

A de-aired water reservoir was added and placed around 1m above the triaxial base providing a pressure head enough for seeping de-aired water through the specimen after it had been flushed with CO_2. The pressure system, pore water pressure gauge and proving ring were calibrated by using a Budenberg Dead Weight Tester. The whole system is illustrated in Figure 4.2.

For undrained monotonic compression tests a standard plastic top cap was employed. After the consolidation and before shearing, the loading ram was lowered until it was just sitting on the top cap. This was confirmed by the slight movement of the dial gauge within the proving ring. For the extension test, however, the connection between the top cap and the loading ram must be fixed so that an extension force could be applied. This was accomplished by making a new top cap having an internal thread so that it could be attached to the ram. The connection for the extension test is illustrated in Figure 4.3.

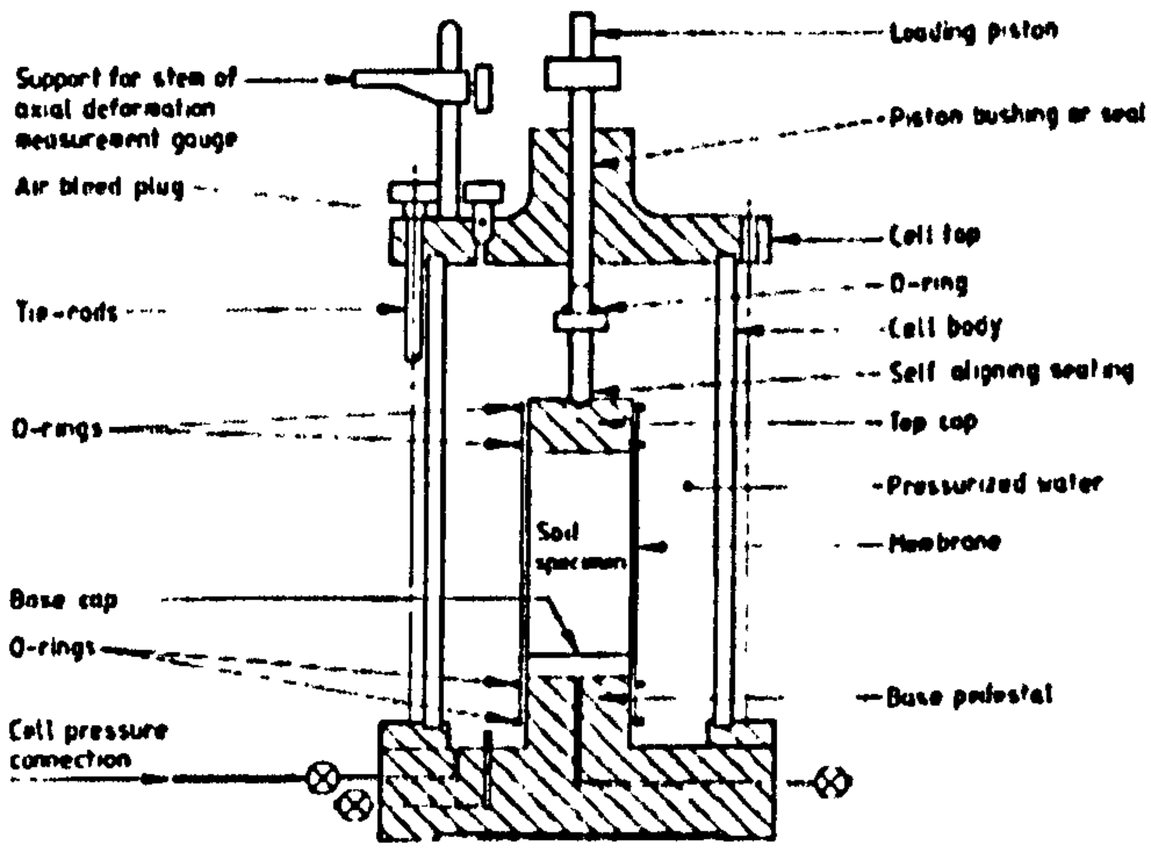

Figure 4. 1 Typical details of triaxial cell (after BS1377, 1990)

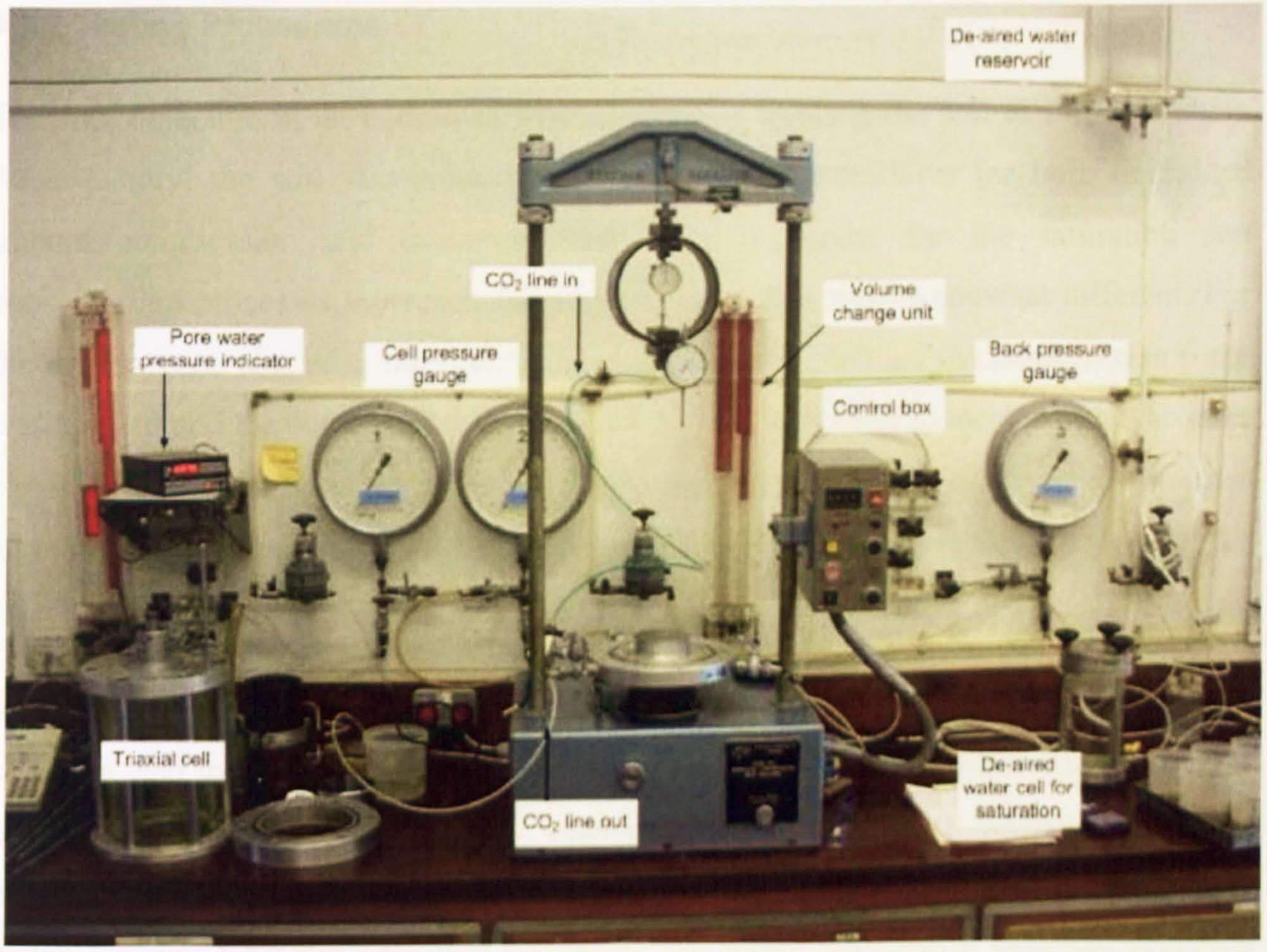

Figure 4. 2 Undrained monotonic triaxial test set up

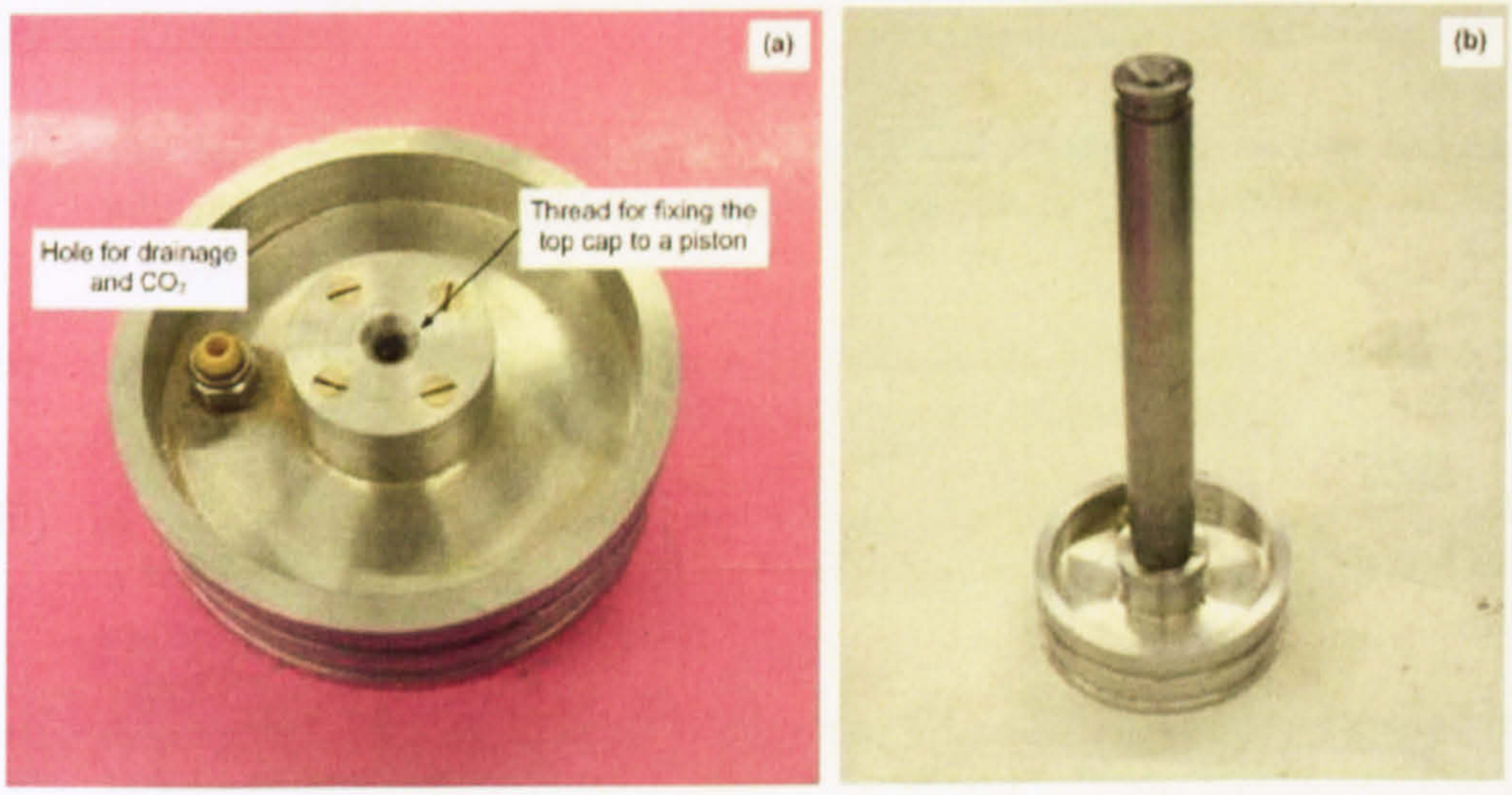

Figure 4. 3 Top cap and piston for undrained monotonic triaxial extension test

4.2.2 Testing Procedures

The first objective in an undrained triaxial test was to bring the soil to full saturation. Subsequently, the soil was consolidated. The testing procedures for both undrained triaxial compression and extension tests were the same for the saturation and consolidation processes; however, the shearing processes were somewhat different. For the compression test, after the consolidation had been completed the compression force was applied and the force read from the proving ring was used to calculate the deviator stress. In this case the major principal stress was the summation of the deviator stress and the cell pressure; and, the minor principal stress was the cell pressure.

For the extension test, the top cap was fixed to the specimen, and the axial load was reduced by lowering the base at a constant rate. The force read from the proving ring was also used to calculate the deviator stress. However, the horizontal stress now became the major principal stress; whereas, the vertical stress became the minor principal stress. For both compression and extension tests, during the shearing the pore water pressure was also recorded and hence the major and minor effective principal stresses were obtained. The test procedures for the undrained monotonic triaxial compression and extension tests are described in detail below:

A) <u>Sample Preparation</u>

(i) The base pedestal was greased; a rubber membrane was put on and sealed with O-rings; and a porous disc was placed on the pedestal (see Figure 4.4(a)).

(ii) The mould was assembled; any potential leak from the mould and the mould-base interface was plugged using plasticine (see Figure 4.4(b)).

(iii) A full vacuum was applied in-between the inner mould and the rubber membrane; to make sure that the membrane was completely attached to the mould.

(iv) A mixture was weighed in eight portions using Table 3.3 in Chapter 3 Materials and Testing Programmes.

(v) Each portion of the mixture was stirred and mixed thoroughly using a wooden stick until it was well blended.

(vi) Each portion was deposited by means of a dry funnel maintaining the drop height of the mixture to virtually zero (see Figure 4.4(c)); each layer was levelled using the wooden stick.

(vii) After the last (eighth) portion had been deposited, a porous disc was placed, followed by a top cap; the level was checked (see Figure 4.4(d), (e)). Note that for the compression test, a normal top cap was used; but, for the extension test, the top cap shown in Figure 4.3 was employed.

(viii) The top cap was enclosed by the membrane and sealed with O-rings.

(ix) A small nylon pipe was connected from the top of the top cap to the CO_2 line-out (see Figure 4.4(f)). Note that this line was also used for the discharge for seeping de-aired water after CO_2 had been flushed.

(x) A small vacuum of about -20kPa was applied through the back pressure line to sustain the specimen, and then the mould was dismantled. It was ensured that the difference between the applied vacuum and the first step of cell pressure to be applied was lower than the desired consolidation pressure, otherwise, the specimen would be overconsolidated.

(xi) At this stage the dimensions of the specimen were taken. For the height two opposite vertical sides were measured; whereas; for the diameter, top, middle, and bottom were measured using a micrometer and averaged. Note that the average for the diameter was determined from: [top + 2(middle) + bottom] / 4.

(xii) The triaxial cell lid was secured. For the compression test, the loading piston was lowered to just touch the top cap (see Figure 4.4(g)). For the extension test, however, the special loading piston having the external thread was screwed to the specific top cap having the internal thread so that the connection was a fixed one.

(xiii) The triaxial cell was filled with water (see Figure 4.4(h)).

(xiv) The initial pore water pressure and the initial level of the volume change unit were recorded.

B) <u>Saturation</u>

(i) A first cell pressure step of 50kPa was applied; in the meantime, the small vacuum applied for sustaining the specimen was slowly released.

(ii) The specimen was percolated with CO_2 using a pressure of about 10kPa for 10 minutes. Note that the line for discharging the CO_2 was submerged in a half-full jar of water so that the bubbles could be observed. The specimen was flushed with de-aired water from the reservoir for around 10 minutes, or until visibly fully wet. At this stage, the *B* value was already over 0.90.

(iii) A first back pressure step of 40kPa was applied, keeping a stress difference of 10kPa. The next increment for the cell and back pressure was 50kPa. For example, for the second step, cell pressure = 100kPa and back pressure = 90kPa.

(iv) To check for the next increment of cell and back pressure, the drainage valve was closed and the pore water pressure was observed over a 1-minute interval. If the change was less than 1% of the confining pressure, it was assumed to be stabilised, and the next step of the pressure could be applied.

(v) To check *B* value:

- The drainage valve was closed.
- A change in cell pressure of 50kPa ($\Delta\sigma_3$) was applied.
- The change of pore water pressure (Δu) due to the increase of cell pressure of 50kPa was recorded.
- Then *B* was calculated by $B = \Delta u / \Delta\sigma_3$.
- Only *B* values equal to or greater than 0.97 indicating full saturation were accepted; otherwise, a specimen was discarded.

C) Consolidation and shearing

(i) At the end of the saturation the effective stress was 10kPa. Note that for all undrained monotonic triaxial tests, for the sake of the consistency of the test results, the final cell pressure and back pressure before the consolidation were 200kPa and 190kPa, respectively.

(ii) The drainage valve was shut; then, the cell pressure was slowly increased from 200kPa to 290kPa, resulting in a consolidation pressure of 100kPa. Note that the increase of pore water pressure should be virtually equal to the increase of cell pressure; otherwise, there might be leaks in the system or membrane.

(iii) The drainage valve was opened to allow the specimen to consolidate. The consolidation period for all specimens was 1 hr. The water coming out of the specimen was measured and recorded for calculating the void ratio.

(iv) After the consolidation, the drainage valve was closed to create the undrained conditions for the shearing.

(v) With respect to the compression and extension tests, the specimen was sheared by raising and lowering the triaxial base at a rate of 0.5mm/min. The reading was taken manually for every 0.1% strain for the strain range between 0 – 1%. Then it was read every 0.5% until the axial train reached 5%. From 5% strain until finish, the reading was taken every 1% strain.

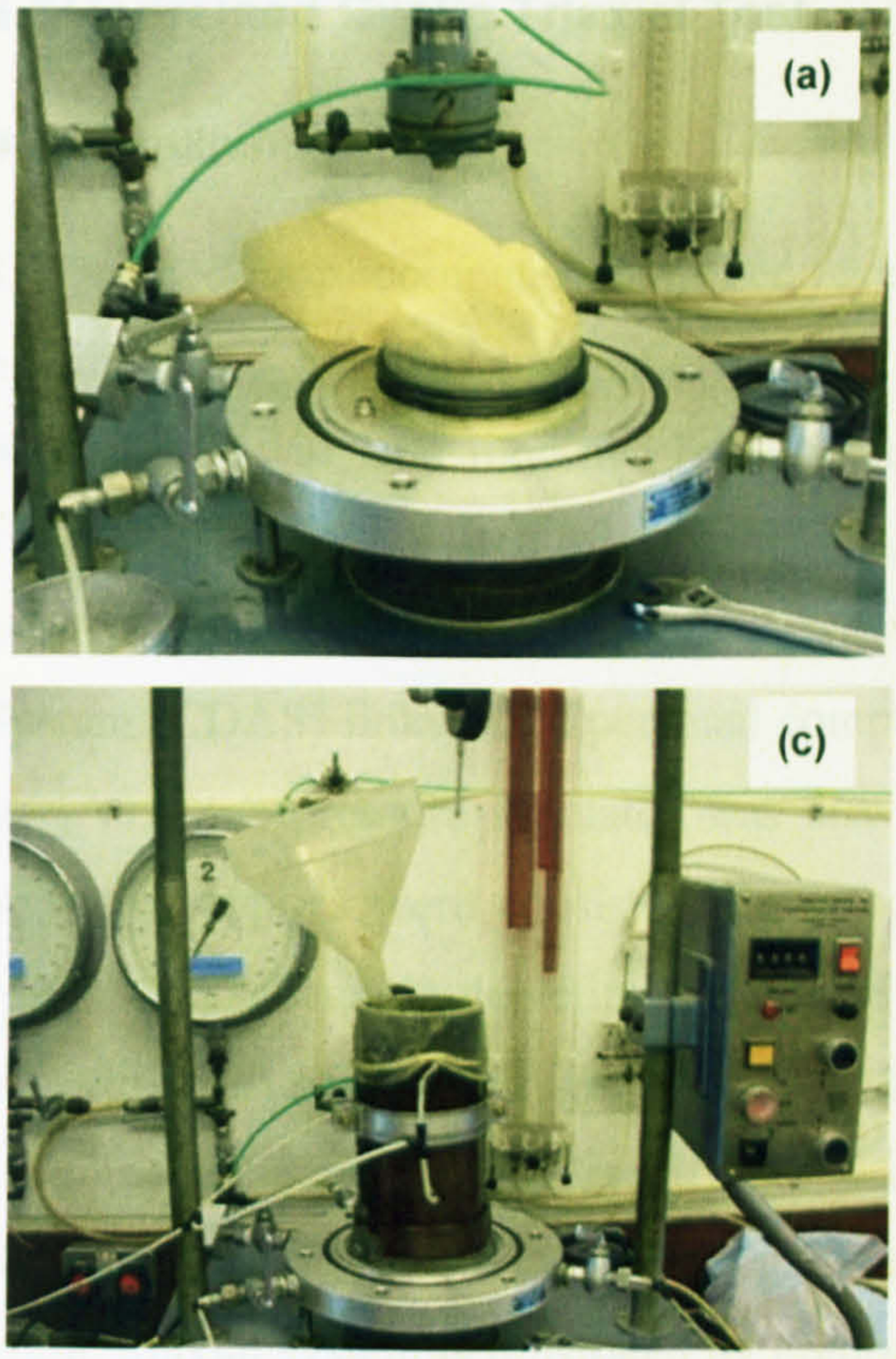

Figure 4. 4 Test procedures for undrained monotonic triaxial test

4.3 Undrained Cyclic Triaxial Test

4.3.1 Equipment

The closed-loop computer-controlled cyclic triaxial testing system employed was manufactured by ELE International Ltd., UK, and Industrial Process Controls Ltd., Australia. It was later modified by Higuchi (2001) at the University of Sheffield. The system basically consisted of a triaxial cell, a loading frame fitted with a double-acting actuator connected to a pneumatic servo valve, and a Control and Data Acquisition System (CDAS) linked to a personal computer. The axial strain was obtained by using an LVDT. A pressure regulator was also included in the system to ensure that the pressure supplies were consistent throughout the test, which is crucial for the servo valve. The schematic depicting the CDAS connected to a personal computer and the actuator is illustrated by Figure 4.5. In addition, the system was enhanced by adding a vacuum gauge and a CO_2 facility for aiding the sample preparation and saturation, similarly to that used for the undrained monotonic triaxial test. The picture of the whole cyclic triaxial system is illustrated by Figure 4.6.

One important feature of the top cap to be used for the cyclic loading test, was that similar to the undrained monotonic triaxial extension test, it had to be attached to the loading piston in order that the cyclically repeated extension load could be applied. In this case the fixed connection employed was by means of a suction-type top cap, as illustrated by Figure 4.7. The fixed connection consisted of a truncated-cone shape steel (see Figure 4.7(a)) connected to the loading piston and the rubber protruded from the top of the top cap. The protruded rubber just fitted and surrounded the truncated-cone shape steel (see Figure 4.7(b)). There was a hole through the truncated-cone shape steel which was used to apply a full vacuum, creating a fixed connection. The details of the ELE cyclic triaxial system (UTM Hardware Reference, 1998; Higuchi, 2001; Meca, 2004) and its important component parts will be described in the following sections.

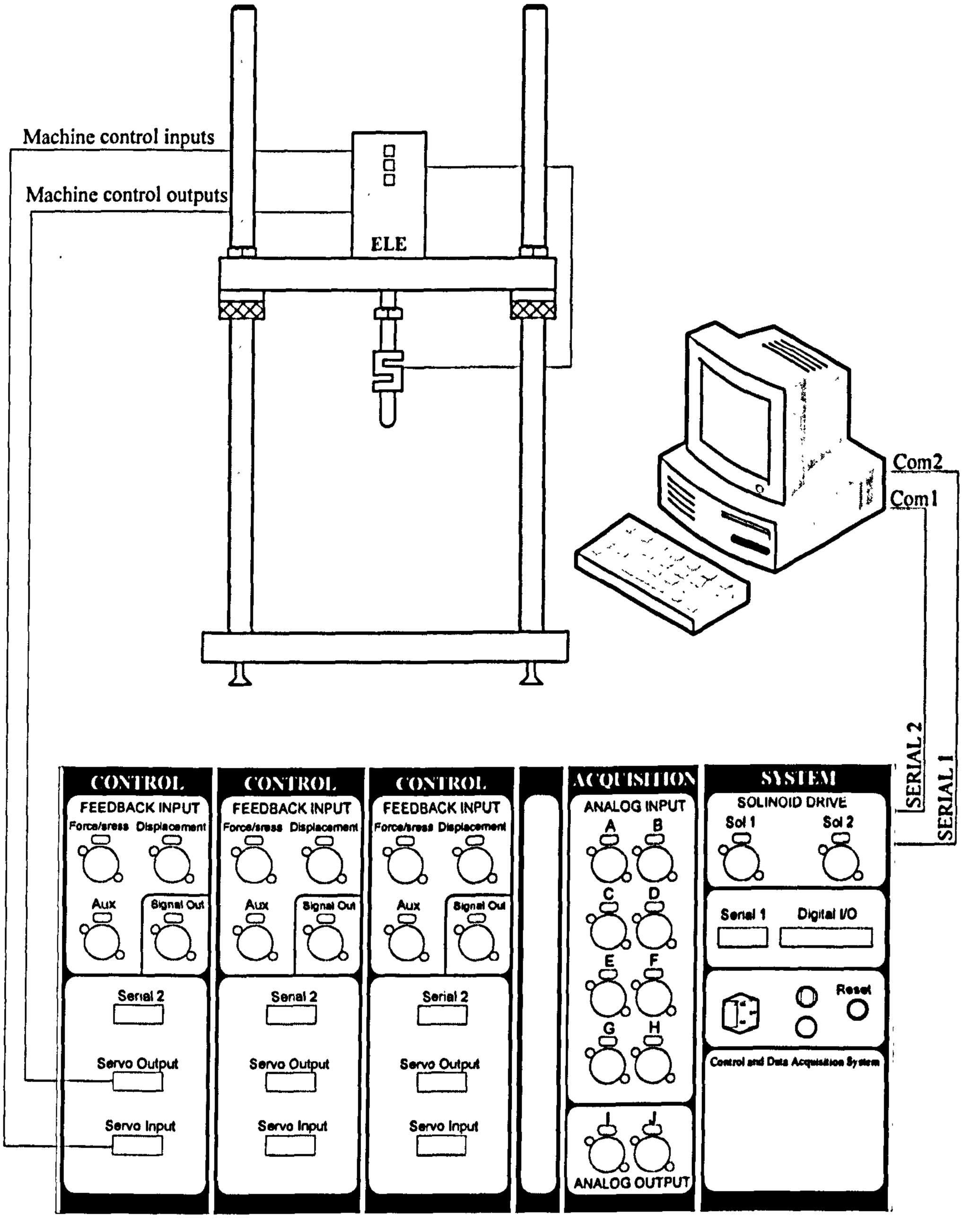

Figure 4. 5 CDAS connected to PC and loading frame (after UTM Hardware Reference, 1998)

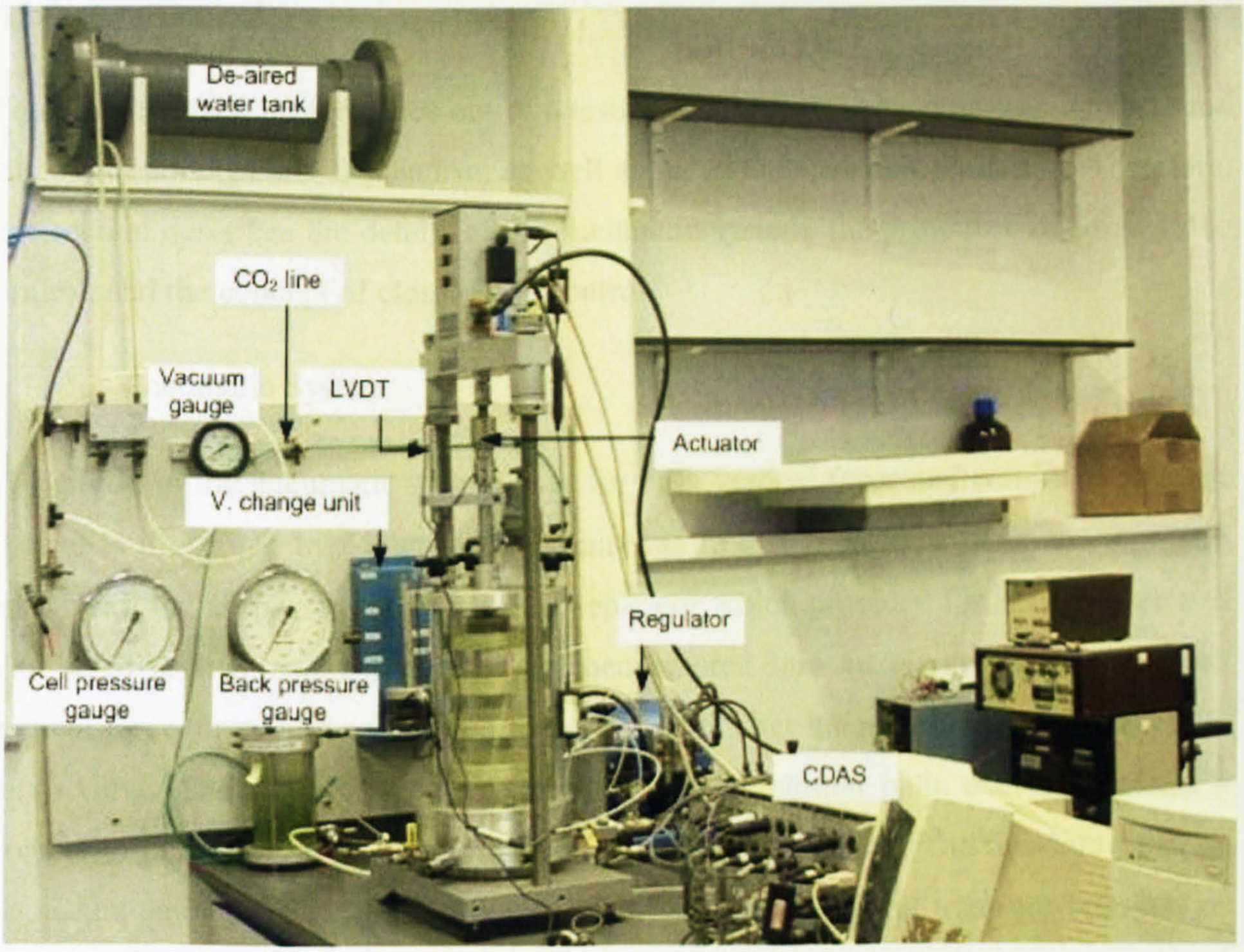

Figure 4. 6 Test set up for undrained cyclic triaxial test

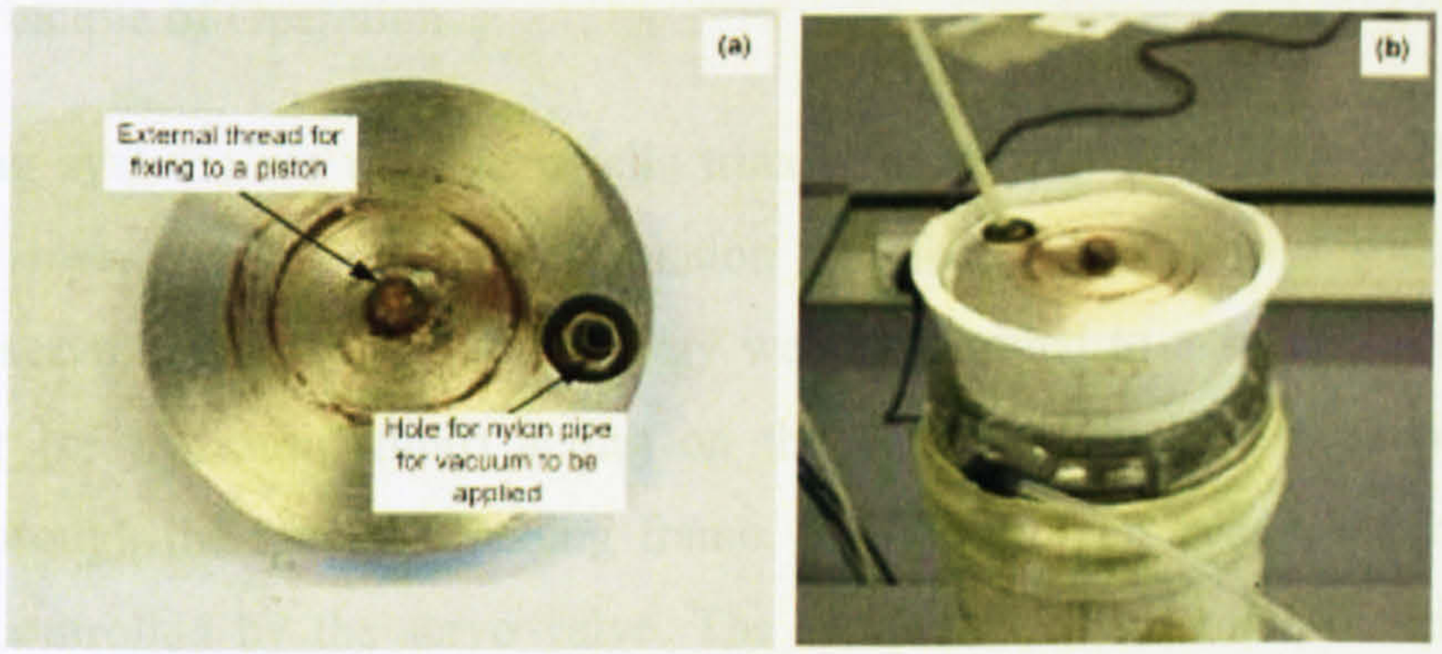

Figure 4. 7 Specific-designed top cap for undrained cyclic triaxial test

A) System Control

To obtain the best performance out of a testing machine, it is necessary to comprehend its control concept and mechanism as well as its advantages and limitation. Therefore, this section describes the details of the pneumatic system, the principles of servo valve control, and the concept of closed-loop control.

(i) Pneumatic System

The circuit of the pneumatic system used for both vertical force and confining pressure control is illustrated by Figure 4.8. The air was first filtered by a filter and regulator unit. Next, the air passed through a mist separator which provided further filtration and also acted as a moisture trap. The air then entered into an air accumulator for the vertical force air supply and passed through a final filter before entering the pneumatic servo valve. The confining pressure air supply had a similar path, except it entered a voltage-to-pressure converter before entering an air accumulator. The five-litre capacity air accumulator provided the improvement of the regulation and transient response of the system under pulsed repeated loading operation.

(ii) Principle of Operation

Servo testing systems are used for cyclic triaxial tests because they provide accurate control and measurement of the deformation and force applied to a soil specimen. Within the servo testing system, the energy was transmitted to a specimen using high pressure air (or hydraulic fluid) acting on the actuator which was coupled to the specimen through the reaction loading frame. The flow of air pressure (or hydraulic fluid) was controlled by the servo valve. The servo valve had small electric currents which were used to open and close the control spool (Figure 4.9) of the valve. Because such valves have very high power amplification, large specimens as well as large rates of work can be easily controlled by just controlling the electric current input.

Typically transducers such as load cells and strain gauges are mounted on the system for measuring the parameters required. These transducers not only convert the mechanical movement into standard electronic signals via the Control and Data Acquisition System (CDAS), but also provide the output display on a personal computer user interface screen.

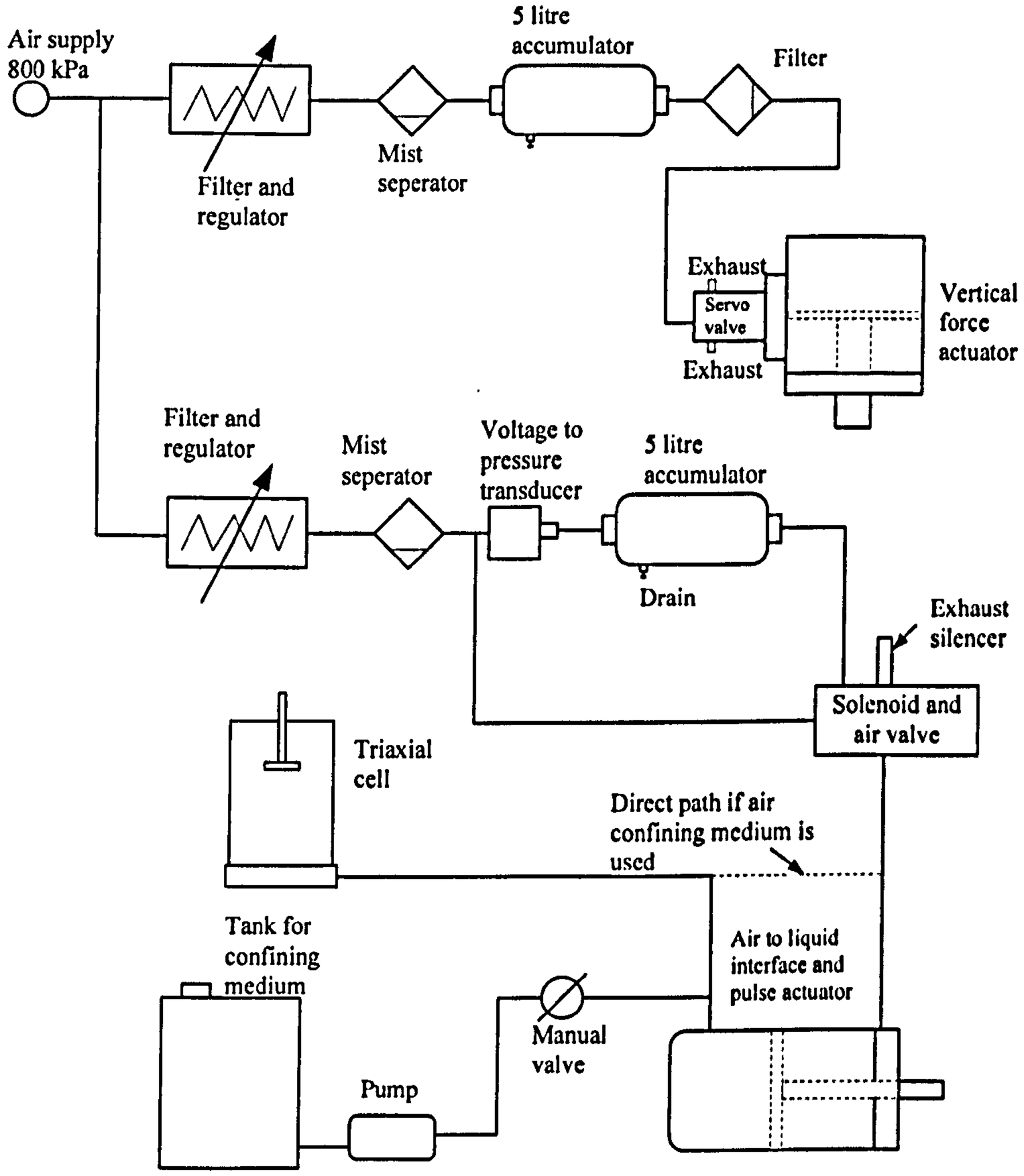

Figure 4. 8 Pneumatic circuit (after UTM Hardware Reference, 1998)

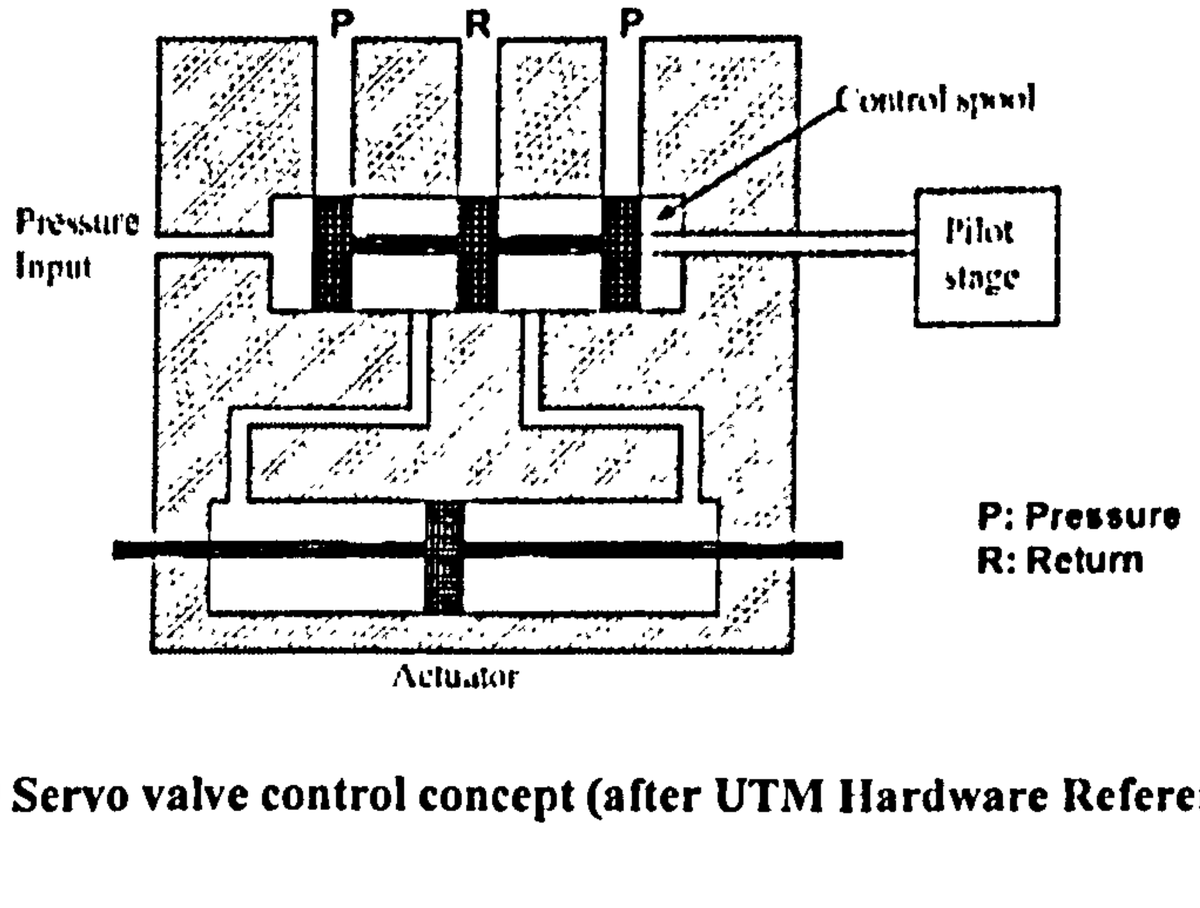

Figure 4. 9 Servo valve control concept (after UTM Hardware Reference, 1998)

(iii) Closed-Loop Servo Control

Figure 4.10 shows the diagram for the closed-loop servo system. The transducer transmitted the signal to a summing junction within the CDAS enclosure. The receiving signal then was compared with the required input (demand). The difference between the two signals is called the error which was used to drive the servo valve to regulate the flow of air pressure to eliminate the error. This concept can be expressed as the following equation:

$$\text{Drive ERROR} = \text{Input DEMAND} - \text{Position FEEDBACK} \qquad \textbf{(Eq. 4. 1)}$$

From the diagram, it can be seen that the response of the system does not rely on the alertness of a tester as the control loop is closed electronically. Note that this feedback loop can be used for any transducer attached to the system.

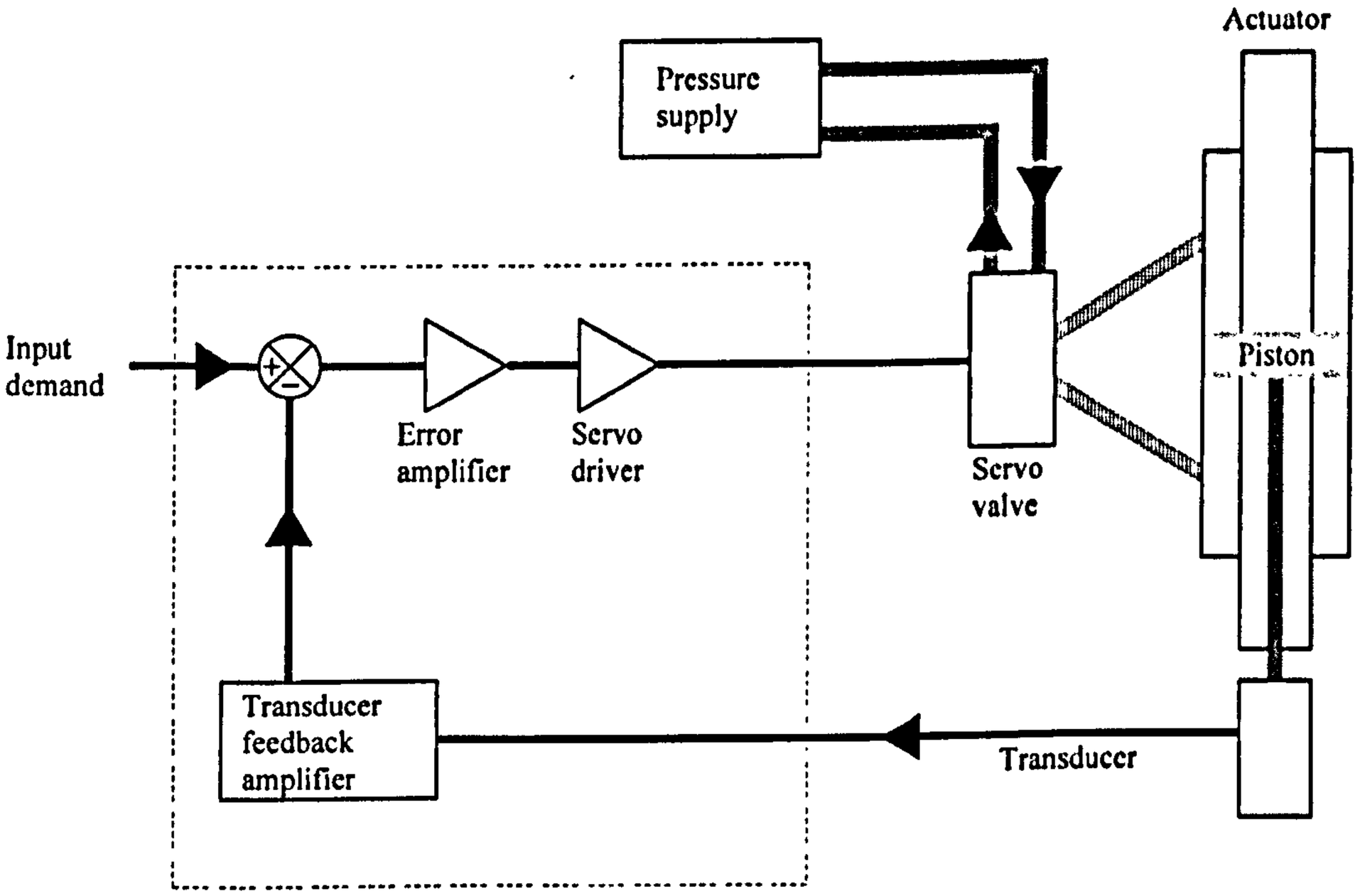

Figure 4. 10 Closed loop servo-block diagram (after UTM Hardware Reference, 1998)

B) Hardware Components

(i) UTM 5 P Loading Frame and Actuator

The loading frame manufactured by ELE International Ltd., was of heavy construction to limit the deflection and vibrations of the frame which could influence the accuracy of measurements during repeated cyclic loading. It had a heavy, flat base steel plate

supported on four levelling screws. Two threaded rods supported a crosshead beam, providing the height adjustment, and accommodating the servo-controlled actuator and its control system. The actuator mounted on the crosshead beam was a low friction, double acting, and high-speed design with a very high frequency response of up to 70Hz.

(ii) Modified Triaxial Cell

The triaxial cell manufactured by ELE could accommodate specimens having dimensions of up to 200mm high and 100mm diameter. The cell was rated to a maximum confining pressure of 1700kPa.

The cyclic deviator stress to be applied in this research was a continuous sinusoidal-wave form comprising both repeated compression and extension. Therefore, the top platen had to be a fixed type. For the sake of convenience, the suction-type top platen was selected. As a result, the total height of a specimen plus the top cap was such that the head room left was not enough for a submersible load cell. Therefore, the triaxial cell was lengthened by 50mm by adding an aluminium ring at the base. This value was calculated to accommodate the bender elements as well.

(iii) Pressure Reservoir

A pressure reservoir was used to preserve a steady air pressure supply to the high precision servo valve. For practical use, the air pressure was maintained at around 500kPa throughout the test. The reservoir had two water/oil traps at both inlet and outlet ports to ensure that the air was clean. Note that if the frequency of the actuator to be used is high, a higher capacity of pressure reservoir should be considered.

(iv) Cell Pressure System

The cell pressure system comprised an electro-pneumatic servo valve, a pressure transducer, a bladder type air/water pressure assembly, and a pressure gauge. The air pressure regulated by the servo valve was supplied to the air/water pressure assembly, which in turn pressurised the water in the assembly, hence transmitting the pressure into the triaxial cell.

The servo valve manufactured by Festo Co., provided a pressure output range of 0 – 1000kPa for an input range of 0 – 10V. The mechanism of the servo valve is illustrated by Figure 4.9. Note that the pressure can be regulated either by the CDAS or by software. In both control modes, the cell pressure was controlled via the servo valve.

The pressure transducer manufactured by ELE International Ltd., was located next to the output port of the servo valve and had a range of pressure from 0 to 1000kPa with a resolution of ± 0.5kPa. The required pressure was monitored on a computer screen through the software.

(v) Back Pressure System and Volume Change Unit

The transducer used for measuring and monitoring the back pressure was the same as used for the cell pressure. The continuous measurement of volume change was done by connecting the water outlet of the air/water interface tank to the volume change measurement apparatus, and then to the cell base used to apply back pressure to the specimen.

The volume change unit used was manufactured by ELE International Ltd. It had a capacity of 80 ml and a sensitivity of 0.01ml. The unit comprised a cylinder, a piston fitted with a Bellofram, and an LVDT. The lower chamber of the cylinder was connected to the air/water pressure unit whereas the upper chamber was connected to the cell base. The LVDT attached to the piston was used to monitor as well as to calculate the volume change in association with the area of the piston.

(vi) Pore Pressure Transducer

The measurement of pore water pressure was done by using a pore pressure transducer manufactured by ELE International Ltd. The transducer had a range of 0 -1000kPa. The signal from the transducer was amplified by an in-line gain amplifier manufactured by Industrial Process Controls Ltd. which provided a resolution of ± 0.1kPa.

(vii) Submersible Load Cell

The compression and extension axial loads were controlled and monitored by employing a submersible load cell manufactured by Wykeham Farrance. The load cell had a load range of ± 5 kN, with a final resolution of ± 2.5N. The load cell was

calibrated using a Bundenberg Dead Weight Tester together with a load cell calibration frame.

(viii) Deformation Transducer

The measurement of vertical deformation of the specimens was done using an LVDT manufactured by ELE International Ltd. The LVDT had a linear range of 50mm and a resolution of ± 0.01mm. The body of the LVDT was clamped to the loading piston while its post and bracket were clamped to the top of the triaxial cell. During testing, the deformation data was collected by the CDAS, and was displayed, monitored, and recorded by the personal computer for further analysis by spreadsheet software, usually Microsoft Excel. The LVDT was calibrated before use by using a 0.001mm resolution Mistutoya digital micrometer.

(ix) Top Platen Loading Cap and Connecting Device

The top platen loading cap and connecting device was made by the Department of Civil and Structural Engineering, Sheffield University. It was designed to have a fixed connection between the loading piston and the top cap so that a tension force could be applied. The loading piston consisted of a load rod connected to the submersible load cell. The load cell was attached to a steel truncated-cone shape. The connection to the top cap, was a socket-like rubber protrusion designed to just fit and surround the steel. The fixed connection was achieved when a full vacuum was applied through the hole in the top of the cone while it was inserted into the rubber.

(x) Control and Data Acquisition System (CDAS)

The control and data acquisition system (CDAS) was manufactured by IPC Ltd. The CDAS comprised a power supply module, a microprocessor module, an analogue input/output module, and a closed-loop digital signal processing module. It was a compact, self contained unit that provided all critical control, timing and data acquisition functions for the testing frame and transducers. The CDAS was connected to a personal computer on which was installed the cyclic triaxial testing software provided by ELE International Ltd. The module had eight normalised (± 10V range) transducer input channels. These channels were digitised by accurate, high speed 12 bit Analogue to Digital (A/D) converters for data analysis and presentation.

For feedback control operation, the CDAS had three normalised input channels. One was dedicated to the position of the actuator, the second was dedicated to the actuator force, and the third was a general purpose input (Aux) for on-specimen transducers etc. Each of these three channels fed into the control module and were buffered and brought out to a connector (Signal Out) for optional data acquisition.

Connected to the PC, the CDAS automatically controlled the operation of the loading frame for individual types of test. The CDAS directly controlled the servo valve to apply the requested loading rate as well as wave form. It could also apply a voltage via the Digital to Analogue Converter (D/A) to adjust the air pressure to the required level for tests requiring confining stress. While the specimen was being subjected to cyclic loading forces, the CDAS captured data from the transducers and transferred these, via RS232 serial link, to the PC for data processing, display, and storage.

4.3.2 Principles of Undrained Cyclic Triaxial Test

During earthquake shaking, a soil element at plane x - x shown in Figure 4.11 may be considered to be subjected to a series of cyclic shear strains or stresses caused by shear waves that reverse many times. The idealised stress conditions for the soil during the earthquake can be illustrated by Figure 4.12. It is recognised that if a ground is horizontal or gently sloping, there will be no shear stresses on the horizontal plane before the earthquake. During the earthquake, however, the normal stresses on this plane remain constant, but cyclic shear stresses are induced during the period of shaking (Prakash, 1981).

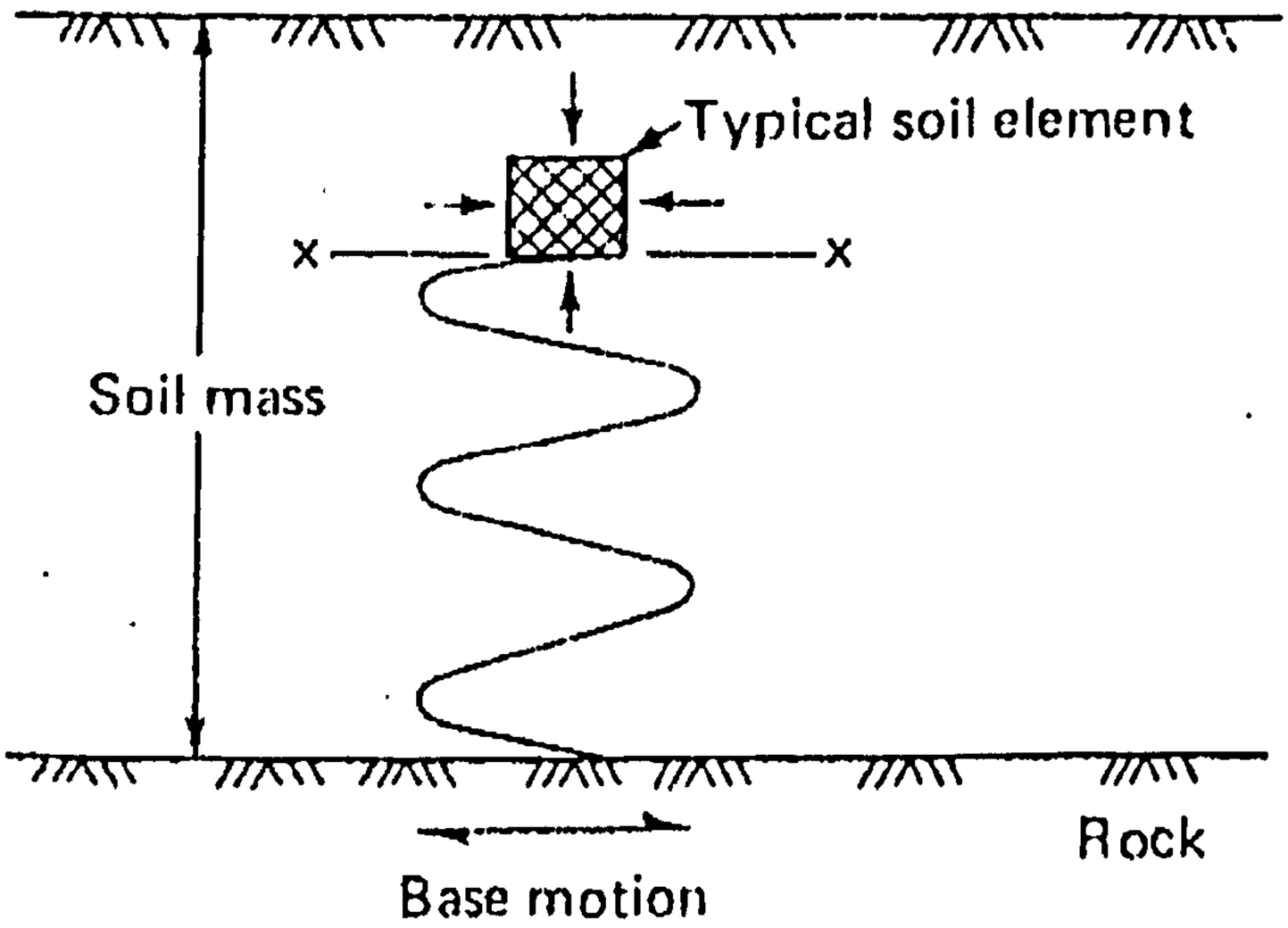

Figure 4. 11 Transmission of shear waves from rock base into the overlying soil (after Prakash, 1981)

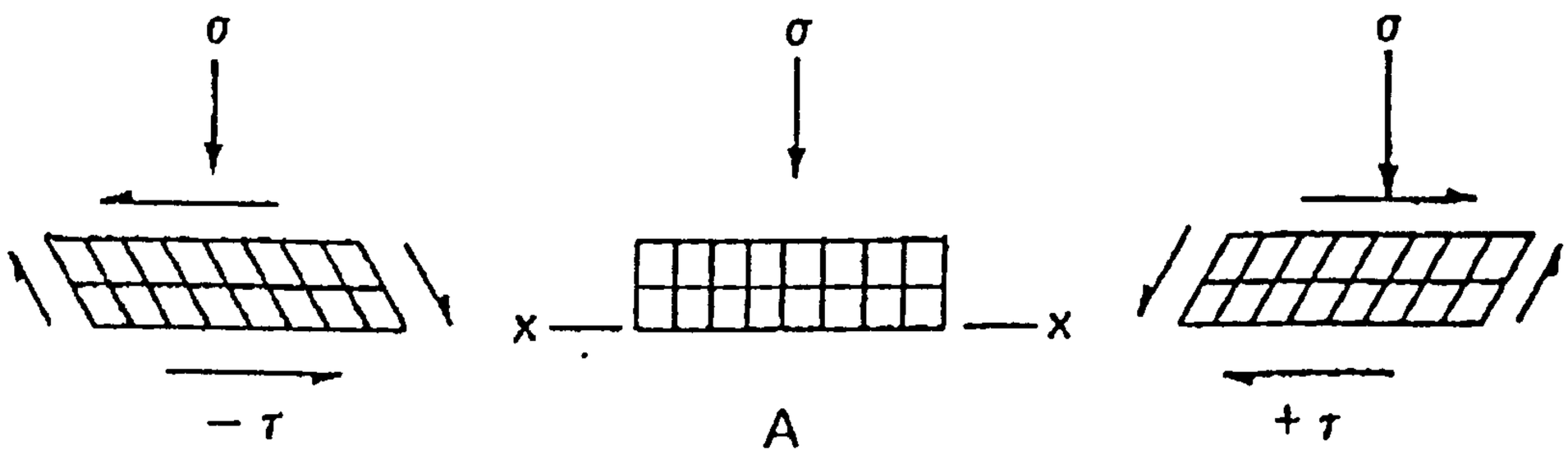

Figure 4. 12 Idealised stress condition for soil element during an earthquake (after Prakash, 1981)

The reversal of shear stresses caused by an earthquake can be illustrated graphically using the Mohr diagram by Figure 4.13. Stage (a) represents the stress conditions for a soil before the shaking; it is under all-round pressure with no shear stress, as shown in column 2. When an earthquake takes place, both surface and body waves are generated. However, it is the shear wave that causes the shear stress and shear strain in the soil. This can be simulated by applying shear stresses as illustrated by stages (b) and (c) in Figure 4.13. The simulation of simultaneous cyclic stress changes on both the vertical and horizontal planes acting on a specimen as shown in column 3 of Figure 4.13 is very difficult to maintain. However, it can be approximated by applying the stress conditions shown in column 4 (Prakash, 1981).

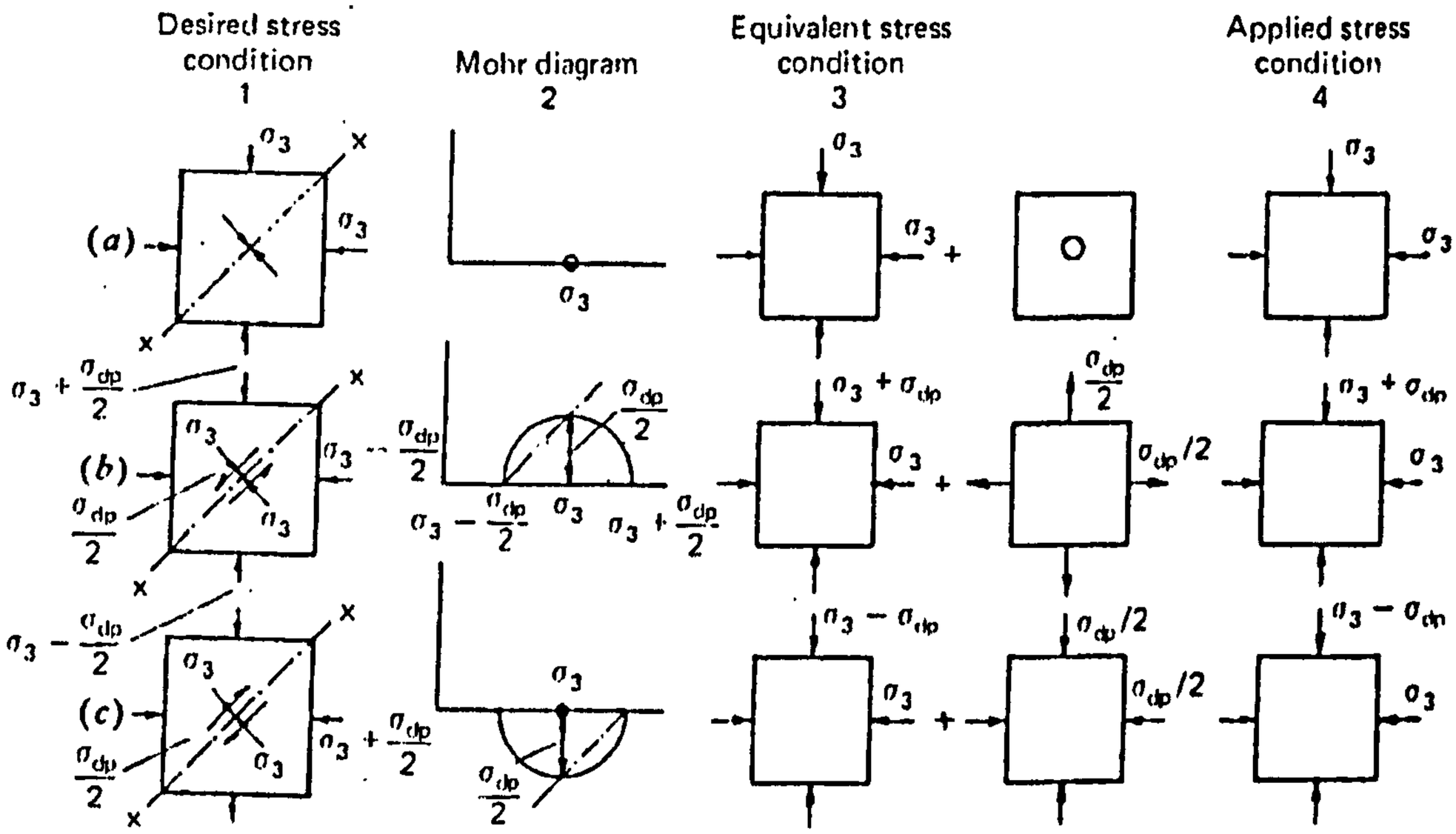

Figure 4. 13 Stress conditions for cyclic triaxial test under simulated earthquake loading (after Seed and Lee, 1996; Prakash, 1981)

4.3.3 Cyclic Stress Parameters

The main purpose of the cyclic triaxial test is to determine the cyclic strength of a soil. However, during cyclic loading the stress-strain behaviour and the build up of excess pore water pressure are also observed. The cyclic strength of an isotropically consolidated soil is influenced by two major factors, namely the density and the initial effective stress (Vaid *et al.*, 2001). In common practice, the cyclic deviator stress q_{cyc} that causes the soil to liquefy after a particular number of cycles N is normalised by the consolidation pressure σ'_{3c}. This is known as the cyclic stress ratio CSR, and is defined as $q_{cyc} / 2\sigma'_{3c}$. It should be noted that σ_{cyc} shown in Figure 4.13 and q_{cyc} are in fact the same. Also note that the CSR for the cyclic simple shear test is defined as τ_{cyc} / σ'_v, where σ'_v denotes the vertical effective stress.

During cyclic triaxial testing, the maximum cyclic shear stress τ_{cyc} generated by the cyclic deviator stress q_{cyc} (or σ_{cyc}) occurs on a plane at 45-degrees to the principal planes, as previously illustrated by Figure 4.13 (column 1), and can be calculated by the following equation:

$$\tau_{cyc} = \frac{q_{cyc}}{2} \qquad \textbf{(Eq. 4. 2)}$$

where:

q_{cyc} = $(\sigma'_1 - \sigma'_3)_{cyc}$

σ'_1 = major principal effective stress, and

σ'_3 = minor principal effective stress.

The so-called cyclic deviator stress q_{cyc} is in fact an averaged single amplitude deviator stress obtained from peak applied loads both in compression and extension during cyclic loading, and can be calculated from the following equation:

$$q_{cyc} = \frac{\Delta P_c + \Delta P_e}{2A_c} \qquad \textbf{(Eq. 4.3)}$$

where:

ΔP_c = peak cyclic load in compression,

ΔP_e = peak cyclic load in extension, and

A_c = area of specimen after consolidation.

The measurement of peak cyclic loads, in both compression and extension, as well as the sinusoidal wave form normally employed in the cyclic triaxial test is illustrated by Figure 4.14. It should be noted that the measurement should be taken only when the wave form is uniform. If the wave form observed during cycling loading being applied is not consistent, that test must be discarded.

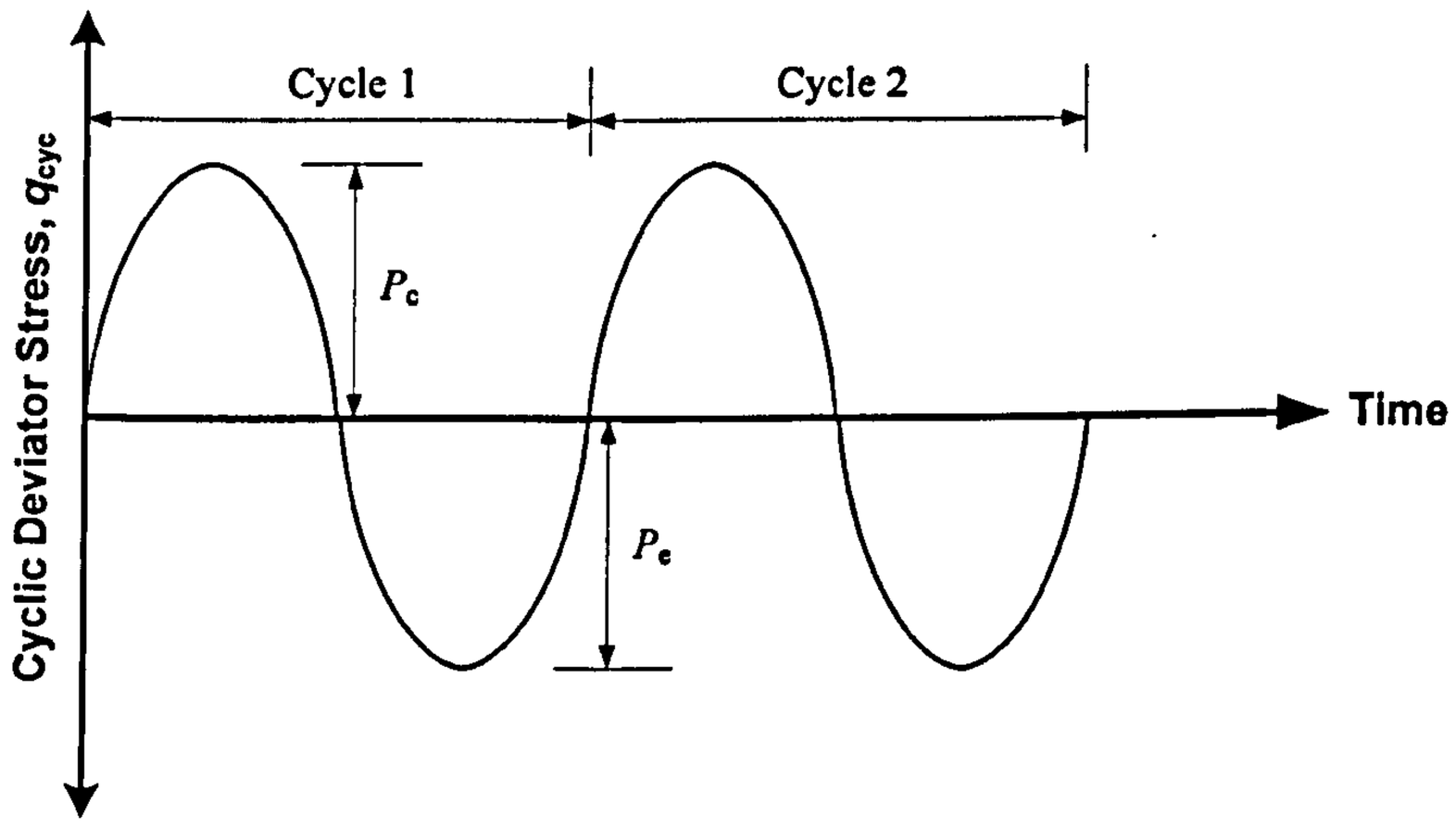

Figure 4. 14 Descriptions of sinusoidal wave form and cyclic loads

The magnitude of cyclic load to be applied on a specimen at any cyclic stress ratio *CSR* can be estimated by the following equation (ASTM, 1996b):

$$P_c = 2 \times \sigma'_{3c} \times CSR \times A_c \qquad \text{(Eq. 4. 4)}$$

where:

σ'_{3c} = consolidation pressure, and

CSR = cyclic stress ratio.

4.3.4 Testing Procedures (including the bender element test)

The undrained cyclic triaxial test was conducted through a personal computer running the software called UTM 4 Cyclic and Shear Triaxial Test, Version V2.0 provided by IPC Global (UTM for Windows, 2006). Note that UTM stands for The Universal Testing Machine.

The main menu basically consisted of File menu, Run menu, Options menu, View menu, and Help menu. The File menu was mainly for managing files and creating templates; all new tests always began from this menu. Printing the report of a test was also included in the File menu. The Run menu was simply for commencing, stopping, and resuming the test. Note that the Run menu was deactivated if the input section was incomplete. The Options menu was for displaying the test print report and controlling of the wave shapes. The main function for the View menu was simply to display the levels of all transducers and wave forms before and during testing.

A) Initial Set Up

(i) CDAS, PC, vacuum pump, and pressure pump, were turned on accordingly.

(ii) The pressure regulator was adjusted to 5Bars .

(iii) The base pedestal accommodating the bender element acting as a transmitter was greased; a rubber membrane was put on and sealed with O-rings; the centred-hollow porous disc was placed in position. (see Figure 4.15(a)).

(iv) The mould was assembled; any potential leak from the mould and the mould-base interface was plugged using plasticine (see Figure 4.15(b)).

(v) A full vacuum was applied between the inner mould and the rubber membrane; to make sure that the membrane was completely attached to the mould.

B) Sample Preparation

(i) A mixture was weighed in eight portions using Table 3.3 in Chapter 3 Materials and Testing Programmes.

(ii) Each portion of the mixture was stirred and mixed thoroughly using a wooden stick until it was well blended.

(iii) Each portion was deposited by means of a dry funnel maintaining a virtually zero drop height for the mixture (see Figure 4.15(c)); each layer was levelled by using the wooden stick.

(iv) After the last (eighth) portion had been deposited, the centred-hollow porous disc similar to that used at the base was placed, followed by a top cap, also accommodating the other bender element but acting as a receiver; the level was checked (see Figure 4.15(d)). The direction of the receiver bender element had to be the same as the transmitter; otherwise, the signals might not have been detected properly.

(v) The top cap was enclosed by the membrane and sealed with O-rings (see Figure 4.15(e)).

(vi) A small nylon pipe was connected from the top of the top cap to the CO_2 line-out (see Figure 4.15(f)). Note that this line was also used for the discharge for de-aired water after the CO_2 had been flushed.

(vii) A small vacuum of about -20kPa was applied through the back pressure line to sustain the specimen; then the mould was dismantled. The difference between the vacuum applied and the first step of cell pressure to be applied was kept lower than the desired consolidation pressure. Otherwise, the specimen would be overconsolidated.

(viii) At this stage the dimensions of the specimen were taken. For the height two opposite vertical sides were measured; whereas; for the diameter, top, middle, and bottom were measured using a micrometer and averaged. Note that the average for the diameter was determined from: [top + 2(middle) + bottom] / 4.

(ix) The cyclic triaxial cell was fixed in place.

(x) The loading piston with the truncated-cone shape attached was lowered and inserted into the rubber socket surrounding the top cap (see Figure 4.15(g)). Note that at the top of the truncated-cone shape was a hole used for connecting the vacuum line through the top of the cell.

(xi) The full vacuum was applied through the small nylon pipe connected to the top of the truncated-cone shape steel creating the connection between the specimen and loading piston.

(xii) The triaxial cell was filled with water.

(xiii) The initial pore water pressure and the initial level of volume change unit level were recorded. Note that this step was done by the personal computer.

C) Input of Test Control Parameters

(i) The UTM 4 application was opened.

(ii) A test from the File menu was begun by either opening a new file or using a template.

(iii) A file name was entered.

(iv) Test information entered including:

- General descriptions of the test.
- Specimen dimensions.

(v) Test set up parameters entered, including:

- For the saturation: cell pressure increment and differential pressure in kPa.
- For isotropic consolidation: effective stress adjustment in kPa.
- For anisotropic consolidation (not used).
- For cyclic loading: pulse width (ms), peak to peak amplitude (kPa), termination cycle count (cycles), and termination strain (%). The pulse width, in other words, the frequency of peak to peak deviator stress (kPa) to be applied. For example, in this research the frequency of 0.1Hz was used throughout. Thus, the pulse width = (1/0.1) x 1000 = 10000ms.
- For shear loading (not used).

D) Saturation

(i) A first cell pressure step of 50kPa was applied; in the meantime, the small vacuum applied for sustaining the specimen was slowly released.

(ii) The specimen was percolated with CO_2 using a pressure of about 10kPa for 10 minutes. Note that the line for discharging the CO_2 was submerged in a half-full jar of water so that the bubbles could be observed. The specimen was flushed with de-aired water from the reservoir for around 10 minutes, or until visibly fully wet. At this stage, the *B* value was already over 0.90.

(iii) A first back pressure step of 40kPa was applied, keeping a stress difference of 10kPa. The next increment for the cell and back pressure was 50kPa. For example, for the second step, cell pressure = 100kPa and back pressure = 90kPa.

(iv) To check for the next increment of cell and back pressure, the drainage valve was closed and the pore water pressure was observed over a 1-minute interval. If the change was less than 1% of the confining pressure, it was assumed to be stabilised, and the next step of the pressure could be applied.

(v) To check *B* value:

- The drainage valve was closed.
- A change in cell pressure of 50kPa ($\Delta\sigma_3$) was applied.
- The change of pore water pressure (Δu) due to the increase of cell pressure of 50kPa was recorded.
- Then B was calculated by $B = \Delta u / \Delta\sigma_3$.
- Only B values equal to or greater than 0.97 indicating full saturation were accepted; otherwise, a specimen was discarded.

E) Consolidation, Bender Element Test and Cyclic Loading Test

(i) At the end of the saturation the effective stress was 10kPa. Note that for all undrained cyclic triaxial tests, for the sake of the consistency of the test results, the final cell pressure and back pressure were 200kPa and 190kPa, respectively.

(ii) The drainage valve was shut; then, the cell pressure was slowly increased from 200kPa to 290kPa, resulting in a consolidation pressure of 100kPa. Note that the increase of pore water pressure should be virtually equal to the increase of cell pressure; otherwise, there might be leaks in the system or membrane.

(iii) The drainage valve was opened to allow the specimen to consolidate. The consolidation period for all specimens was 1 hr. The water coming out of the specimen was measured and recorded for determining the void ratio which was done by the personal computer.

(iv) After the consolidation, the BE test was conducted using frequencies of 2, 4, 7, 11, and 16kHz.

(v) After the BE test was completed, the drainage valve was shut to create the undrained conditions for the cyclic loading test.

(vi) The specimen was cyclically loaded using a continuous sinusoidal wave form at a frequency of 0.1Hz. Note that, unlike the undrained monotonic triaxial test, the undrained cyclic triaxial test was stress-controlled.

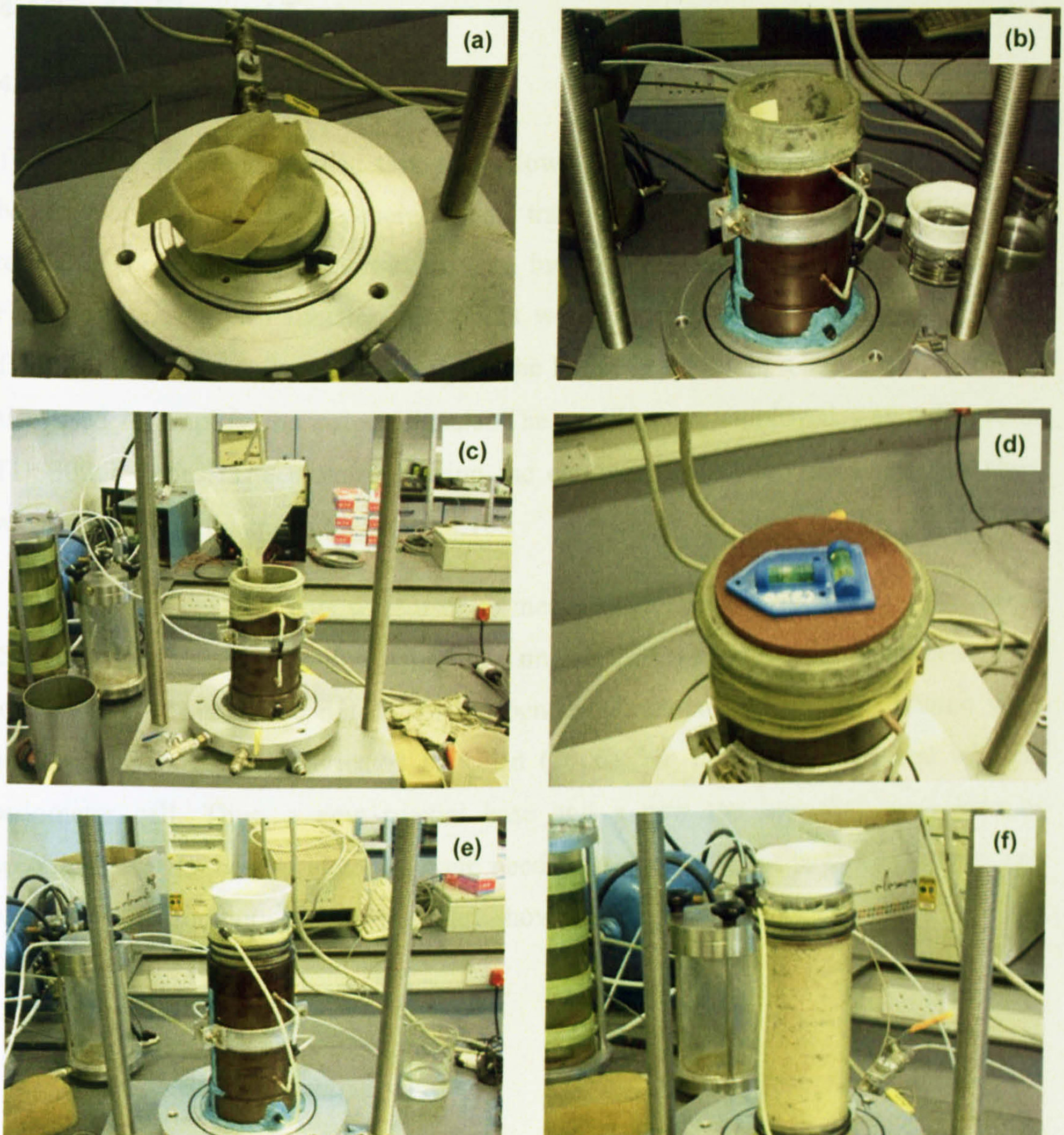

Figure 4. 15 Test procedures for undrained cyclic triaxial test and bender element test

4.4 Bender Element Test

4.4.1 Equipment

To perform a bender element test, the following devices are needed: (1) at least two bender elements, one is for generating and transmitting the signals and the other is for receiving the generated shear waves, (2) a function generator and (3) an oscilloscope. For this research, two function generators were employed: Farnel FG1 and Thandar TG4001. The former was used to trigger the latter. In addition, a signal amplifier was also used to amplify the output signals. The oscilloscope employed was a Textronix TDS3000b series. The picture showing the equipment used for measuring the shear wave velocity is illustrated by Figure 4.16.

The bender elements were used to measure the shear wave velocity, and hence the small-strain shear modulus, using the same specimen used for the undrained cyclic triaxial test. It should be noted that the bender elements used in this research were already developed and fabricated by Chan (2006), but they had been used with an oedometer cell. Thus, a new triaxial base and a new top cap that were able to accommodate the bender elements were needed. As a result, the base and the top cap were designed and built in-house, and are shown in Figure 4.17.

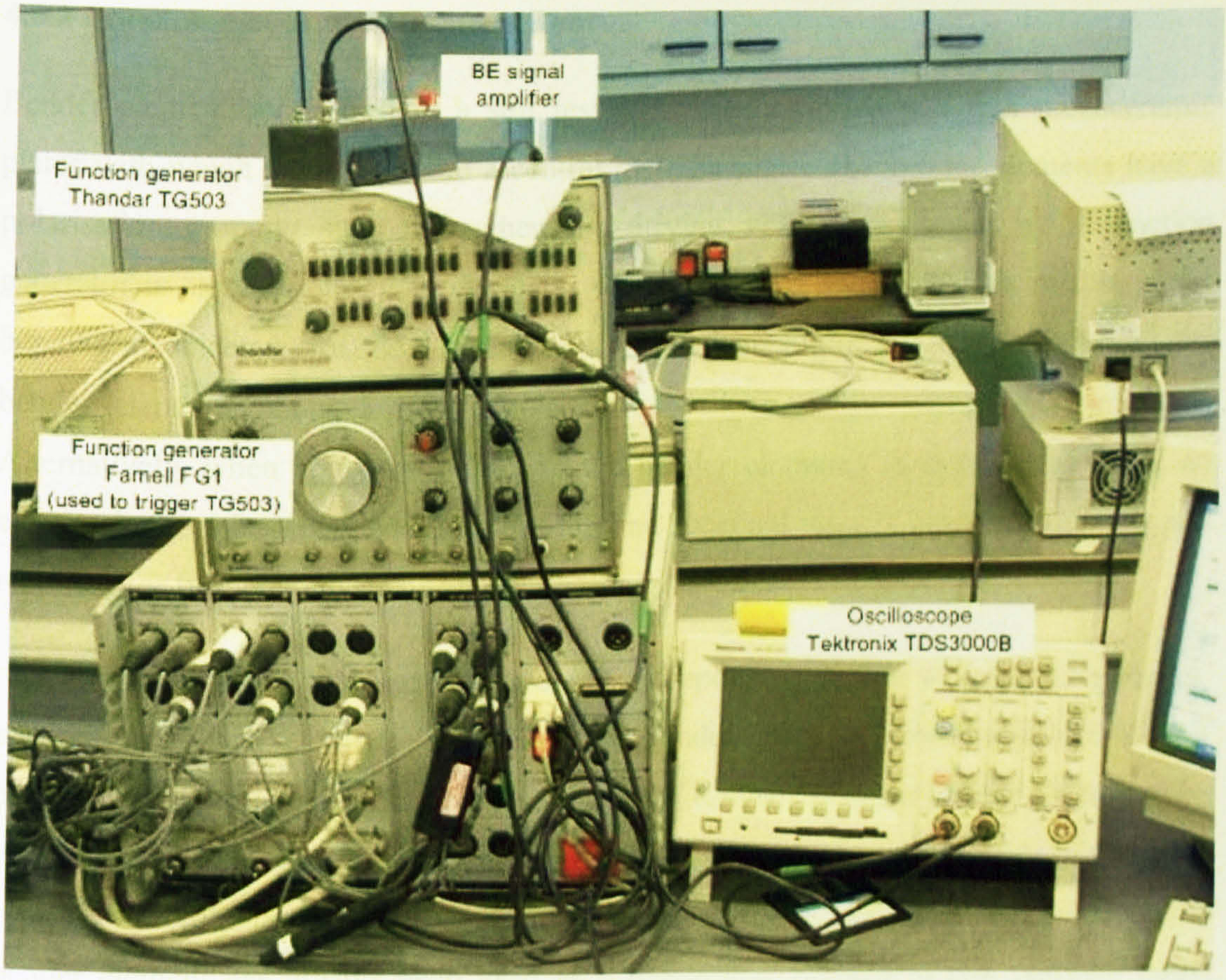

Figure 4. 16 Connection between oscilloscope and function generators

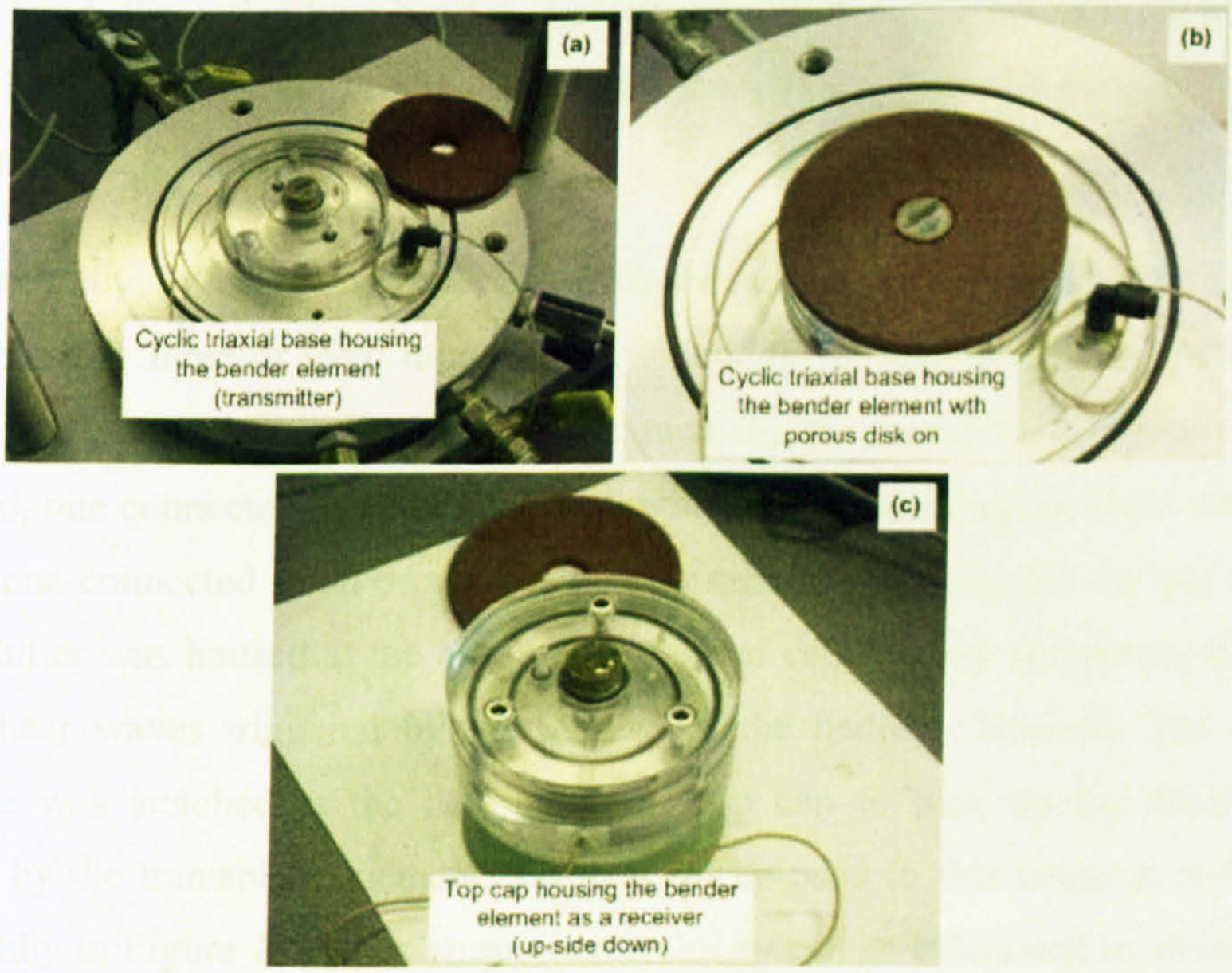

Figure 4. 17 Base and top cap housing bender elements

4.4.2 Principles of Bender Element Test

Bender elements employed in a soil test normally comprise two thin piezoceramic plates with which are attached to a central metallic plate. The bender elements have a polarisation property such that when the driving voltage generated by a function generator is applied, one plate elongates while the other shortens. This results in the bending displacement of the element, as illustrated by Figure 4.18. By protruding the bender elements about 5 mm into a soil specimen, shear waves are generated. Alternatively, when applying a force to the bender elements to make them bend, an electrical signal is generated. Both driving and received signals can be visualised and recorded for further analysis by an oscilloscope.

There are two types of bender element, depending on the wiring configuration, namely series and parallel. The details of bender element fabrication and wiring configurations employed can be found in Chan (2006). Comparing the parallel-type connection and the series-type connection, if the same voltage is applied to the parallel type, it will produce as much as twice the displacement. As such, the parallel-type bender element has always been used as a transmitter because it can produce more displacement thereby providing stronger shear waves that are easier to be detected. On the other hand, the series-type bender element is used as a receiver because it is more sensitive in terms of picking up the generated shear waves than the parallel type (Lee and Santamarina, 2005).

Generally, at least two bender elements are needed for the measurement of shear waves; however, three or even more bender elements are also possible, depending on the space and boundary conditions of a specimen. In the case of two bender elements being used, one connected to a function generator is for generating the shear waves and the other one connected to an oscilloscope is for receiving the signals. In this research the transmitter was housed at the base of the triaxial cell thereby simulating the travel path of shear waves triggered by the motion of the bedrock beneath. The receiver meanwhile was attached at the bottom of the top cap to pick up the shear waves generated by the transmitter element. The test set up used in this research is depicted schematically in Figure 4.19. The shear wave velocity can be calculated by dividing the tip to tip distance between the transmitter and the receiver by the arrival time of shear waves, as shown below:

$$V_s = \frac{l_{t-t}}{t_o} \qquad \textbf{(Eq. 4. 5)}$$

where:

V_s = shear wave velocity,

l_{t-t} = tip to tip distance between transmitter and receiver, and

t_o = arrival time.

Note that there was a debate about which distance should be used in the shear wave velocity calculation, between (1) tip to tip of the bender elements, and (2) the full specimen height. However, studies by Viggiani and Atkinson (1995) showed that the length to be used in shear wave velocity determination should be taken from the distance between the tips of the bender elements. Hence, the tip-to-tip distance has been used as a standard in the BE test (e.g., Lee and Santamarina, 2005; Chan, 2006). After obtaining the shear wave velocity, the small strain shear modulus G_{max} can be calculated by Eq. 2.10.

Several types of wave form have been employed in the BE test, e.g., pulse sine wave, step wave, pulse square wave, and continuous sine wave, as illustrated by Figure 4.20. However, from recent reports it has been shown that the pulse sine wave produces signals that are easier to interpret (Viggiani and Atkinson, 1995; Jovičić *et al*, 1996; Blewett *et al.* 2000; Leong *et al.*, 2005). As a result, a pulse sine wave was used to generate the shear waves in this research.

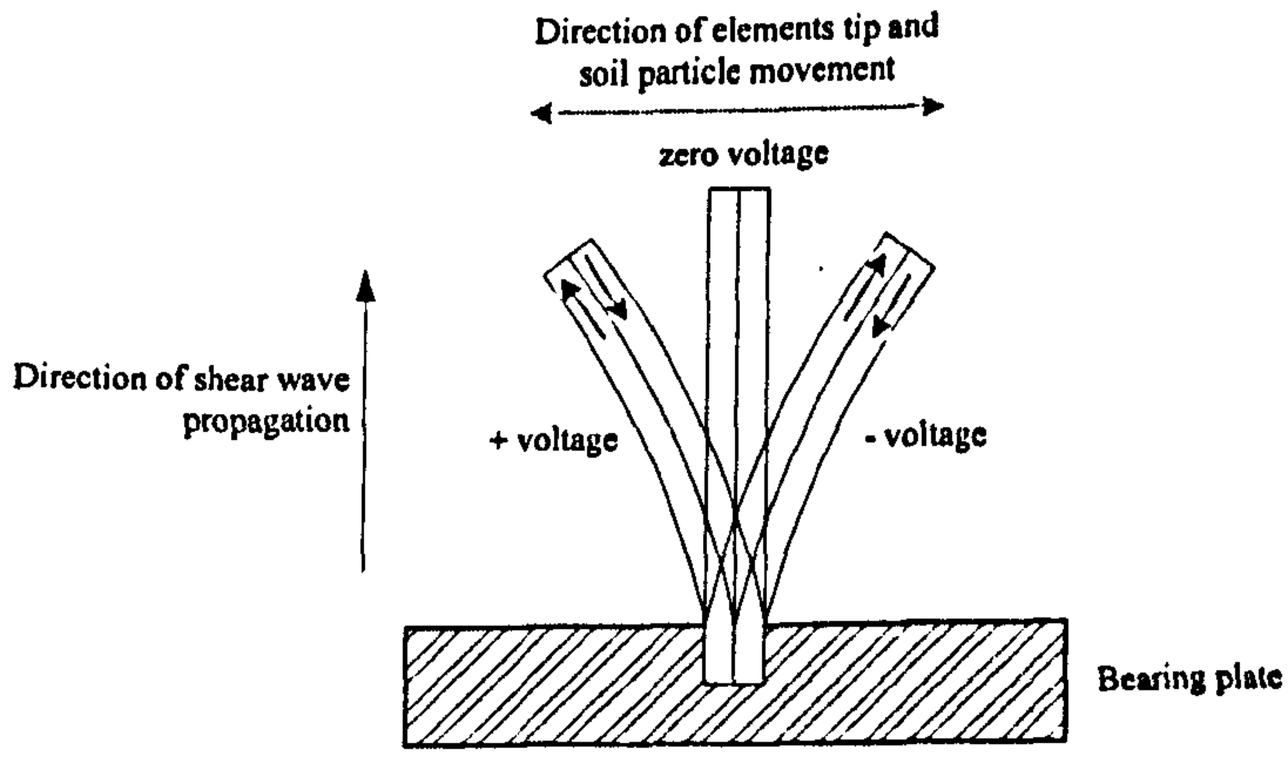

Figure 4. 18 Bending of piezoelectric bender element caused by changing between positive and negative voltage (after Kramer, 1996)

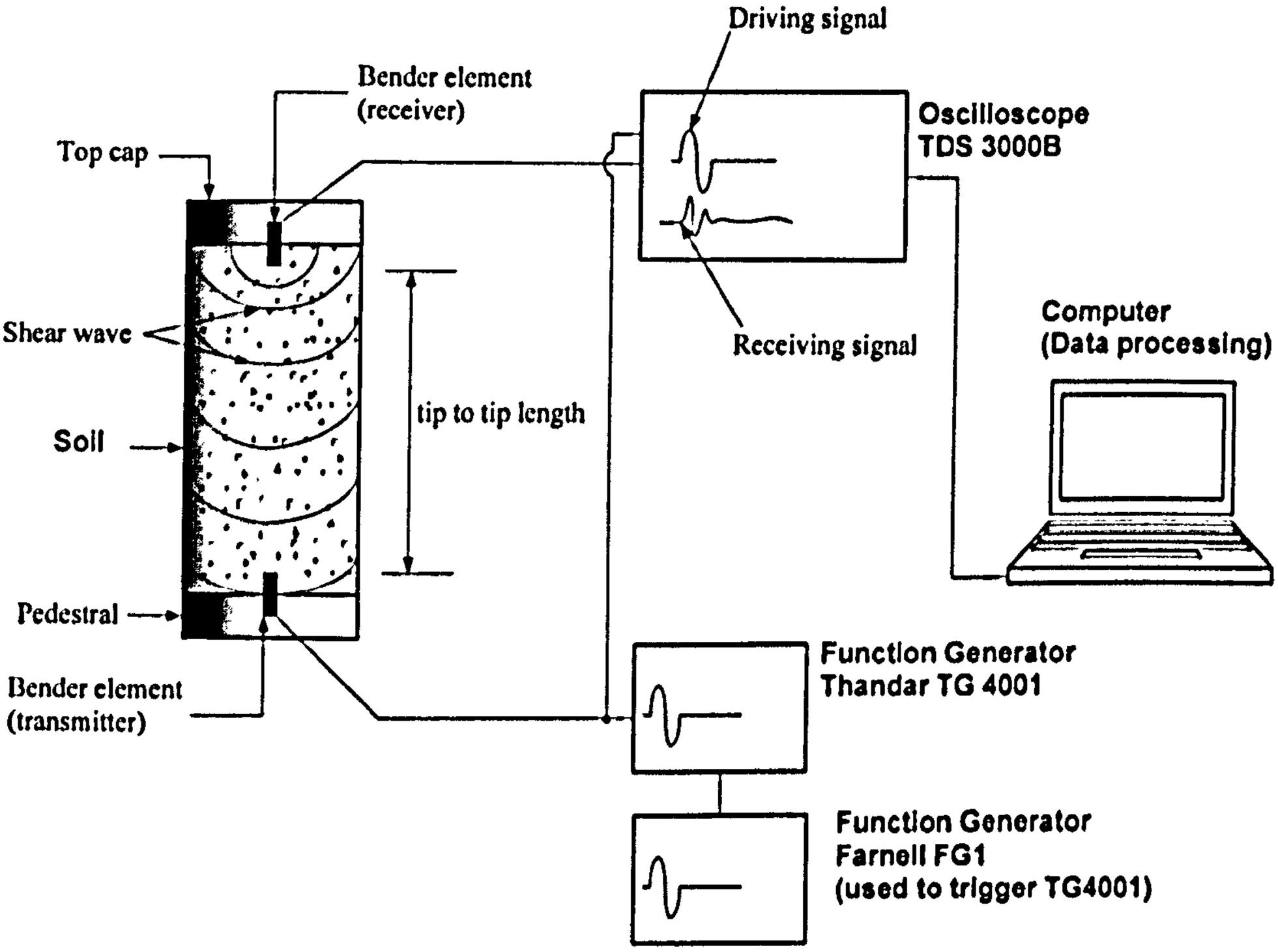

Figure 4. 19 Set up for bender element test

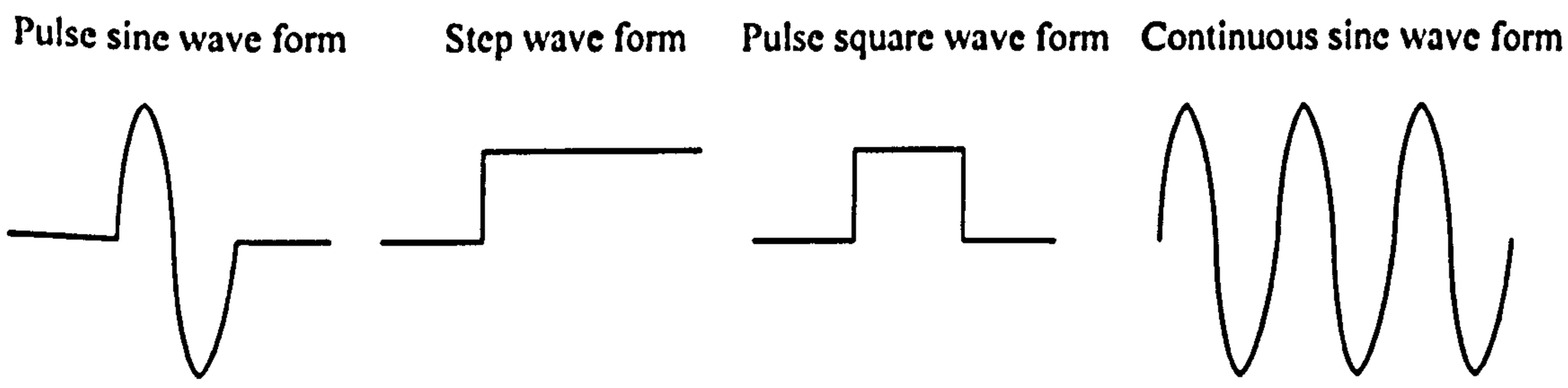

Figure 4. 20 Examples of wave forms (driving signals) used in BE test